ANALYIS AND DESIGN OF AXIALLY LOADED DRILLED SHAFTS SOCKETED INTO ROCK

By

Lianyang Zhang

S. B., Naval Architecture and Ocean Engineering (1985)
Shanghai JiaoTong University, China
S. M., Geotechnical Engineering (1988)
Tongji University, China

Submitted to the Department of Civil and Environmental Engineering
in partial fulfillment of the requirements for the degree of

Master of Science
in Civil and Environmental Engineering

at the

MASSACHUSETTS INSTITUTE OF TECHNOLOGY

June 1997

Signature of Author .....
Department of Civil and Environmental Engineering
May 14, 1997

Certified by .....
Herbert H. Einstein
Professor of Civil and Environmental Engineering
Thesis Supervisor

Accepted by .....
Joseph M. Sussman
Chairman, Department Committee on Graduate Studies

ANALYIS AND DESIGN OF AXIALLY LOADED DRILLED SHAFTS SOCKETED INTO ROCK

By

Lianyang Zhang

Submitted to the Department of Civil and Environmental Engineering
on May 14, 1997 in partial fulfillment of the requirements
for the Degree of Master of Science in Civil and Environmental Engineering

ABSTRACT

Drilled shafts socketed into rock are widely used to transfer heavy structural loads through weak overburden soil to underlying rock. In current design practice, empirical relations derived from load tests are often used to predict ultimate loads. To predict the load deformation response at working loads, theoretical solutions have been developed.

This thesis contains a literature review of current design methods, which shows: (a) Available empirical relations for estimating the ultimate side shear resistance give a wide range of values. This is because the relations are derived from different databases. (b) Available relations for estimating the end bearing resistance assume a linear relationship between the end bearing resistance and the unconfined compressive strength. However, the linear relations do not predict the field tests reasonably. And (c) Current design methods just model the rock mass as a single half space or at best, as a two-layer medium (i.e., the rock adjacent to and beneath the shaft) for the prediction of load-displacement response. This is a very crude approximation to the multi-layered rock mass in reality.

Because of the limitations of the current design methods, a new design model is proposed. The new design method can reasonably predict the ultimate side shear resistance and the end bearing resistance. It also considers the multi-layer nature of the rock mass for the prediction of load-displacement response. For the ultimate side shear resistance, a new relation is recommended by analyzing the available power-curve relations. For the end bearing resistance, a database of 35 loading tests is developed. By analyzing the database, a new relation between the end bearing resistance and the unconfined compressive strength is derived. A theoretical analysis is conducted using the Hoek-Brown strength criterion. The theoretical results basicaliy support the new relation. For the prediction of the displacement of drilled shafts at working load, a model which can consider the multi-layer nature of rock masses is developed. Governing differential equations and boundary conditions are derived for a shaft socketed in a rock mass with any number of layers. Closed-form solutions for a shaft socketed in a three-layer rock mass is presented. The model is validated by comparing it with the available theoretical solutions. Two examples including three test shafts are given to show the use of the design method. The results show that the proposed method can satisfactorily predict the ultimate loads and the displacements at working loads.

Thesis Supervisor: Herbert H. Einstein
Title: Professor of Civil and Environmental Engineering

ACKNOWLEDGEMENTS

I would like to express my gratitude and appreciation to my advisor, Professor H. Einstein, for his guidance, support, continuous interest and constructive criticism throughout the course of this research and during the writing of this thesis.

I would also like to thank my wife, Connie, for her love and understanding. She has sacrificed so much and provided the most support to me, while taking good care of our lovely baby, Janet.

Contents

List of Figures

List of Tables

CHAPTER 1

INTRODUCTION

1.1 General

Large diameter drilled shaft foundations are often used to transfer heavy structural loads through weak overburden soil to more competent underlying bedrock. The diameter of a shaft usually varies from 0.5 m to 6.0 m and the depth may exceed 70 m, depending on the required capacity and available equipment. In the United States, the typical diameter of the shaft ranges from 0.6 m to 1.8 m, the depth ranges from 7.0 m to 30 m, and the strength of the shaft concrete ranges from 20 MPa to 45 MPa (Baker 1994). Drilled shaft foundations have the following major advantages:

1. High load capacity and relatively low cost.
2. Simple length adjustment in the field.
3. Low noise and vibration during construction.

4. Quick and easy excavation. In areas with deep soft soil underlain by rock, drilled shafts are the most efficient deep foundation system.

Because of the above advantages, drilled shaft foundations have become an appropriate and economical foundation system for heavily loaded structures.

Drilled shafts are sometimes called bored piles, drilled piers, caissons, or cast-in-place concrete piles. When drilled in rock, the portion of the shaft drilled into rock is referred to as a rock socket. As in other deep foundations, the rock socket derives its load capacity from two components (Figure 1.1):

1) shearing resistance at the shaft-rock interface around the vertical cylindrical surface of the socket, and

2) end bearing resistance at the base of the shaft.

In addition to the basic geomaterial strength and deformation characteristics, other factors such as the degree of roughness of the interface between the concrete and the rock mass play important roles in the behavior of rock sockets (Kodikara et al. 1992; Hassan and O'Neill 1997).

During the past two decades, great advances have been made in understanding the behavior of drilled shaft foundations. Numerous studies have been carried out to investigate the influence of various factors on the design, construction and performance

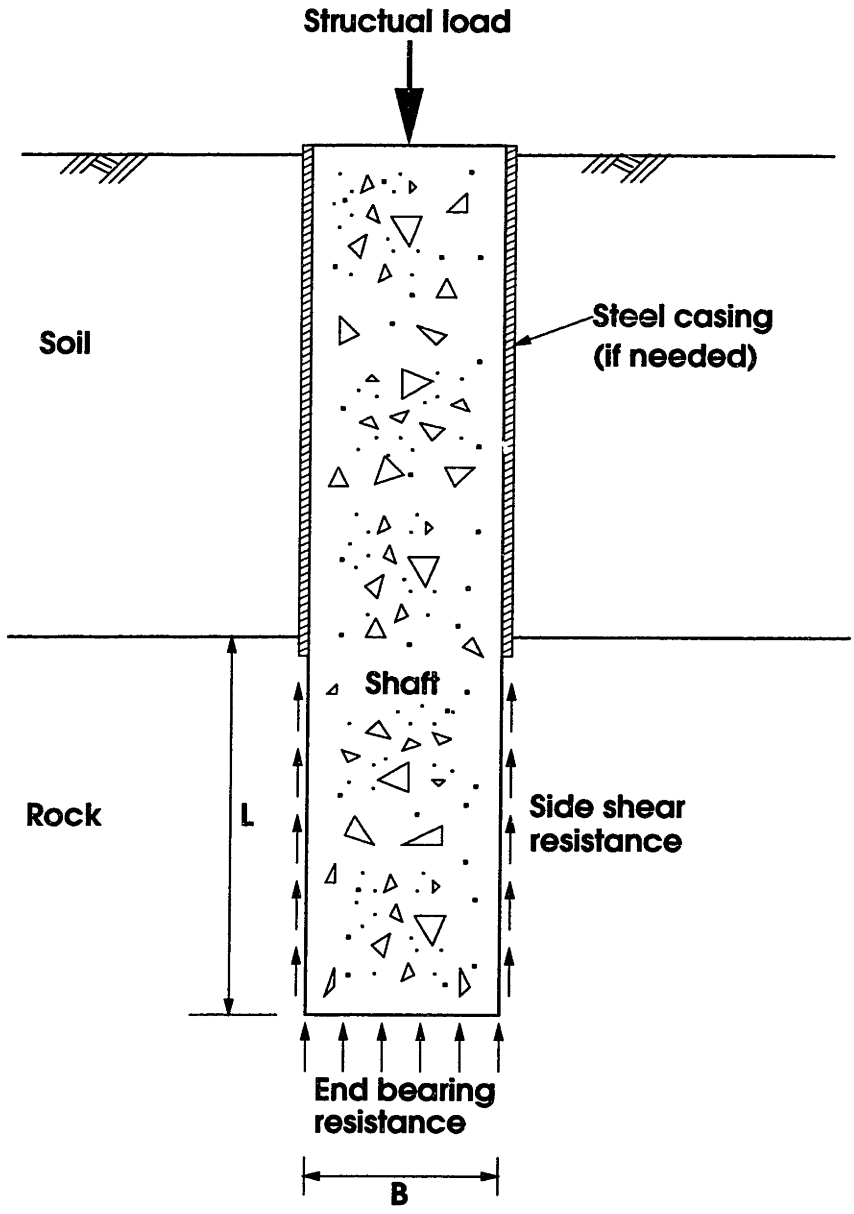

Figure 1.1 A drilled shaft sockted into rock.

of drilled shafts. These investigations have focused on the following three methods:

1. *Load tests on full scale instrumented drilled shafts.* This method is considered the most reliable and dependable technique to determine the bearing capacity and develop new design methods.

2. *Laboratory model tests.* Tests are conducted in a laboratory using reduced scale drilled shaft models as well as idealized soil/rock profiles and load conditions to study the load transfer mechanisms and stress/strain variation behavior of drilled shaft foundations.

3. *Numerical analysis.* This is a useful method to study the general behavior of drilled shaft foundations under different loading and subgrade conditions and perform parametric studies for design applications.

The full scale load test is believed to be the most useful and dependable method to determine the bearing capacity of drilled shaft foundations, and it can yield useful information on load transfer mechanisms. However, field load tests are very expensive and very often tests have to be terminated well before failure as the actual ultimate loads are significantly higher than the anticipated values. In recent years, centrifuge testing has been used as an alternative to study the behavior of rock socketed shafts as a small applied load in a scaled model subjected to high g-level in the centrifuge is equivalent to

a much higher prototype applied load (e.g., Leung and Ko 1993; Dykeman and Valsangkar 1996).

Rational design methods for drilled shafts socketed into rock require determination of both the ultimate load capacity and the expected displacement at the working load. To determine the ultimate load capacity, it is necessary to predict both the ultimate side shear resistance and the end bearing resistance. Based on field load tests, several researchers have proposed relations between rock properties and the ultimate side shear resistance. However, these relations give a wide range of values, which makes it difficult for a designer to choose an appropriate one. As for the end bearing resistance, although some empirical relations are available, they do not give reasonable values in most cases. This may be the reason why current design methods consider the end bearing resistance very crudely. The load-displacement response is usually predicted using charts developed from finite element solutions. Available finite element solutions just model the rock mass as a single half space or, at best, as a two-layer medium (i.e., the rock adjacent to and beneath the socketed shaft). In practice, however, the rock mass is often multi-layered and distinct differences in material properties exist from layer to layer. To reasonably consider the multi-layer nature of rock mass, new solutions need to be developed.

Because of the limitations discussed above, new design methods need to be developed. The new design methods should not only reasonably predict the ultimate side shear resistance and the end bearing resistance, but also consider the multi-layered nature of rock mass.

1.2 Scope and Objectives of Research

The research reported in this thesis is concerned with analysis and design of drilled shafts socketed into rock. The scope of investigations concentrates on the following:

1. Behavior of drilled shafts socketed into rock and subjected to axial compressive loading, i.e., the ultimate load capacity and the displacement at working load.
2. Short-term loading conditions, i.e., no creep effect.

The objectives of this research are the following:

1. To derive a reasonable relation between rock properties and the ultimate side shear resistance of rock-socketed shafts by comparing the available relations.
2. To derive a reasonable relation between rock properties and the end bearing resistance of rock-socketed shafts by developing and analyzing a database of field load tests which include data on end bearing resistance.
3. To develop a model to predict the displacement of rock-socketed shafts at working load. The model has to reasonably consider the multi-layered nature of rock mass.

4. To use the above results to develop a simple design method for rock-socketed shafts.

1.3 Organization

This introduction is followed by Chapter 2 which is a literature review. In the literature review, the mechanism of load transfer of drilled shafts socketed into rock is discussed. Special attention is paid to the methods for estimating the ultimate side shear resistance and the end bearing resistance. The theoretical solutions for estimating load-displacement response are also reviewed.

Chapter 3 presents a general description of an approximate design model for axially loaded drilled shafts socketed into rock. It includes the determination of the ultimate load capacity and the displacement at working load.

In Chapter 4, the methods for estimating the ultimate side shear resistance and the end bearing resistance of drilled shafts socketed into rock are recommended. The relation for predicting the ultimate side shear resistance is derived by analyzing the available relations. A database of 35 loading tests is developed to investigate the end bearing capacity of drilled shafts in rock. Based on this database, a new relation is developed to predict the end bearing capacity of drilled shafts from unconfined compressive strength. Hoek-Brown strength criterion is used to theoretically analyze the end bearing resistance of rock sockets. The results show that the agreement between the new relation and the theoretical solution is reasonable.

Chapter 5 presents the development of a new model to predict the settlement of drilled shafts at working load. Closed-form solutions are derived for a drilled shaft in a three-layer medium. The validation of the proposed model is demonstrated by comparing its results with available theoretical solutions.

Chapter 6 summarizes the recommended design method for axially loaded drilled shafts socketed into rock. Two design examples including three test shafts are provided as a means of verifying and illustrating the use of the design method.

Chapter 7 provides summary, conclusions and recommendations for further research.

CHAPTER 2

LITERATURE REVIEW

2.1 General

Rational design methods for drilled shafts socketed into rock require determination of both the ultimate load capacity and the expected displacement at working load. In most of the current design methods, the ultimate side shear resistance and the end bearing resistance are predicted using empirical relations derived from field load tests. The load-displacement response is predicted using rules developed from finite element solutions or analytical solutions. In the following, a literature review regarding axially loaded drilled shafts socketed into rock is presented. The review concentrates on the following issues:

1) Load transfer mechanism of drilled shafts socketed into rock.

2) Available methods for estimating the ultimate side shear resistance and the end bearing resistance.

3) Available theoretical solutions for predicting load-displacement response of drilled shafts.

4) Current design methods for axially loaded drilled shafts socketed into rock.

2.2 Mechanism of Load Transfer

Axially loaded drilled shafts socketed into rock are designed to transfer structural loads in one of the following three ways (CGS 1992):

1. Through side shear only;
2. Through end bearing only;
3. Through the combination of both side shear and end bearing.

Situations where support is provided solely by side shear resistance are those where the base of the drilled hole cannot be cleaned so that it is uncertain if any end bearing resistance will be developed. Alternatively, where sound bedrock underlies low strength overburden material, it may be possible to achieve the required support in end bearing only, and assume that no side shear support is developed in the overburden. However, where the shaft is drilled some depth into sound rock, a combination of side shear resistance and end bearing resistance can be assumed (Kulhawy and Goodman 1980).

The relative magnitude of the support developed in the side shear and end bearing depends on the following factors:

1. The moduli of the materials in which the shaft is socketed and that of the shaft itself.

2. The magnitude of loading in relation to the ultimate side shear resistance.

3. The method of construction.

The mechanism of load transfer and displacement of a socketed shaft, and the distribution of support between the side shear and end bearing are illustrated in Figure 2.1. In this model all the side shear resistance is replaced by a spring with stiffness k_s, and all the end bearing is replaced with a second spring of stiffness k_b. The support provided in side shear Q_s and end bearing Q_b are each equal to the product of the spring stiffness and the displacement, i.e., $Q_s = k_s w_s$ and $Q_b = k_b w_b$ (Winterkorn and Fang 1975).

In the first case, much of the support is developed in the upper part of the shaft, that is, the side shear resistance per unit displacement is greater than the end bearing resistance developed for the same displacement. Thus the spring constant k_s is greater than the spring constant at the base, k_b (i.e., $k_s > k_b$). The displacement of the shaft is a combination of elastic shortening of the shaft and the displacement of the base. Because most of the displacement occurs in the upper part of the shaft, that is, w_s is greater than w_b (i.e., $w_s > w_b$), the portion of support developed in side shear is much greater than that developed in end bearing (i.e., $Q_s >> Q_b$).

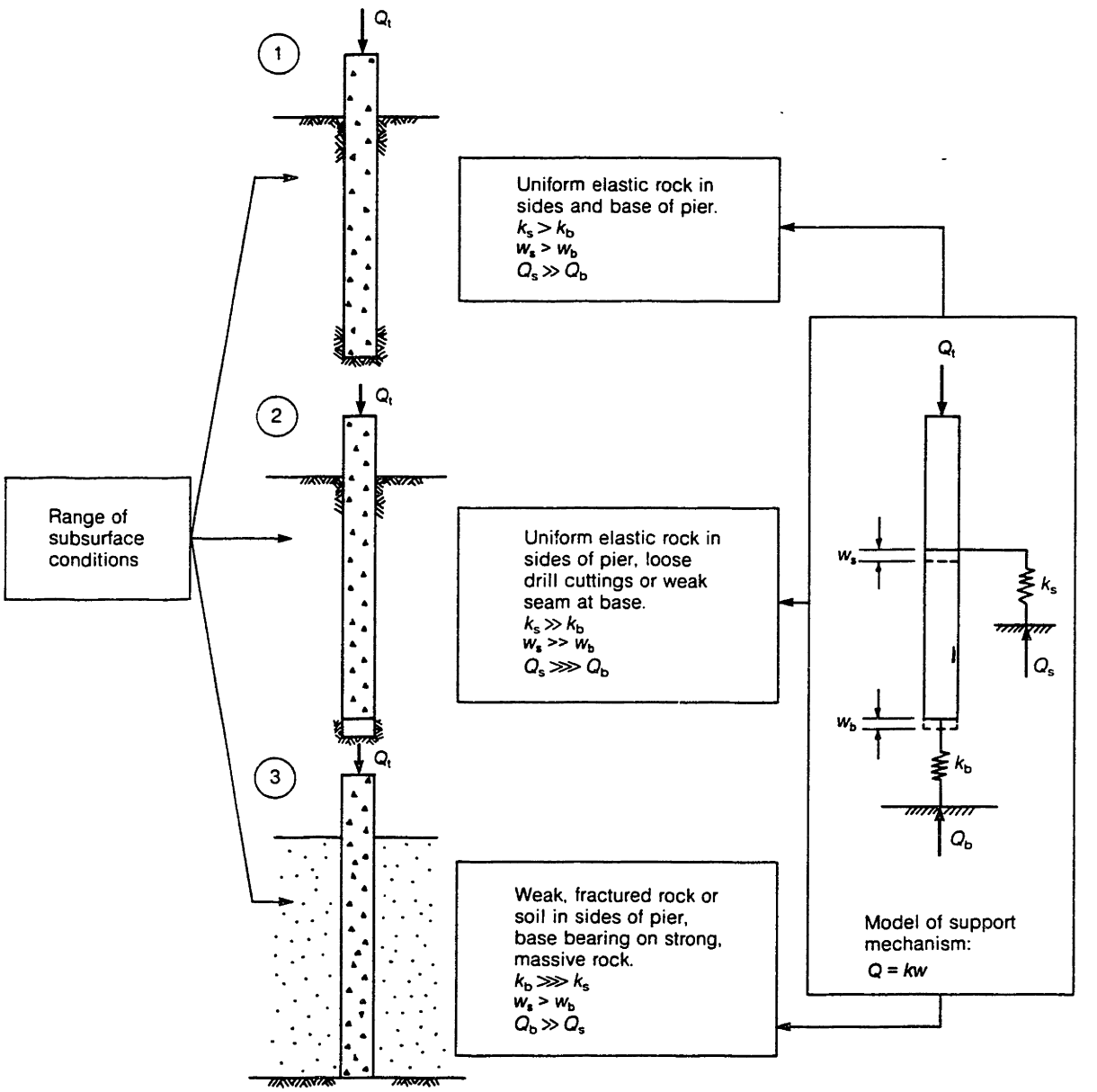

k_s = stiffness of a spring represent the side shear resistance;
k_b = stiffness of a spring represent the end bearing resistance;
w_s = displacement of the shaft side; w_b = displacement of the shaft base;
Q_s = total side shear resistance; Q_b = total end bearing resistance.

Figure 2.1 Simplified load transfer mechanism for socketed shafts (Winterkorn and Fang 1975)

In the second case, material with very low bearing capacity occurs at the base of the shaft (e.g., side shear sockets) such that the spring constant k_b is much smaller than the spring constant k_s (i.e., $k_s >> k_b$). Provided that the applied load does not exceed the ultimate side shear resistance, most of the displacement will occur in the upper part of the shaft (i.e., $w_s >> w_b$) and the major portion of the load will be carried in side shear (i.e., $Q_s >>> Q_b$).

In the third case, the shaft has been drilled through material with a low modulus to end bearing on a much higher modulus material, so the spring constant k_b is much greater than the spring constant k_s (i.e., $k_b >>> k_s$). However, much of the displacement will occur due to elastic shortening of the shaft, and a relatively small amount due to displacement of the high modulus material below the base of the shaft (i.e., $w_s > w_b$). Under these conditions, most of the load is carried in end bearing (i.e., $Q_b >> Q_s$).

2.3 Axial Bearing Capacity

As stated above, when designing a drilled shaft socketed into rock, it is necessary to determine both the ultimate side shear resistance and the end bearing resistance. The ultimate side shear resistance and the end bearing resistance are usually predicted using empirical relations derived from field load tests. There are two basic types of field load tests: tension or pull-out tests which measure only side shear resistance, and compression tests which measure either side shear resistance, end bearing resistance, or both simultaneously.

Tension tests can be used to measure side shear resistance directly. In compression test programs, the test drilled shafts are instrumented (e.g., strain gages and load cells) in order to determine both the load carried in side shear, Q_s, and the load carried in end bearing, Q_b. Alternatively, end bearing may be eliminated by creating a gap beneath the base of the shafts or by using a collapsible base. Such drilled shafts are referred to as side shear shafts, and the portions socketed into rock are termed side shear sockets. Similarly, side shear resistance may be eliminated to produce an end bearing socket. When a test is conducted to failure, under such conditions, it is possible to determine the ultimate unit side shear resistance, τ_{max}, and the maximum unit end bearing resistance, q_{max}, as follows:

$$\tau_{max} = \frac{Q_s}{A_s} \tag{2.1a}$$

$$q_{max} = \frac{Q_b}{A_b} \tag{2.1b}$$

where

$A_s = \pi\ LB$ is the perimeter area of the shaft;

$A_b = \pi\ B^2/4$ is the base area of the shaft;

L is the socket length and

B is the socket diameter.

The ultimate side shear resistance τ_{max} and the end bearing resistance q_{max} are usually correlated to the unconfined compressive strength of the rock, σ_c. For example, τ_{max} is often related to σ_c by the adhesion factor, α,

$$\alpha = \frac{\tau_{max}}{\sigma_c} \tag{2.2}$$

2.3.1 Ultimate Side Shear Resistance

Up until approximately the mid 1970's, prediction of the ultimate side shear resistance of rock sockets was based on crude extrapolation from empirical relations that were originally developed from drilled shafts in clay (Johnston 1992). The adhesion factor of drilled shafts in clay is known to decrease as the clay shear strength increases as suggested, for example, by Tomlinson (1971). As a result, very low adhesion factors were commonly assigned to stronger geomaterials such as rock. Field testing research programs conducted in various parts of the world (e.g., Rosenberg and Journeaux 1976; Horvath 1978 and Williams 1980) showed, however, that the adhesion factors for rock sockets could be significantly higher than those of drilled shafts in clay. They generally agreed that high adhesion factors in rock sockets are due to the interface roughness. Because of the high adhesion factors in rock sockets, a series of new relations for rock

sockets was developed. Some of the more commonly used relations are reviewed in the following.

(a) Empirical relations for ultimate side shear resistance

Using the format of Eq. (2.2), many relations between the ultimate side shear resistance and the unconfined compressive strength have been suggested, based on field test data. Three of them are listed below:

Reynolds and Kaderabek (1980): $\tau_{max} = 0.3\sigma_c$ (2.3)

Gupton and Logan (1984): $\tau_{max} = 0.2\sigma_c$ (2.4)

Reese and O'Neill (1987): $\tau_{max} = 0.15\sigma_c$ (2.5)

In the above relations, the ultimate side shear resistance is just a simple constant times σ_c. Based on field test results, many power-curve relationships were also developed, some of which will be presented in the following.

Rosenberg and Journeaux (1976) suggest the following relation between the ultimate side shear resistance and the unconfined compressive strength

$$\tau_{max} = 0.375(\sigma_c)^{0.515} \quad (2.6)$$

where τ_{max} and σ_c are in MPa.

Meigh and Wolshi (1979) propose the following relation:

$$\tau_{max} = 0.22(\sigma_c)^{0.6} \tag{2.7}$$

where τ_{max} and σ_c are in MPa.

Based on analysis of 202 data points from laboratory and field load tests, Horvath (1982) suggests the following relation:

$$\tau_{max} = 0.2 \text{ to } 0.3(\sigma_c)^{0.5} \tag{2.8}$$

where τ_{max} and σ_c are in MPa.

The roughness of the socket wall is an important factor controlling the development of side shear resistance. Depending on the type of drilling technique and the hardness of the rock, a drilled socket will have a certain degree of roughness. Research has shown that the benefits gained from increasing the roughness of a socket wall can be quite significant, both in terms of peak and residual shear capacity. Studies by Williams et al. (1980) and others have shown that smooth-sided sockets exhibit a brittle type of failure, while sockets having an adequate roughness exhibit ductile failure. Williams and Pells (1981) suggest that rough sockets generate a locked-in normal stress such that there is practically no distinguishing difference between residual and peak side resistance.

As a result of these observations, classifications have been developed so that roughness can be quantified. One such classification proposed by Pells et al. (1980) is based on the size and frequency of grooves in a socket wall (Table 2.1). Based on this classification, Rowe and Armitage (1987b) have proposed the following relation for sockets with different roughness:

$$\tau_{max} = 0.45(\sigma_c)^{0.5} \quad \text{for sockets with roughness R1, R2 or R3} \qquad (2.9a)$$

$$\tau_{max} = 0.6(\sigma_c)^{0.5} \quad \text{for sockets with roughness R4} \qquad (2.9b)$$

where τ_{max} and σ_c are in MPa.

Horvath et al. (1980) also developed a relation from model socket behavior using various roughness profiles. They found that as socket profiles go from smooth to rough, the roughness factor increases significantly, as does the peak side shear resistance. These findings were confirmed in a later study by Horvath et al. (1983), and the following equation was proposed for the roughness factor (*RF*):

$$RF = \frac{h_m L_t}{RL} \qquad (2.10)$$

where

h_m is the average height of grooves in the socket (see Figure 2.2);

L_t is the total travel length along the socket wall profile (see Figure 2.2);

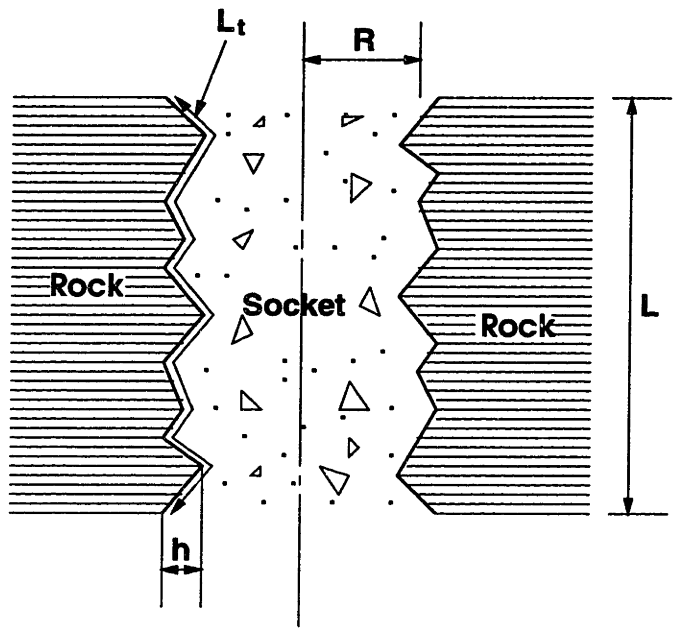

h_m = average of groove heights;
L_t = total travel length along the socket wall profile;
R = norminal radius of the socket;
L = norminal length of the socket.

Figure 2.2 Parameters for defining roughness factor RF

Table 2.1. Roughness classes after Pells et al. (1980)

Roughness Class	Description
R1	Straight, smooth-sided socket, grooves or indentation less than 1.00 mm deep
R2	Grooves of depth 1-4 mm, width greater than 2 mm, at spacing 50 to 200 mm.
R3	Grooves of depth 4-10 mm, width greater than 5 mm, at spacing 50 to 200 mm.
R4	Grooves or undulations of depth greater than 10 mm, width greater than 10 mm, at spacing 50 to 200 mm.

R is the nominal radius of the socket; and

L is the nominal length of the socket.

Using Eq. (2.10), the following relation was developed between the ultimate side shear resistance and RF:

$$\tau_{max} = 0.8\sigma_c(RF)^{0.45} \tag{2.11}$$

Williams et al. (1980) and Williams and Pells (1981) propose a design method that considers both the ultimate load capacity and settlement criteria for rock sockets. For ultimate side shear resistance, a data base of 71 load tests on shafts in mudstones, shales, and sandstones, conducted mostly in Australia, is analyzed and the following relation is developed:

$$\tau_{max} = \alpha_w \beta_w \sigma_c \tag{2.12}$$

where α_w is a reduction factor reflecting the strength of the rock, as shown in Figure 2.3; and β_w is the ratio of side resistance of jointed rock mass to side resistance of intact rock (which will be discussed in detail in next section). When the rock mass is such that the joints are tightly closed and seams are infrequent, β_w is essentially equal to 1.0. Comparing Eq. (2.12) with Eq. (2.2), it can be found that $\alpha_w\beta_w$ is just the adhesion factor, α. Since α_w is derived from field test data, the effect of joints is already included in α_w. If α_w is multiplied by β_w which is obtained from laboratory tests (Williams et al. 1980), the effect of joints will be considered twice. So Eq. (2.12) is not appropriate.

Kodikara et al. (1992) develop a rational model for predicting the relationship of τ_{max} to σ_c based on a specific definition of interface roughness, initial normal stress on the interface and the stiffness of the rock during interface dilation. Figure 2.4 shows the various parameters needed to define interface roughness in that model, which is confirmed through constant normal stiffness interface shearing tests of reconstituted

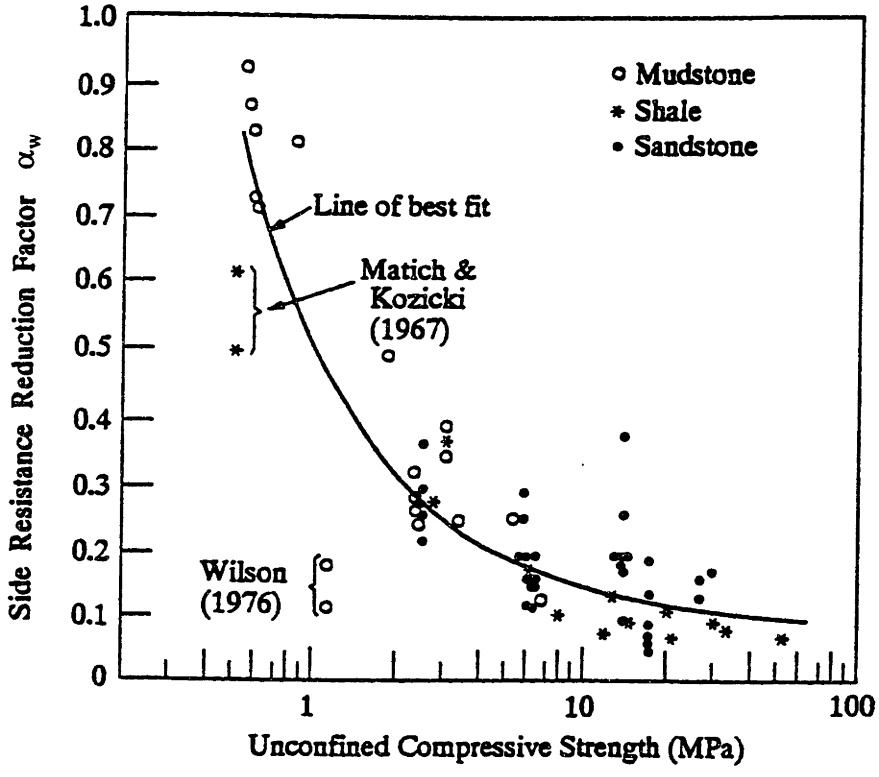

Figure 2.3 Side resistance reduction factor for rock sockets (after Williams and Pells 1981)

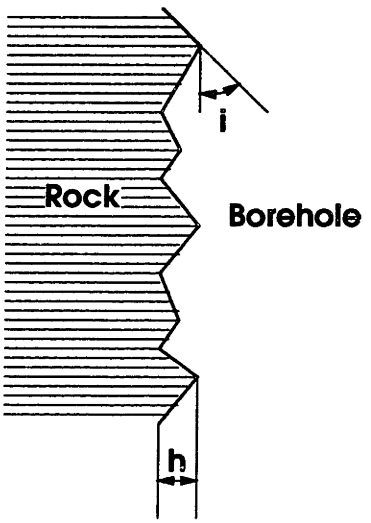

i_m = mean asperity angle;
i_{sd} = standard deviation of asperity angles;
h_m = mean asperity height;
h_{sd} = standard deviation of asperity heights.

Figure 2.4 Borehole roughness (after Kodikara et al. 1992)

Table 2.2. Definition of borehole roughness and range of parameters for Melbourne Mudstone (after Kodikara et al. 1992)

Parameter	Range of values for sockets in Melbourne Mudstone		
	Smooth	Medium	Rough
i_m (degrees)	10-12	12-17	17-30
i_{sd} (degrees)	2-4	4-6	6-8
h_m (mm)	1-4	4-20	20-80
h_{sd}/h_m	0.35		
B (m)	0.5 - 2.0		
σ_c (MPa)	0.5 - 10.0		
σ_n (MPa)	50 - 500		
E_m (MPa)	50 - 500		

Melbourne Mudstone (Johnston and Lam 1989). It accounts for variability in asperity height and angularity, assuming clean, triangular interface joints. Figure 2.5 shows the predicted adhesion factor, α, for Melbourne Mudstone with the range of parameters and roughness as given in Table 2.2. The adhesion factor, α, is presented as a function of E_m/σ_c, σ_c/σ_n and the degree of roughness, where E_m is the elastic modulus of the rock mass and σ_n is the initial normal stress on the shaft-rock interface. It can be seen that the

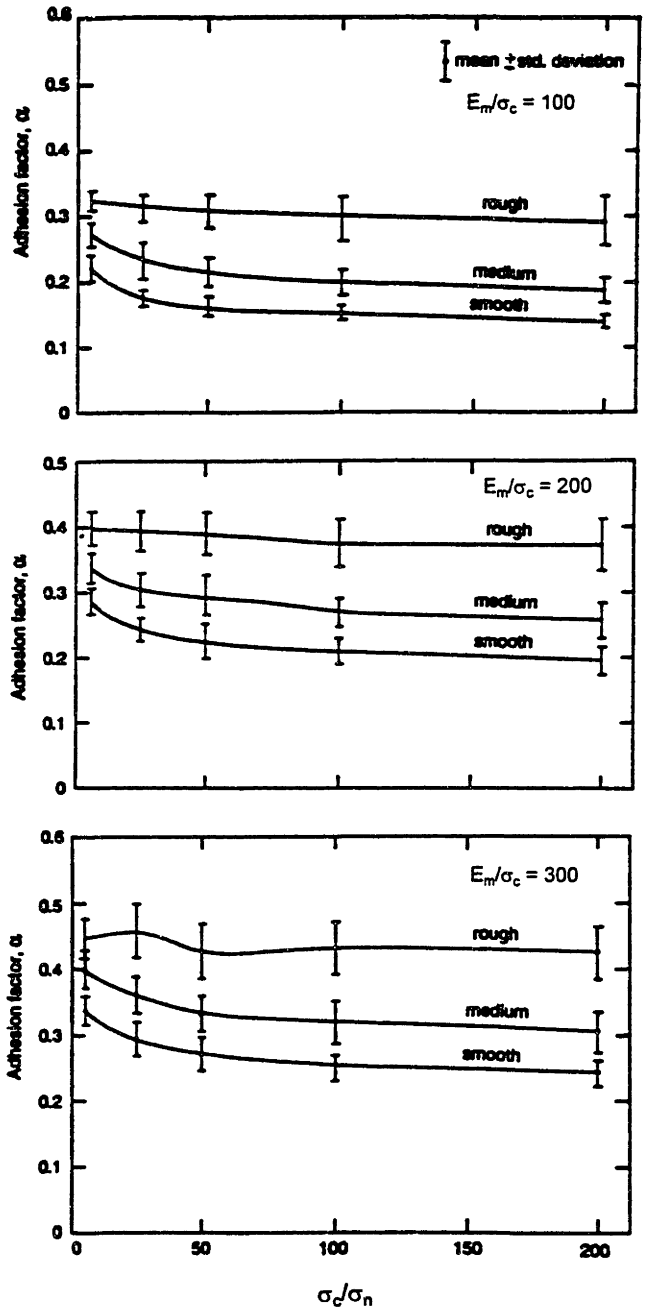

Figure 2.5 Simplified design charts for adhesion factor for Melbourne Mudstone (after Kodikara et al. 1992)

adhesion factor is affected not only by degree of the interface roughness, but also by E_m/σ_c and σ_c/σ_n.

Kulhawy and Phoon (1993) develop a relatively extensive load test data base for drilled shafts in soil and rock and present their data both for individual shaft load tests and as site-averaged data. The results are shown in Figures 2.6 and 2.7, in terms of adhesion factor, α, vs. normalized shear strength, $\sigma_c/2p_a$, where p_a is atmospheric pressure (= 0.1MPa). Understandably, the results of individual load tests show considerably greater scatter than the site-averaged data. On the basis of the site-averaged data, Kulhawy and Phoon (1993) propose the following relations for drilled shafts socketed into rock:

Mean Behavior: $$\alpha = 2.0[\sigma_c / 2p_a]^{-0.5} \quad (2.13a)$$

Upper bound (very rough): $$\alpha = 2.0[\sigma_c / 2p_a]^{-0.5} \quad (2.13b)$$

Lower bound: $$\alpha = 2.0[\sigma_c / 2p_a]^{-0.5} \quad (2.13c)$$

Eq. (2.13) can be rewritten in a general form as

$$\alpha = \Psi[\sigma_c / 2p_a]^{-0.5} \quad (2.14)$$

This leads to a general expression for ultimate side shear resistance

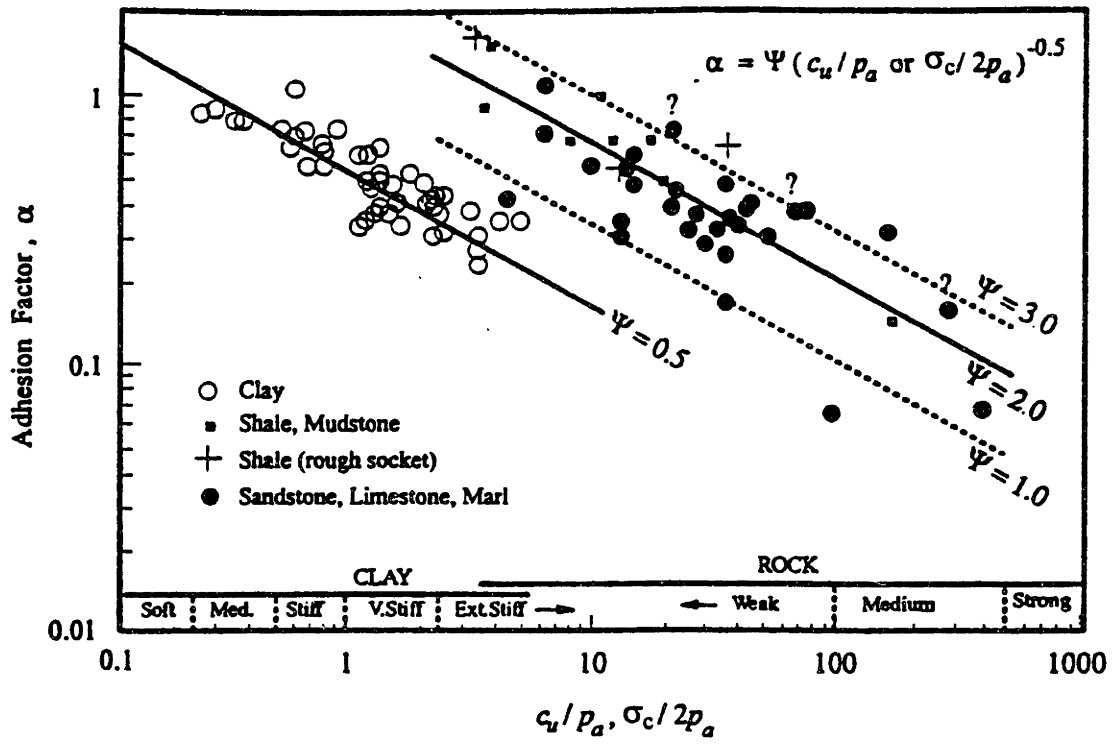

Figure 2.6 Adhesion factor vs. normalized shear strength for site-averaged data (after Kulhawy and Phoon 1993)

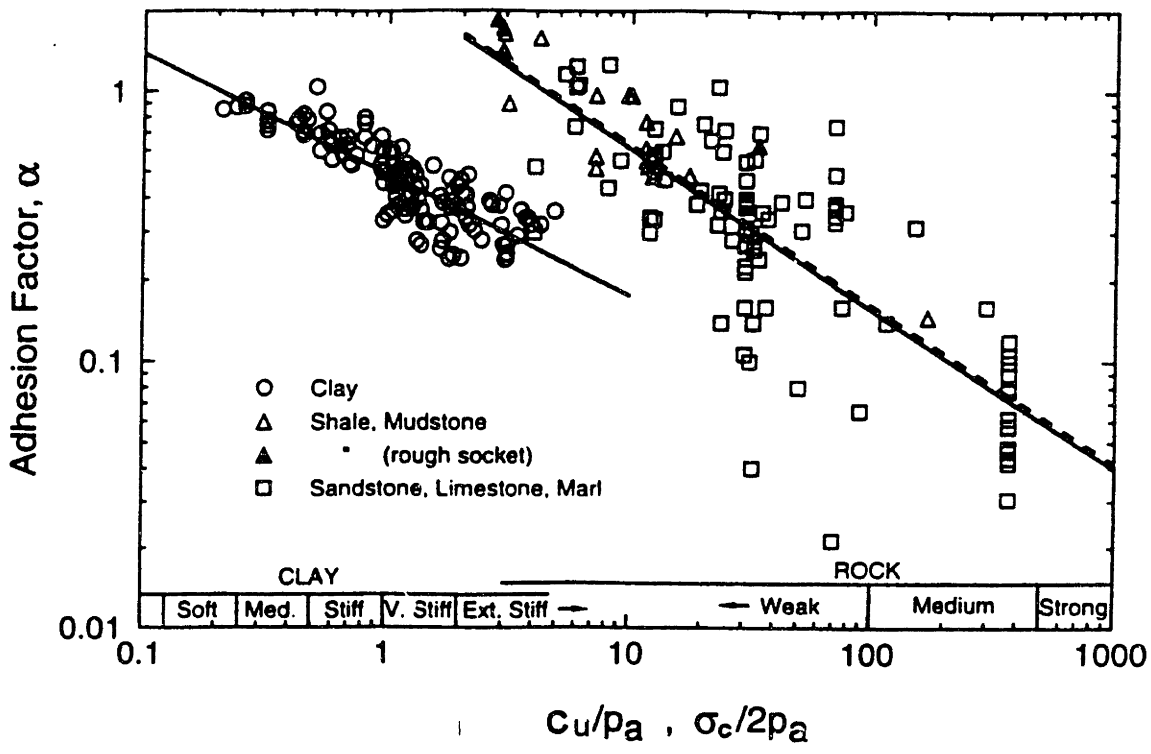

Figure 2.7 Adhesion factor vs. normalized shear strength for individual test data (after Kulhawy and Phoon 1993)

$$\tau_{max} = \Psi[2 p_a \sigma_c]^{0.5} \qquad (2.15)$$

It is very important to note that the empirical relationships given in Eqs. (2.13b) and (2.13c) are bounds to site-averaged data, and do not necessarily represent bounds to individual shaft behavior. The coefficient of determination (r^2) is approximately 0.71 for the averaged data, but is only 0.46 for the individual data, reflecting the much greater variability of the individual test results.

(b) Factors affecting the ultimate side shear resistance

As stated above, the roughness of the socket wall, which is an important factor controlling the development of side shear resistance, has been studied extensively. Other factors such as the joints in the rock mass and the socket geometry have also been studied by some researchers. Williams et al. (1980) suggest that the existence of joints in the rock mass reduces the side shear resistance by reducing the normal stiffness of the rock mass. They develop an empirical relation between the side shear resistance of the jointed rock and the modulus reduction factor, j, as shown in Figure 2.8, in which

$$\beta_w = f(j), \quad j = E_m / E_i \qquad (2.16)$$

where

E_m is the elastic modulus of the rock mass;

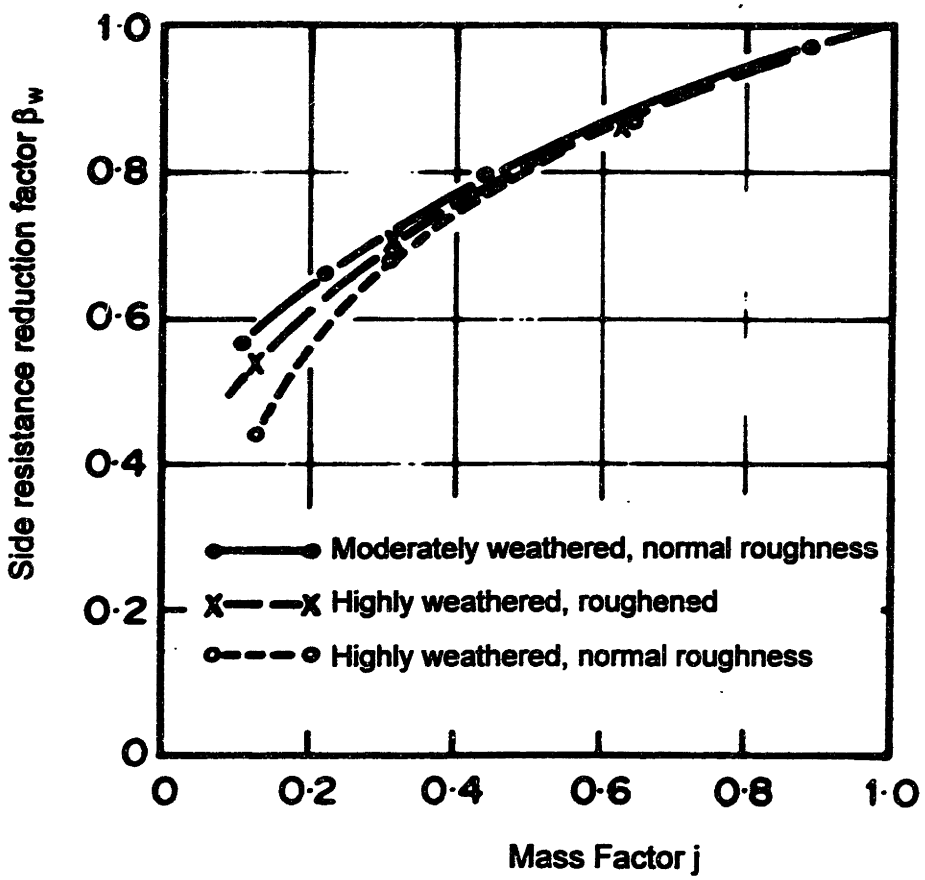

Figure 2.8 Side resistance reduction factor reflecting variation of mass factor (after Williams et al. 1980)

E_i is the elastic modulus of the intact rock;

β_w is the side shear resistance reduction factor as in Eq. (2.12).

Pabon and Nelson (1993) study the effect of soft horizontal seams on the behavior of laboratory model sockets. The study includes four instrumented model sockets in manufactured rock, three of which have soft seams. They conclude that a soft seam significantly reduces the normal interface stresses generated in the rock layer overlying it. Consequently the side shear resistance of rock sockets with soft seams is much lower than that of the intact rock socket.

The effect of socket geometry on side shear resistance is studied by Williams and Pells (1981). They test 15 rock sockets in Melbourne Mudstone, with diameters ranging from 335 mm to 1580 mm, and 27 rock sockets in Hawkesbury Sandstone, with diameters ranging from 64 mm to 710 mm. The results of these tests indicate that the socket length, L, does not have a discernible effect on side shear resistance. They argue that the interface dilation creates a locked-in normal stress with the result that the shear displacement behavior exhibits virtually no peak or residual behavior. They also report that the socket diameter has a negligible effect on side shear resistance. On the other hand, tests by Horvath et al. (1983) indicate that the unit side shear resistance decreases as the sock diameter increases. Williams and Pells (1981) explain this phenomenon by referring to the theory of expansion of infinite cylindrical cavity, which suggests that cylinders with smaller diameters develop higher normal stresses for a given absolute

value of dilation. However, they offer no physical explanation why the socket diameter does not affect their own test results.

2.3.2 End Bearing Resistance

The optimum design of drilled shafts should consider both side shear resistance and end bearing resistance. Unlike the ultimate side shear resistance, numerous theories have been proposed for estimating the end bearing resistance. According to Pells and Turner (1980), the theoretical approaches fall into three categories:

1) Methods which assume rock failure to be plastic.

2) Methods which idealize the zone of failure beneath the base in a form which allows either the brittleness strength ratio or the brittleness modulus ratio to be taken into account (Ladanyi 1966; Davis and Booker 1974).

3) Methods based on limiting the maximum stress beneath the loaded area to a value less than required to initiate fracture.

There is a significant variation in the predicted end bearing resistance from different theories. For example, the predicted bearing resistance of rock with an internal friction angle $\phi = 35°$ ranges from $8\sigma_c$ to $25\,\sigma_c$ depending on which theory is used. Because of the wide variation of theoretical results, empirical and semi-empirical

relations have been developed. Since they are more commonly used than theoretical results, the empirical and semi-empirical relations will be discussed in the following.

Similar to ultimate side shear resistance, many researchers have attempted to correlate end bearing resistance, q_{max}, to the unconfined compressive strength of rock. Some of the suggested relations are as follows:

Coates (1967): $$q_{max} = 3\sigma_c \quad (2.17)$$

Teng (1962): $$q_{max} = (5-8)\sigma_c \quad (2.18)$$

Rowe and Armitage (1987b): $$q_{max} = 2.7\sigma_c \quad (2.19)$$

The bearing capacity of foundations on rock is largely dependent on the strength of the rock mass. Discontinuities can have a significant influence on the strength of the rock mass depending on their orientation and the nature of material within discontinuities (Pells and Turner 1980). As a result, relations have been developed to account for the size and frequency of discontinuities within a rock mass. The Canadian Foundation Engineering Manual (CGS 1992) proposes that the ultimate bearing pressure be calculated using the following equation:

$$q_{max} = 3\sigma_c K_{sp} D \quad (2.20)$$

where

$K_{sp} = [3 + s / B][10(1 + 300g / s)^{0.5}]$ is an empirical factor;

s is the spacing of the discontinuities;

B is the socket width or diameter;

g is the aperture of the discontinuities;

$D = 1 + 0.4(L/B) \leq 3.4$ is the depth factor;

L is the socket length.

It is recommended in the Canadian Foundation Engineering Manual that the above formula for K_{sp} is valid for s/B ratios between 0.05 to 2.0 and for values of g between 0 and 0.02 m.

Kulhawy and Goodman (1980) present an approach that accounts for the presence of discontinuities using either the discontinuity spacing or the rock quality designation (RQD). The authors present the following relationship originally proposed by Bishnoi (1968):

$$q_{max} = JcN_{cr} \tag{2.21}$$

where

J is a correction factor depending on joint spacing (see Figure 2.9);

c is cohesion; and

N_{cr} is a modified bearing capacity factor, which is a function of the friction angle ϕ and discontinuity spacing (see Figure 2.10).

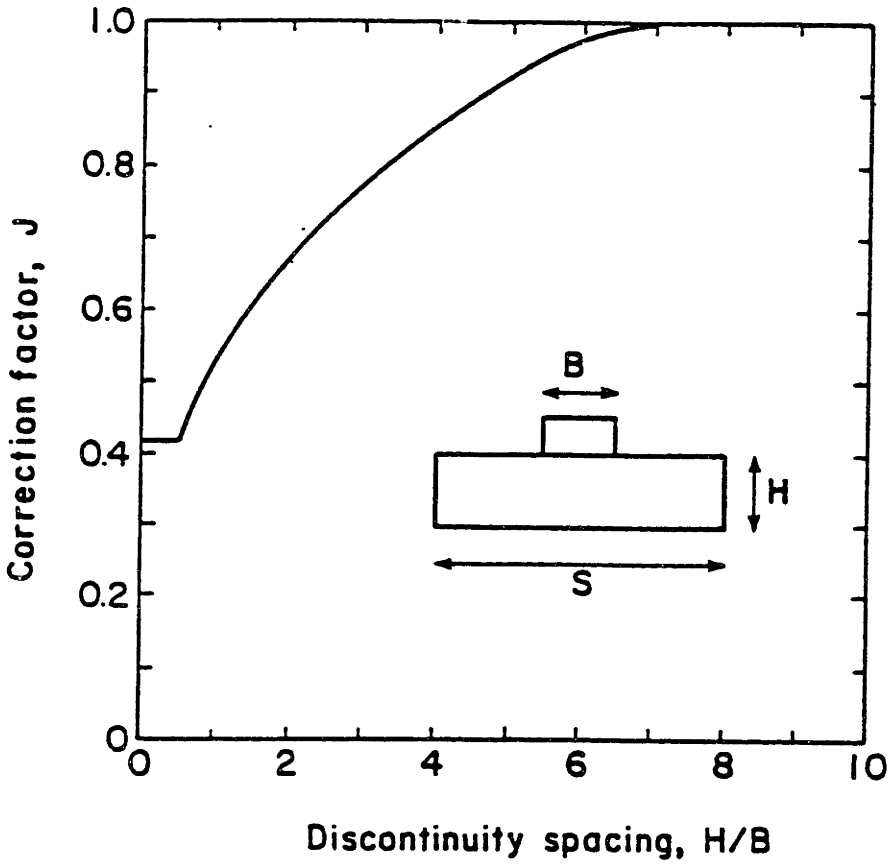

Figure 2.9 Correction factor for discontinuity spacing (after Kulhawy and Goodman 1980)

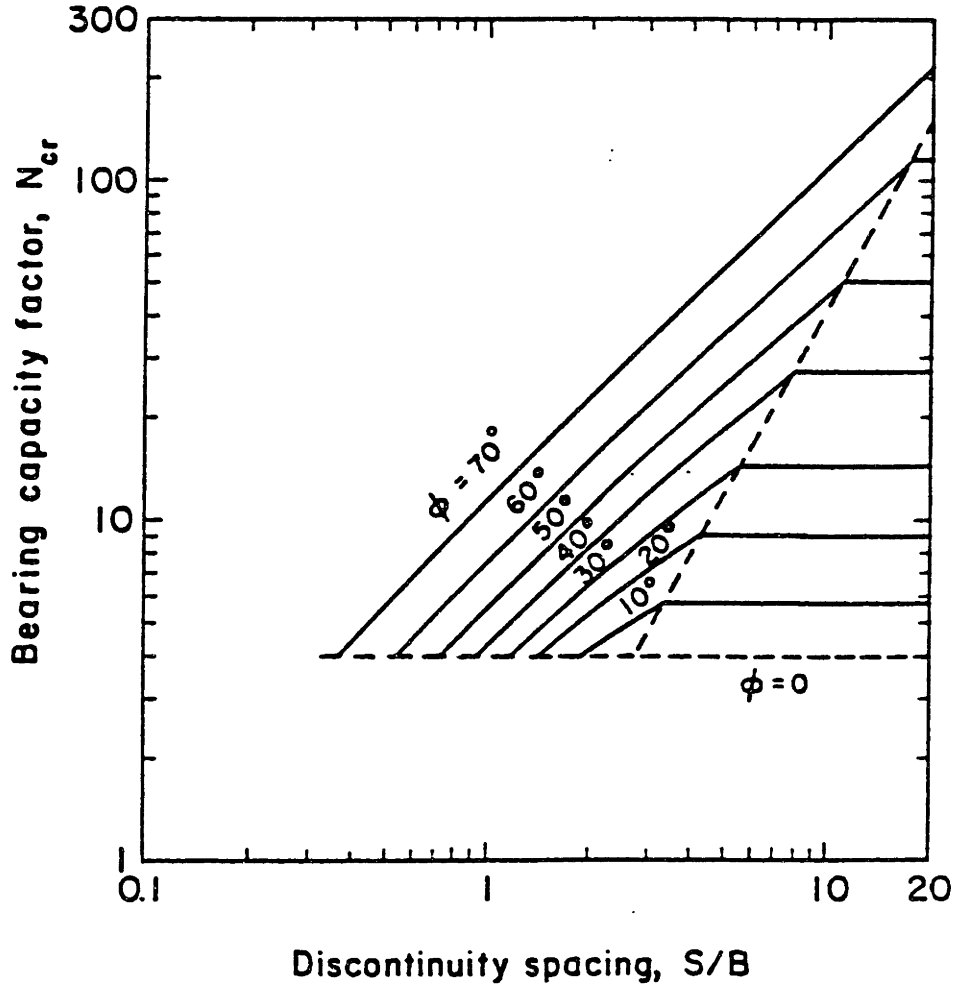

Figure 2.10 Bearing capacity factor for open joints (after Kulhawy and Goodman 1980)

Correction factor of J considers the effect of horizontal joints. The variation of J with the discontinuity spacing is shown in Figure 2.9, where H is the spacing of horizontal joints. For the value of N_{cr} the authors consider the joints being either open or closed. According to Goodman (1980), the presence of open joints would allow failure to occur by splitting (Because the joints are open, there is no confining pressure and failure is likely to occur by uniaxial compression of the rock columns) and this mode of failure needs to be included in the calculation of the end bearing resistance. Several charts are given by Kulhawy and Goodman (1980), following the method of Bishnoi (1968), to determine N_{cr} for both open and closed joints. Figure 2.10 shows N_{cr} for open joints. Design charts are also presented by the same authors to reduce values of Young's modulus, compressive strength, and cohesion due to presence of discontinuities.

2.4 Axial Load-Displacement Behavior of Drilled Shafts

2.4.1 General Load-Displacement Behavior of Drilled Shafts

The general load-displacement curve for a drilled shaft under axial loading is as shown in Figure 2.11 (Kulhawy 1991). The whole curve can be described in three stages:

1. As load is first applied to the head of the shaft, a small amount of displacement occurs which induces the mobilization of side shear resistance from head to base. During this initial period, the shaft behaves essentially in a linear manner, and the displacement

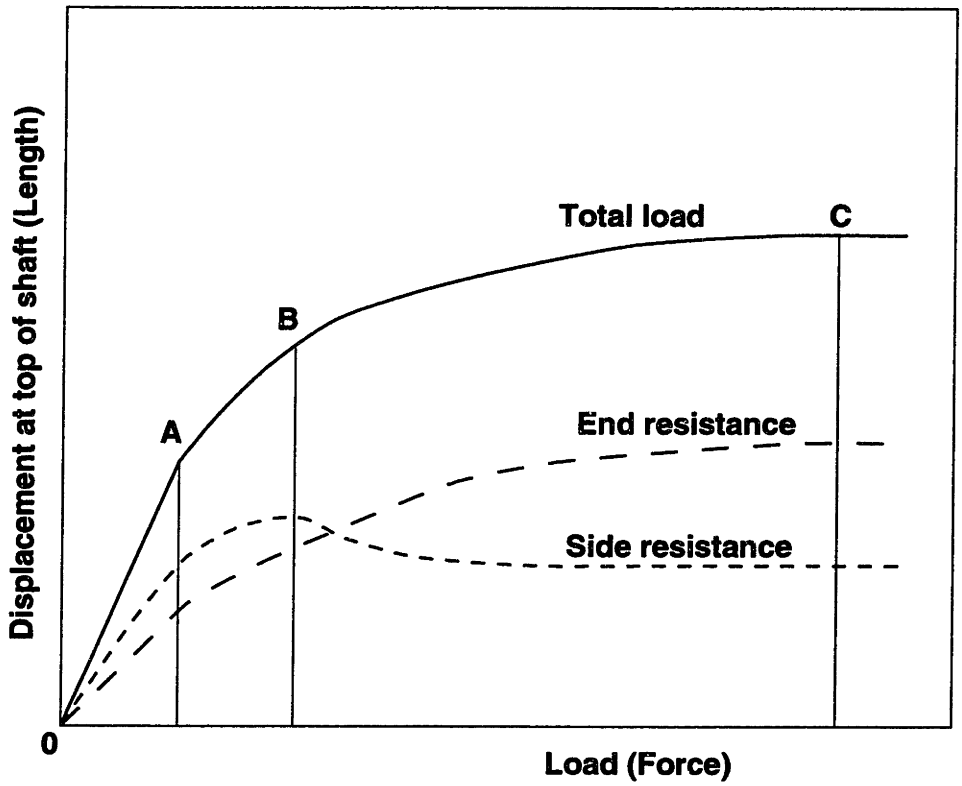

Figure 2.11 Generalized load-displacement for drilled shafts under compressive loading (after Kulhawy 1991)

can be computed accurately using the theory of elasticity. This linear behavior is illustrated in Figure 2.11 as the line OA. The side shear along the shaft is smaller than the ultimate side shear resistance (see Figure 2.12a).

2. As load is increased to point A in Figure 2.11, the shear stress at some point along the interface will reach the ultimate side shear resistance (see Figure 2.12b), and the shaft-rock 'bound' will begin to rupture and relative displacement (slip) will occur between the shaft and the surrounding rock. As the loading is increased further (beyond point A), this process will continue along the shaft, more of the shaft will slip, and a greater proportion of the applied load will be transferred to the end of the shaft. If loading is continued, eventually the side shear everywhere will reach the ultimate side shear resistance (see Figure 2.12c) and the entire shaft will slip (point B).

3. Beyond point B, a greater proportion of the total axial load will be transmitted directly to the end. When both side shear resistance and end bearing resistance are fully mobilized (point C), any increase of load may produce significant displacement. This indicates that the ultimate bearing capacity of the drilled shaft has been reached.

2.4.2 Theoretical Analysis of Load-Displacement Behavior of Drilled Shafts

Predicting the load-displacement response of drilled shafts is in some cases as important as, or possibly more critical than, predicting the ultimate bearing capacity. Many theoretical methods have been proposed for calculating the displacement of drilled shafts socketed into rock. Mattes and Poulos (1969) are among the first to investigate the

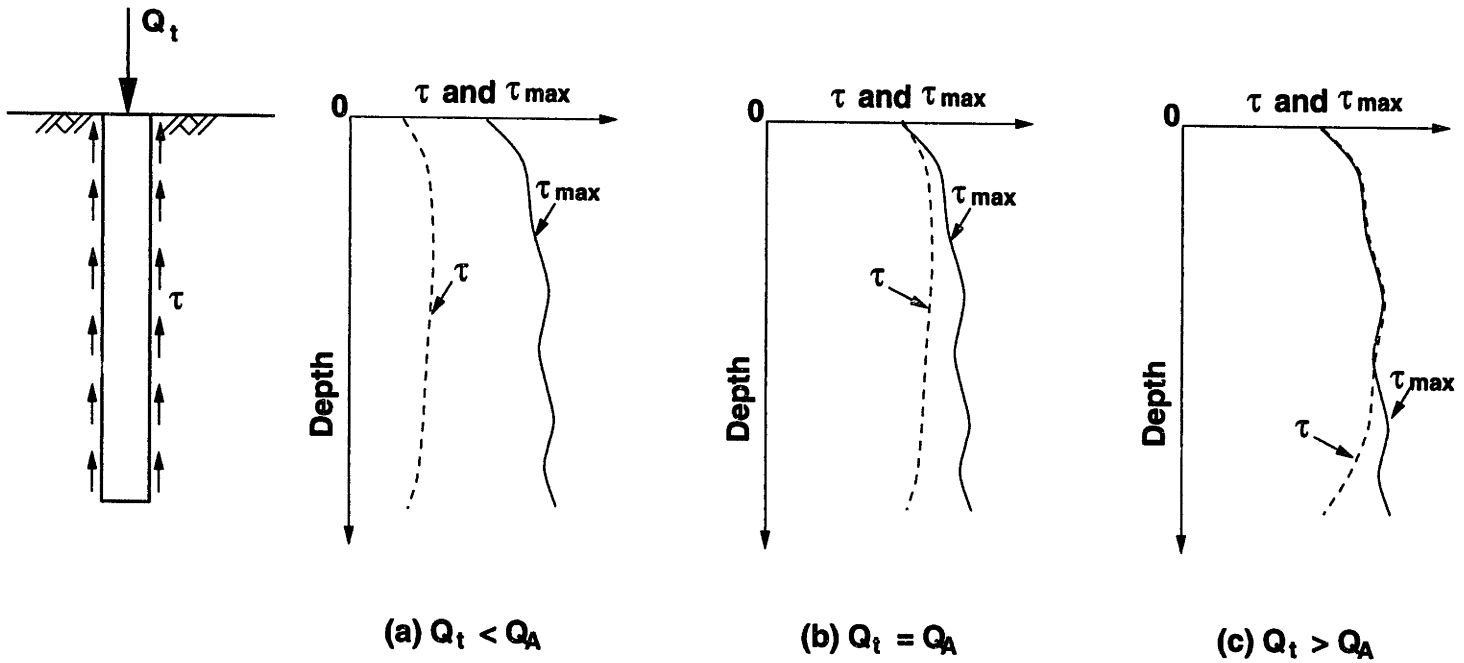

τ = shear stress along the shaft-rock interface;
τ_{max} = ultimate side side shear resistance;
Q_A = the applied load corresponding to point A in Figure 2.11.

Figure 2.12 Shear stresses at different values of applied load.

load-displacement behavior of rock-socketed shafts by integration of Mindlin's equations. Carter and Kulhawy (1988) provide a set of approximate analytical solutions to predict the load-displacement response of rock sockets by modifying the solutions of Randolph and Wroth (1978) for piles in soil. The majority of the theoretical solutions for predicting the displacement of drilled shafts socketed into rock, however, have been developed using finite element analyses (e.g., Osterberg and Gill 1973; Pells and Turner 1979; Donald et al. 1980; Rowe and Armitage 1987a). Most of the techniques proposed for the calculation of the vertical displacements of drilled shafts socketed into rock are based on the theory of elasticity. It has been usual to assume that the drilled shaft is essentially an elastic inclusion within the surrounding rock mass and that no slip occurs at the interface between the shaft and the rock mass, although the solutions of Rowe and Armitage (1987a) and Carter and Kulhawy (1988) can consider the possibility of slip. In the following, some of the more commonly used theoretical and numerical solutions are briefly reviewed.

(a) Finite element solutions considering no slip

Osterberg and Gill (1973) present an elastic finite element analysis for shafts socketed into strong rock. Pells and Turner (1979) extend this work to cover a more representative range of rock stiffness and socket geometry. Their analyses model the rock mass as a single half space and do not consider slip along the socket interface.

Donald et al. (1980) investigate the behavior of shafts socketed into Mohr-Coulomb rock. They assume full bound, i.e., no slip, along the shaft-rock interface. The

plastic analysis, however, is limited to a few separately analyzed cases and the general solution is presented only for elastic rock. Two layers of rock are considered in the analyses, i.e., the rock adjacent to and beneath the socketed shaft (see Figure 2.13).

The solutions from different researchers are quite similar. For simplicity, only the solutions of Pells and Turner (1979) are presented, as shown in Figure 2.14 (for a single half space, i.e., $E_r = E_b$ and $\nu_r = \nu_b$ in Figure 2.13), in which I_p is the nondimensional displacement influence factor defined by

$$I_p = \frac{E_r R w_t}{Q_t} \tag{2.22}$$

where

E_r is the Young's modulus of the rock mass;

R is the radius of the rock-socketed shaft ($R = B/2$);

Q_t is the applied load at the top of the rock-socketed shaft;

w_t is the displacement at the top of the rock-socketed shaft.

(b) Finite element solutions considering slip

Rowe and Armitage (1987) perform an elastic-plastic finite element analysis that accounts for slip along the interface according to the technique developed by Rowe and Pells (1980). Two layers of rock are considered in the analyses (see also Figure 2.13). The interface behavior is established in terms of the Coulomb failure criterion. The roughness

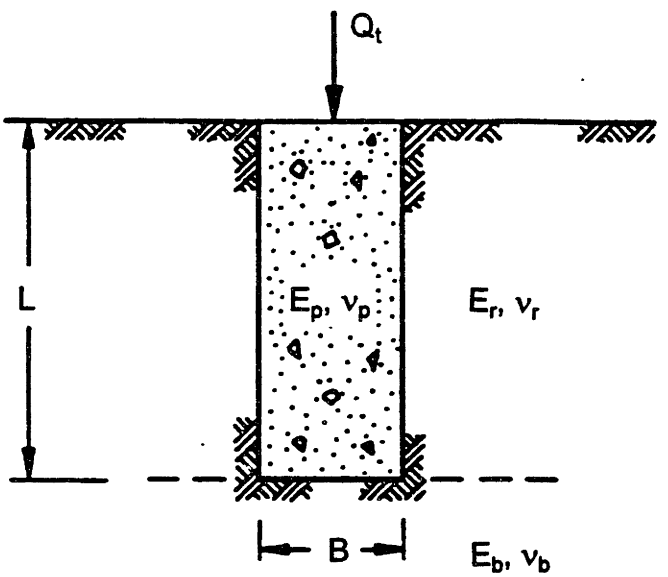

Figure 2.13 A socketed shaft in two layers of rock.

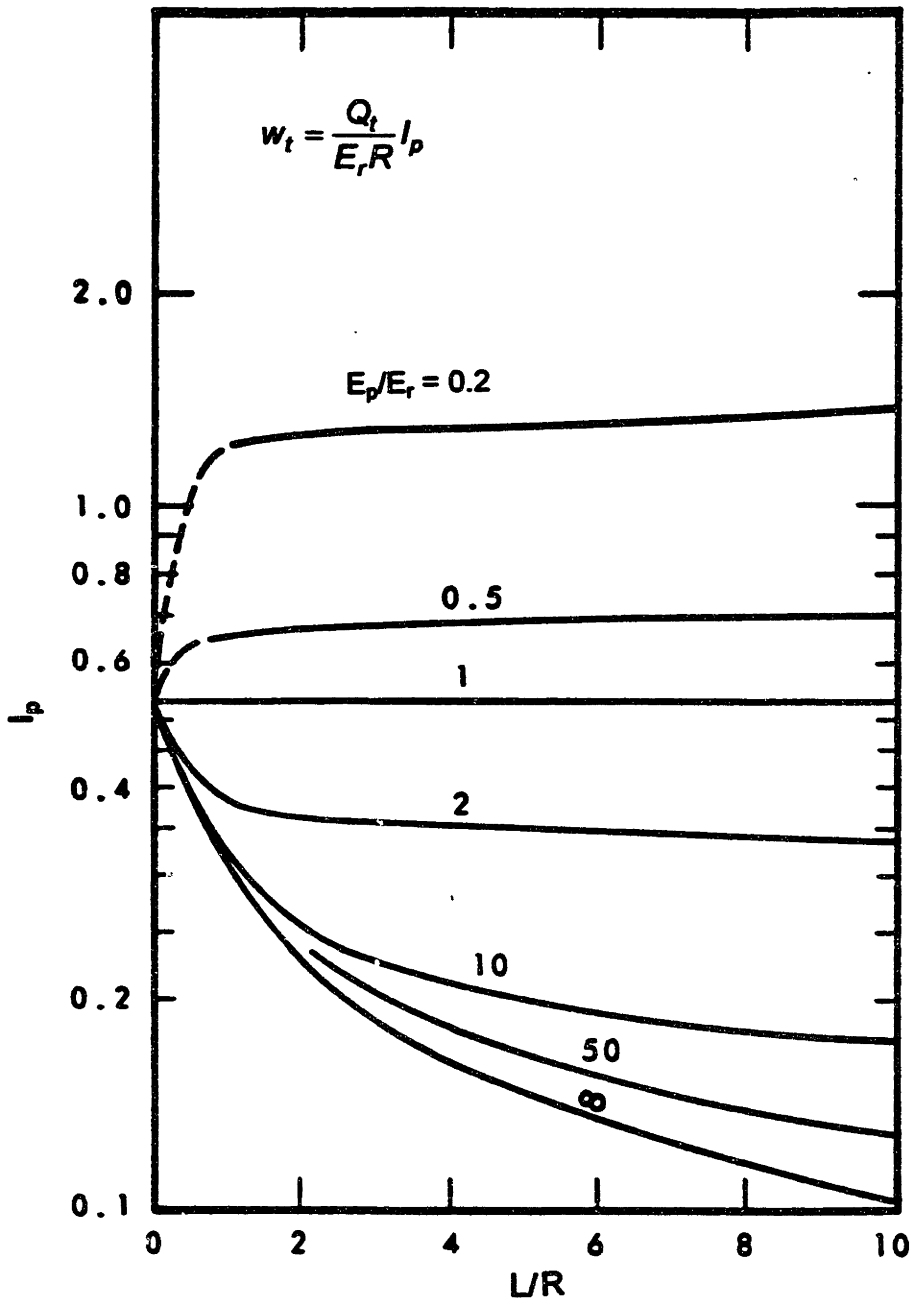

$I_p = E_r R w_t / Q_t$; R = shaft diameter; w_t = displacement at shaft head;
Q_t = total applied load at shaft head; L = length of the shaft;
E_r = Young's modulus of rock mass; E_p = Young's modulus of the shaft;

Figure 2.14 Elastic displacement of a socketed shaft (after Pells and Turner 1979)

of the interface is modeled implicitly through the use of an angle of interface dilatancy that produces additional normal stress on the interface as the shaft deflects vertically due to the applied load. The contribution of the interface dilatancy commences once slip occurs at the interface. The results of this study are presented in three sets of design charts respectively for E_b/E_r = 0.5, 1.0 and 2.0. Figure 2.15 shows the set for E_b/E_r = 2.0. Although the analysis is carried out considering the behavior of a cohesive-frictional-dilative interface, the design charts are developed only for nondilative-cohesive interfaces. These charts will be further discussed in Section 2.5.2. It should be noted that the nondimensional displacement influence factor, I, in Figure 2.15, is defined by

$$I = \frac{E_r B w_t}{Q_t} \tag{2.22a}$$

where

E_r is the Young's modulus of the rock mass adjacent to the shaft;

B is the diameter of the rock-socketed shaft;

Q_t is the applied load at the top of the rock-socketed shaft;

w_t is the displacement at the top of the rock-socketed shaft.

The value of I defined by Eq. (2.22a) is twice that of I_p determine by Eq. (2.22) for the same value of E_r, Q_t and w_t.

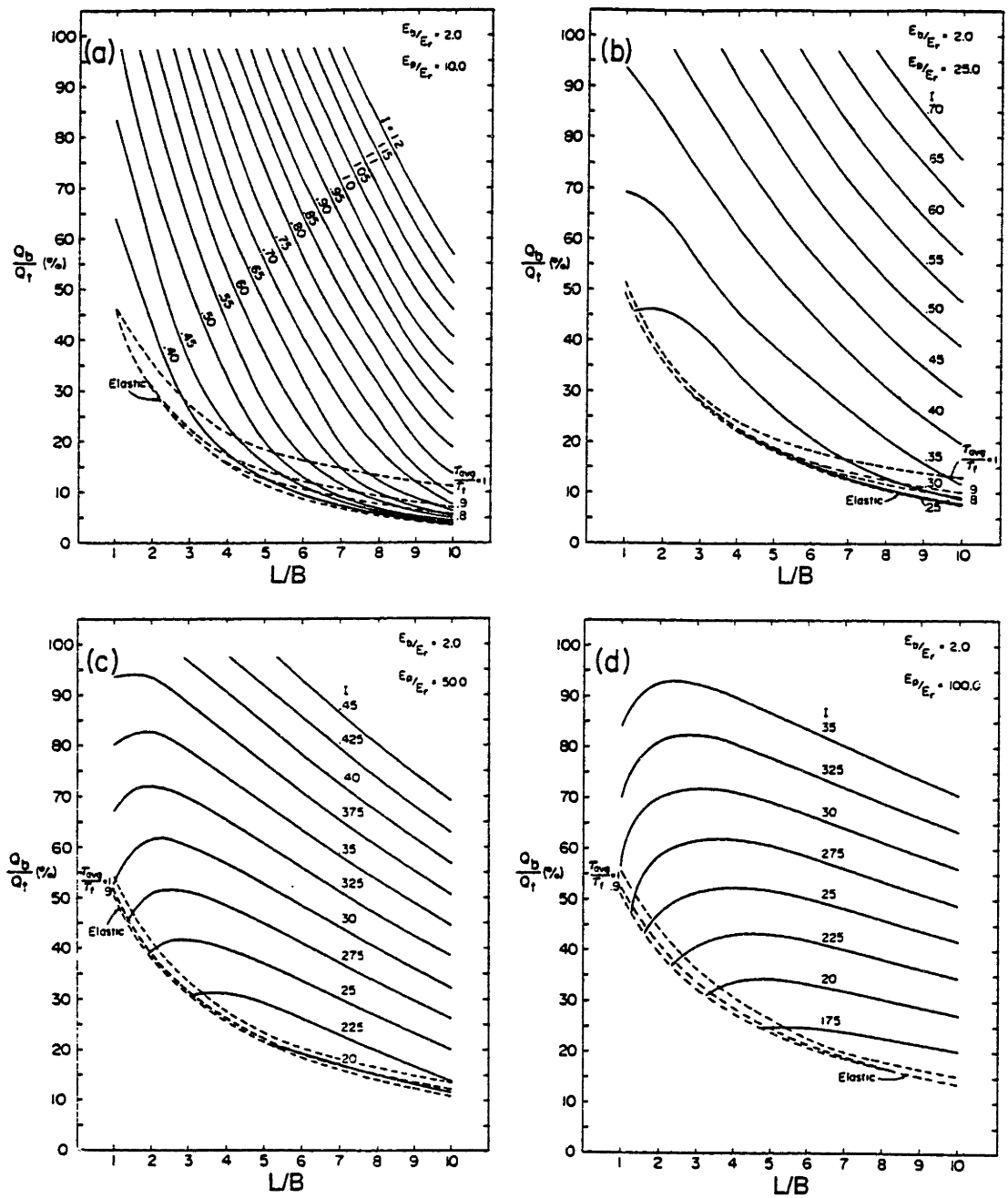

$I = E_r B w_t / Q_t$; B = shaft diameter; w_t = displacement at shaft head;
Q_t = total applied load at shaft head; Q_b = bearing load at shaft base;
E_r = Young's modulus of rock mass; E_p = Young's modulus of the shaft;
τ_{avg} = average side shear resistance; $\tau_f = \tau_{max}$ = ultimate side shear resistance.

Figure 2.15 Design charts for a socketed shaft (E_b/E_r = 2.0) (after Rowe and Armitage 1987a)

(c) Analytical solutions of Carter and Kulhawy (1988)

Carter and Kulhawy (1988) provide a set of approximate analytical solutions to predict the load-settlement response of rock sockets. Two layers of rock are considered in the solutions (see Figure 2.13). The solutions are for a shaft without slip or with full slip.

Solutions considering no slip

Under an applied axial load, the displacements in the rock mass are predominantly vertical, and the load is transferred from the shaft to the rock mass by vertical shear stresses acting on the cylindrical interface, with little change in vertical normal stress in the rock mass (except near the base of the shaft). The pattern of deformation around the shaft may be visualized as an infinite number of concentric cylinders sliding inside each other (Randolph and Wroth 1978) (see Figure 2.16). Randolph and Wroth (1978) have shown that, for this type of behavior, the displacement of the shaft w may be described adequately in terms of hyperbolic sine and cosine functions of depth z below the surface, as given below:

$$w(z) = A_1 \sinh(\mu z) + A_2 \cosh(\mu z) \tag{2.23}$$

in which, A_1 and A_2 are constants which can be determined from the boundary conditions of the problem. The constant μ is given by

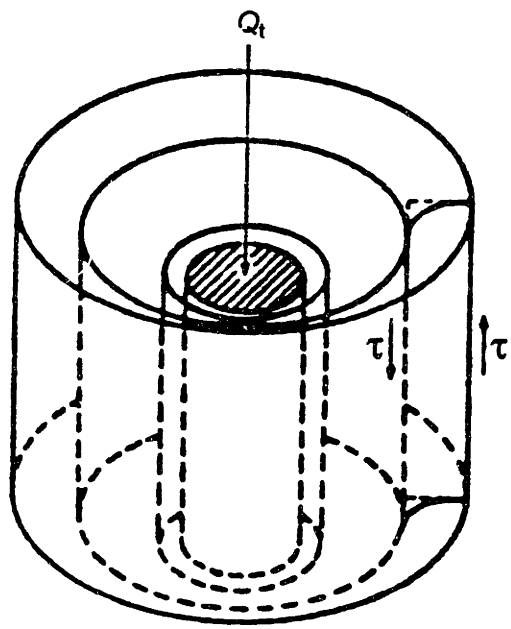

Figure 2.16 Mode of deformation around the shaft (after Randolph and Wroth 1978).

$$(\mu L)^2 = (\frac{2}{\varsigma\lambda})(\frac{L}{R})^2 \tag{2.24}$$

where

$\zeta = \ln[2.5(1 - \nu_r)L/R]$;

$R = B/2$ is the radius of the shaft;

$\lambda = E_p/G_r$;

$G_r = E_r/[2(1 + \nu_r)]$ is the elastic shear modulus of the rock mass surrounding the shaft;

E_p is the Young's modulus of the shaft;

E_r is the Young's modulus of the rock mass surrounding the shaft;

ν_r is the Poisson's ratio of the rock mass surrounding the shaft.

Using the standard solutions for the displacement of a rigid punch resting on an elastic half-space (Poulos and Davis 1974) as the boundary condition at the base of the shaft, the elastic settlement at the head of the shaft is given by (Randolph and Wroth 1978):

$$\frac{G_r R w_t}{Q_t} = \frac{1+\left(\frac{4}{1-\nu_b}\right)\left(\frac{1}{\pi\lambda\xi}\right)\left(\frac{L}{R}\right)\left(\frac{\tanh(\mu L)}{\mu L}\right)}{\left(\frac{4}{1-\nu_b}\right)\left(\frac{1}{\xi}\right)+\left(\frac{2\pi}{\varsigma}\right)\left(\frac{L}{R}\right)\left(\frac{\tanh(\mu L)}{\mu L}\right)} \tag{2.25}$$

where

$\xi = G_b/G_r$

$G_b = E_b/[2(1 + \nu_b)]$ is the elastic shear modulus of the rock mass below the shaft base.

E_b is the Young's modulus of the rock mass below the shaft base;

ν_b is the Poisson's ratio of the rock mass below the shaft base.

The solution given by Eq. (2.25) is plotted in Figure 2.17 for cases where $\nu_r = \nu_b = 0.25$ and $E_r = E_b$. Also plotted are finite element solutions by Pells and Turner (1979). The general agreement between the two solutions is reasonable.

Solutions considering full slip

The case of slip along the entire length of the shaft (beyond point B in Figure 2.11) also has been considered in detail by Carter and Kulhawy (1988). For this case, the shear strength of the interface is given by the Coulomb criterion:

$$\tau = c + \sigma_r \tan\phi \qquad (2.26)$$

where

c is the interface cohesion;

ϕ is the interface friction angle;

σ_r is the radial stress acting on the interface.

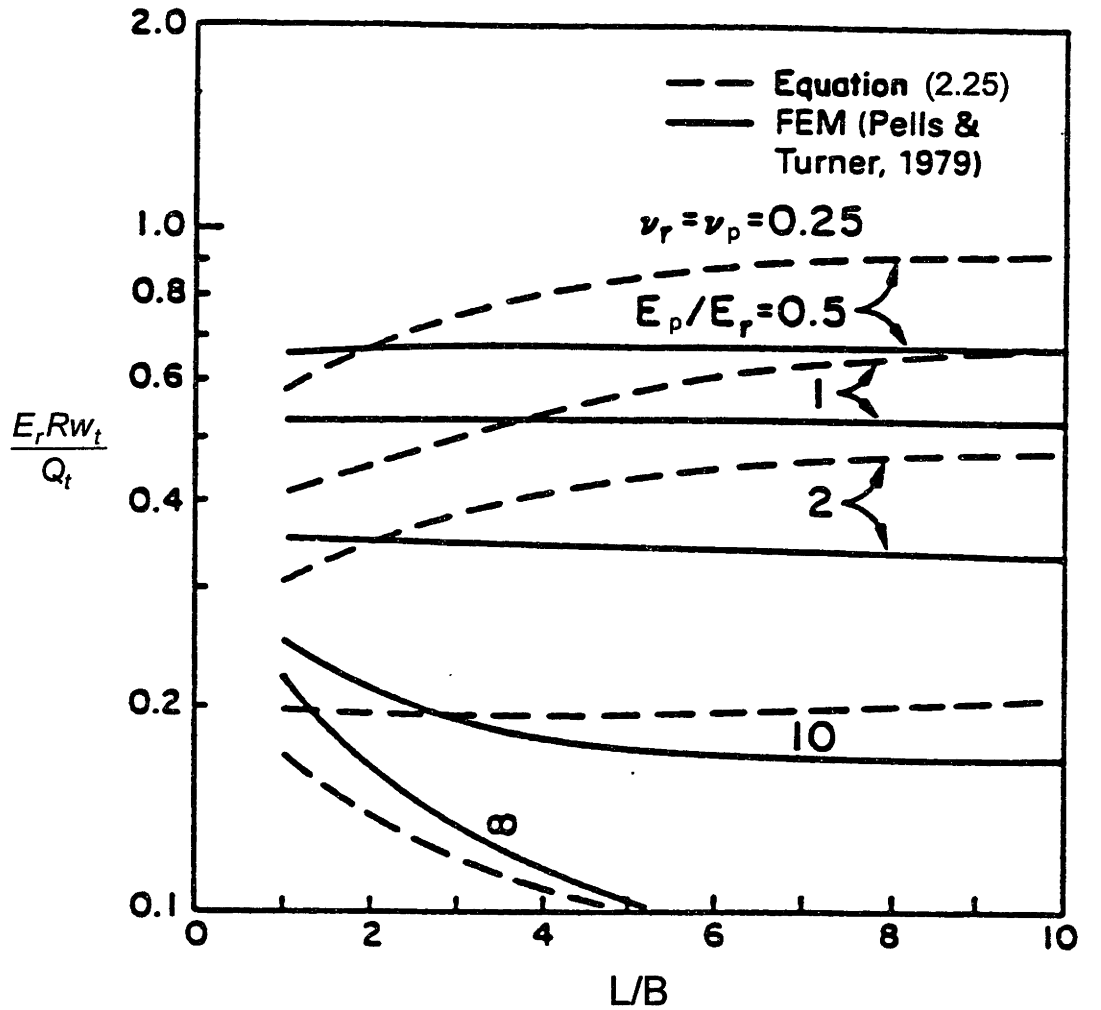

L = length of the shaft; R = shaft diameter; B = diameter of the shaft;
Q_t = total applied load at shaft head; w_t = displacement at shaft head;
E_r, ν_r = Young's modulus and Poisson's ratio of rock mass;
E_p, ν_p = Young's modulus and Poisson's ratio of the shaft.

Figure 2.17 Elastic displacement of a socketed shaft (after Carter and Kulhawy 1988)

As relative displacement (slip) occurs, the interface may dilate, and it is assumed that the displacement components follow the dilation law:

$$\frac{\Delta u}{\Delta w} = \tan \psi \tag{2.27}$$

where

Δu and Δw are the relative normal and shear displacements of the shaft-rock interface (see Figure 2.18);

ψ is the angle of dilation defined by Davis (1968).

To determine the radial displacements at the interface, the procedure suggested by Goodman (1980) and Kulhawy and Goodman (1987) is followed, in which conditions of plane strain are assumed, as an approximation, independently in the rock mass and in the slipping shaft. The rock mass is considered to be linear elastic, even after full slip has taken place, and the shaft is considered to be an elastic column, These assumptions, together with the dilatancy law, allow one to derive an expression for the variation of vertical stress in the compressible shaft. The distribution of the shear stress acting on the shaft then can be calculated from equilibrium conditions, and the vertical displacement can be determined as function of depth z by treating the shaft as a simple elastic column.

The 'full slip' solution for the displacement of the shaft head is derived as

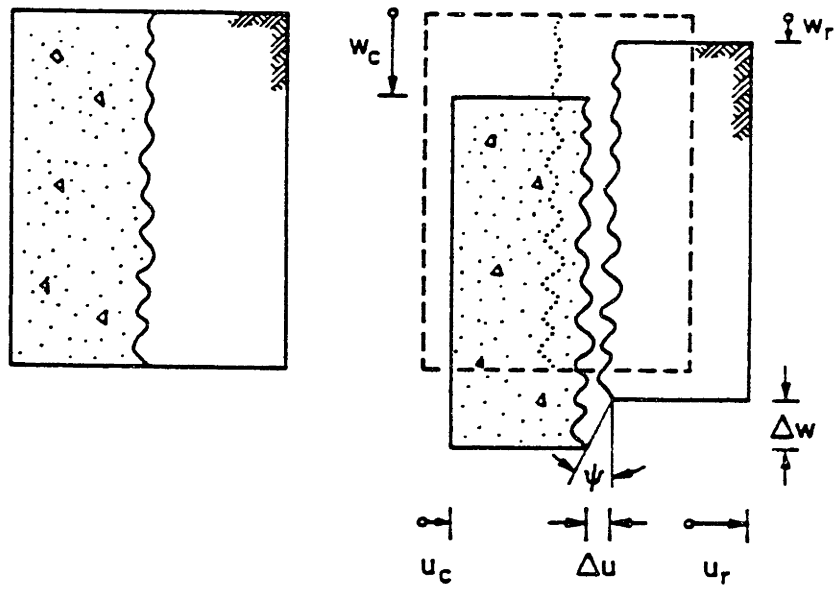

$$\frac{-\Delta u}{\Delta w} = \frac{u_c - u_r}{w_c - w_r} = -\tan\psi$$

u_c and w_c = radial and vertical displacement of the shaft;
u_r and w_r = radial and vertical displacement of rock mass;
ψ = angle of dialation.

Figure 2.18 Schematic illustration of dilatancy at the shaft-rock mass interface (after Carter and Kulhawy 1988)

$$w_t = F_3\left(\frac{Q_t}{\pi E_r B}\right) - F_4 B \tag{2.28}$$

in which

$$F_3 = a_1(\lambda_1 B C_3 - \lambda_2 B C_4) - 4a_3 \tag{2.29}$$

$$F_4 = \left[1 - a_1\left(\frac{\lambda_1 - \lambda_2}{D_4 - D_3}\right)B\right] a_2\left(\frac{c}{E_r}\right) \tag{2.30}$$

$$C_{3,4} = D_{3,4} / (D_4 - D_3) \tag{2.31}$$

$$D_{3,4} = [\pi(1 - \nu_b^2)\left(\frac{E_r}{E_b}\right) + 4a_3 + a_1\lambda_{2,1}]e^{\lambda_{2,1}L} \tag{2.32}$$

$$\lambda_{1,2} = \frac{-\beta \pm (\beta^2 + 4\alpha)^{1/2}}{2\alpha} \tag{2.33}$$

$$\alpha = a_1\left(\frac{E_p}{E_r}\right)\left(\frac{B^2}{4}\right) \tag{2.34}$$

$$\beta = a_3\left(\frac{E_p}{E_r}\right)B \tag{2.35}$$

$$a_1 = (1 + \nu_r)\varsigma + a_2 \tag{2.36}$$

$$a_2 = \left[(1 - \nu_p)\left(\frac{E_r}{E_p}\right) + (1 + \nu_r)\right]\left(\frac{1}{2\tan\phi\tan\psi}\right) \tag{2.37}$$

$$a_3 = \left(\frac{\nu_p}{2\tan\psi}\right)\left(\frac{E_r}{E_p}\right) \tag{2.38}$$

All other parameters in Eqs. (2.28) to (2.38) are as defined before. The adequacy of the closed-form expressions is demonstrated by comparing them with the finite element solution by Rowe and Armitage (1987a, b). The results are shown in Figure 2.19. The overall agreement between the closed-form solutions and the finite element results is good.

Comments

It must be noted that the closed-form solutions just consider "no slip" and "full slip" conditions. They cannot predict the load-displacement response between the occurrence of first slip and full slip of the shaft (i.e., curve AB in Figure 2.11). However, the finite element results indicate that the progression of slip along the socket takes place over a relatively small interval of displacement (Finite element predictions of first slip and full slip have been indicted in Figure 2.19). Therefore it seems reasonable, at least for most practical cases, to ignore the small region of the curves corresponding to progressive slip and to assume that the load-displacement relationship is bilinear, with the slope of the initial portion given by Eq. (2.25) and the slip portion by Eq. (2.28).

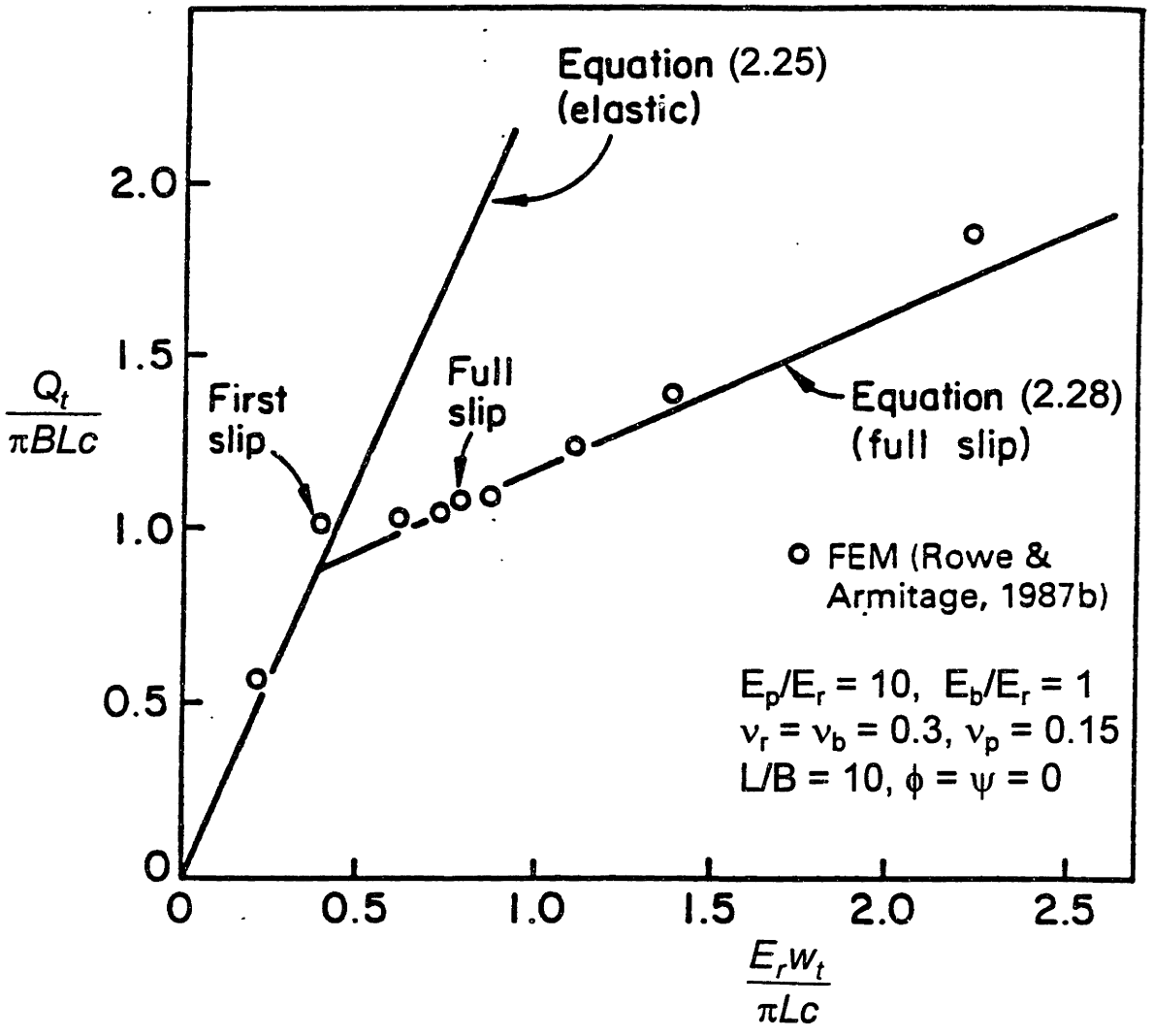

L = length of the shaft; B = diameter of the shaft;
Q_t = total applied load at shaft head; w_t = displacement at shaft head;
E_r, ν_r = Young's modulus and Poisson's ratio of the rock mass adjacent to the shaft;
E_b, ν_b = Young's modulus and Poisson's ratio of the rock mass below the shaft;
E_p, ν_p = Young's modulus and Poisson's ratio of the shaft;
c = interface cohesion; ψ = angle of dilation.

Figure 2.19 Displacement of a socketed shaft considering full slip (after Carter and Kulhawy 1988)

2.5 Current Design Methods

Currently, several methods are available for the design of drilled shafts socketed into rock. In general, a design method uses one of the empirical relations discussed in section 2.3 to estimate the ultimate side shear resistance and the end bearing resistance. The load-displacement response is then predicted using charts obtained with finite element solutions discussed in section 2.4. In this section, two typical design methods will be described to show how the empirical relations and the finite element results are used in design practice.

2.5.1 Williams et al. Design Method

Williams et al. (1980) introduce the concept of normalized elastic and inelastic side shear and end bearing resistance to predict the load-displacement response of rock sockets. Their design method concentrates on satisfying a displacement criterion and involves the following general procedure:

1. Determine a maximum allowable displacement w_t.

2. Select trial shaft dimensions. Generally the shaft diameter will be suggested by construction requirements or allowable concrete stresses and it is necessary only to select a trial shaft length.

3. Assume that the shaft behaves elastically and use the elastic solution of Donald et al. (1980) for a shaft in a semi-infinite half space (see Figure 2.20) to predict the total elastic load, Q_e, at displacement w_t, i.e.,

$$Q_e = \frac{w_t E_m B}{I} \tag{2.39}$$

where

E_m is the Young's modulus of the rock mass;

B is the diameter of the shaft;

I is the nodimensional displacement influence factor which can be obtained from Figure 2.20.

4. Determine the distribution of the elastic load, Q_e, between the side and the base (Q_{se} and Q_{be}) according to elastic load distribution curves (e.g., Figure 2.21 developed by Donald et al. 1980). The elastic unit side shear, τ_e, and the elastic end bearing, q_e, are then determined as

$$\tau_e = \frac{Q_{se}}{2\pi LR} \tag{2.40}$$

$$q_e = \frac{Q_{be}}{\pi R^2} \tag{2.41}$$

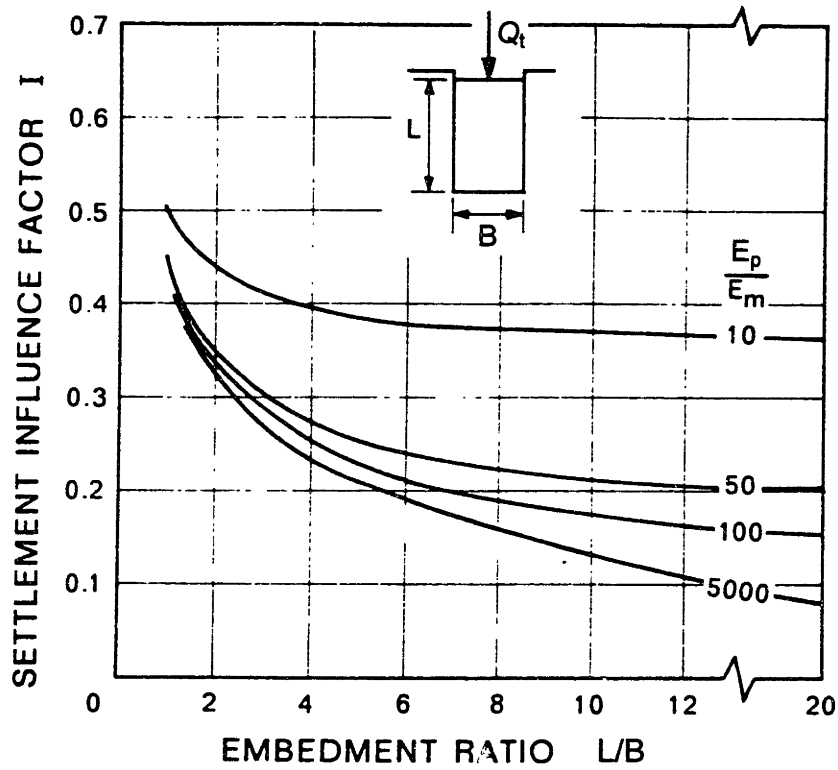

$I = E_m B w_t / Q_e$; L = length of the shaft; B = diameter of the shaft;
Q_e = total load at shaft head corresponding to elastic displacement w_t at shaft head;
E_m = Young's modulus of the rock mass;
E_p = Young's modulus the shaft.

Figure 2.20 Elastic displacement influence factor as a function of embedment ratio and Modular ratio (after Donald et al. 1980)

The elastic side shear ratio, τ_e/τ_{max}, is then calculated, where τ_{max} is calculated using Eq. (2.12), i.e.,

$$\tau_{max} = \alpha_w \beta_w \sigma_c \tag{2.12}$$

5. The solutions in steps 3 and 4 are for the case that the shaft behaves elastically. If the shaft behaves non-elastically, Q_{se} and Q_{be} have to be adjusted to get the corrected (actual) side resistance, Q_s, and the corrected (actual) base load, Q_b. The deviation from elastic behavior is quantified by using the graph shown in Figure 2.22, which is derived from empirical evidence from full-scale load tests on rough sockets in Melbourne Mudstone (Williams 1980) (For shafts in rock masses with different properties, new relations should be derived). Figure 2.22 shows the relationship between τ_e/τ_{max}, and another ratio, τ_p/τ_{max}, termed by Williams et al. (1980) the 'plastic stress ratio', where τ_p is the stress equal to the difference between the elastic side shear stress and the mobilized side shear stress, i.e.,

$$\tau_p = \tau_e - \tau_s \tag{2.42}$$

where τ_s is the mobilized side shear stress, i.e., the actual side shear stress at displacement w_t. Therefore, the corrected (actual) side resistance, Q_s, is

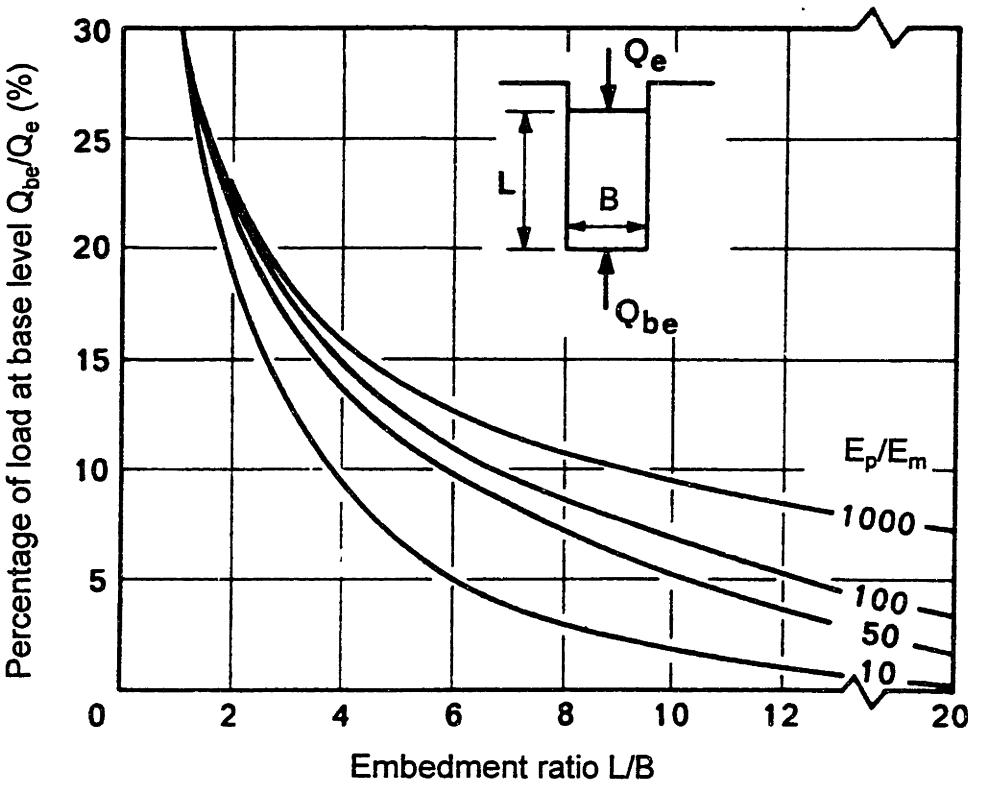

L = length of the shaft; B = diameter of the shaft;
Q_e = total load at shaft head corresponding to elastic displacement w_t at shaft head;
Q_{be} = load at shaft base corresponding to elastic displacement w_t at shaft head;
E_m = Young's modulus of the rock mass;
E_p = Young's modulus the shaft.

Figure 2.21 Elastic load distribution as a function of embedment ratio and Modular ratio (after Donald et al. 1980)

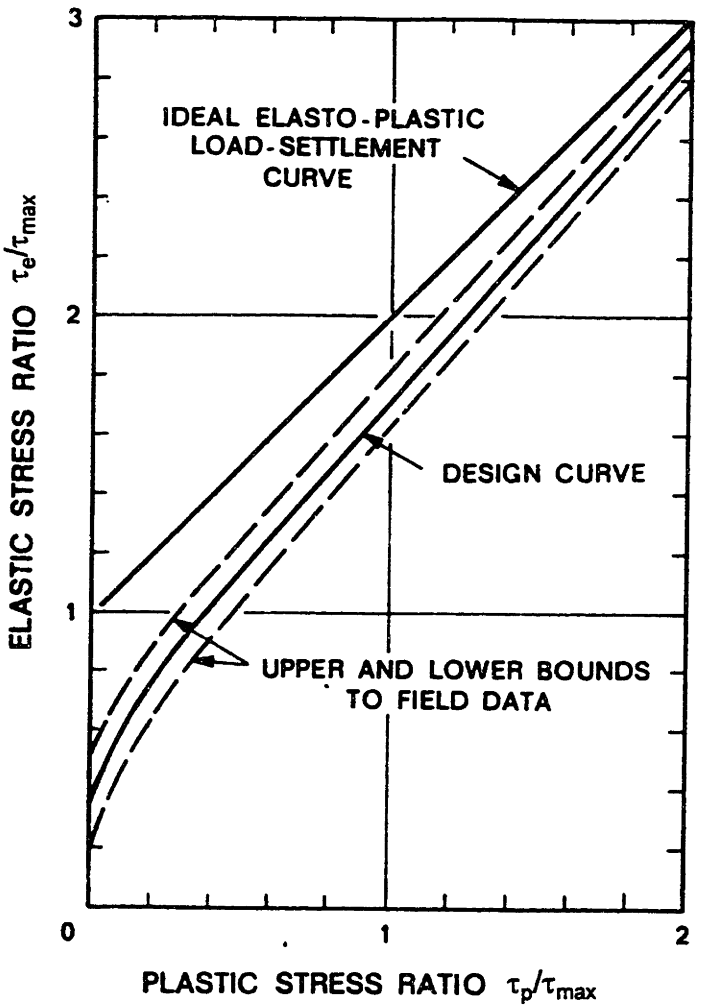

Figure 2.22 Normalized design curves for side resistance (after Williams et al. 1980)

$$Q_s = (\tau_e - \tau_p)\pi LB \tag{2.43}$$

The unit base resistance corresponding to a displacement of 1% of the shaft diameter, q_1, is defined as the ultimate base resistance and is estimated by

$$q_1 = N_s \sigma_c \tag{2.44}$$

where N_s is an empirical factor determined from Figure 2.23. The elastic bearing resistance ratio, q_e/q_1, is then calculated. The deviation, q_p, from the elastic behavior, i.e., the difference between the elastic end bearing and the mobilized end bearing is

$$q_p = q_e - q_b \tag{2.45}$$

where q_b is the mobilized end bearing, i.e., the actual end bearing at displacement w_t. Thus the corrected (actual) base load, Q_b, is

$$Q_b = (q_e - q_p)\pi R^2 \tag{2.46}$$

where q_p can be determined the empirical graph given in Figure 2.24.

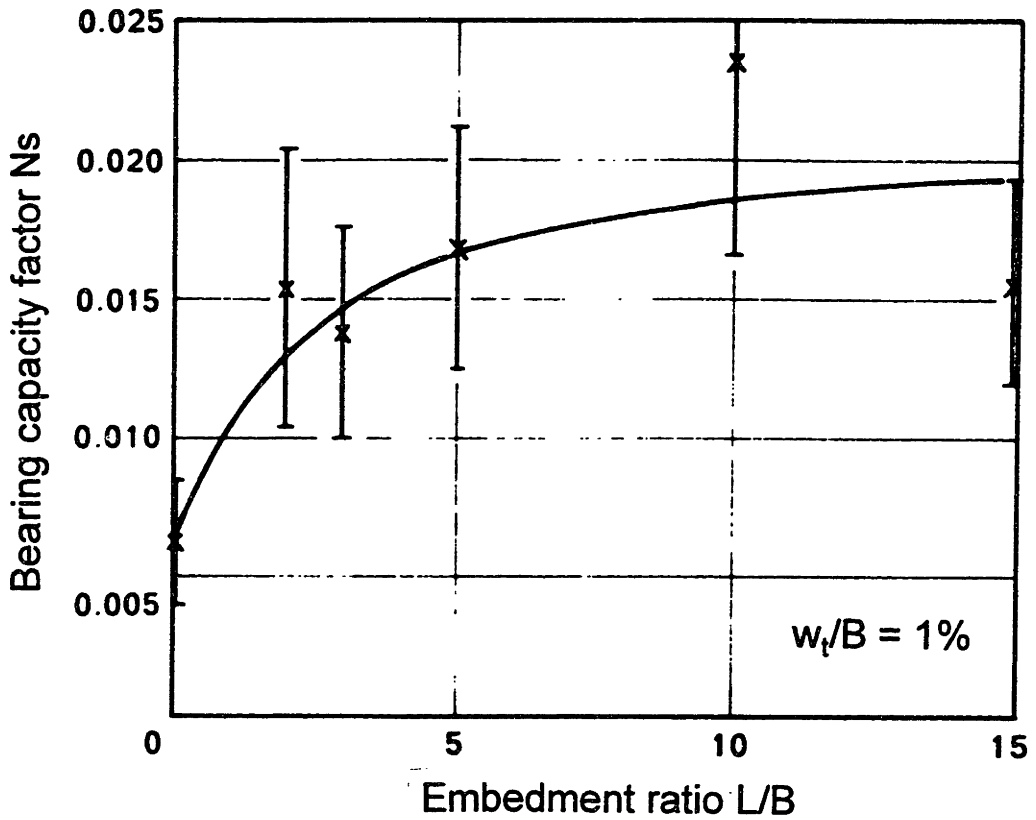

Figure 2.23 Bearing capacity factor N_s vs. L/B
(after Williams et al. 1980)

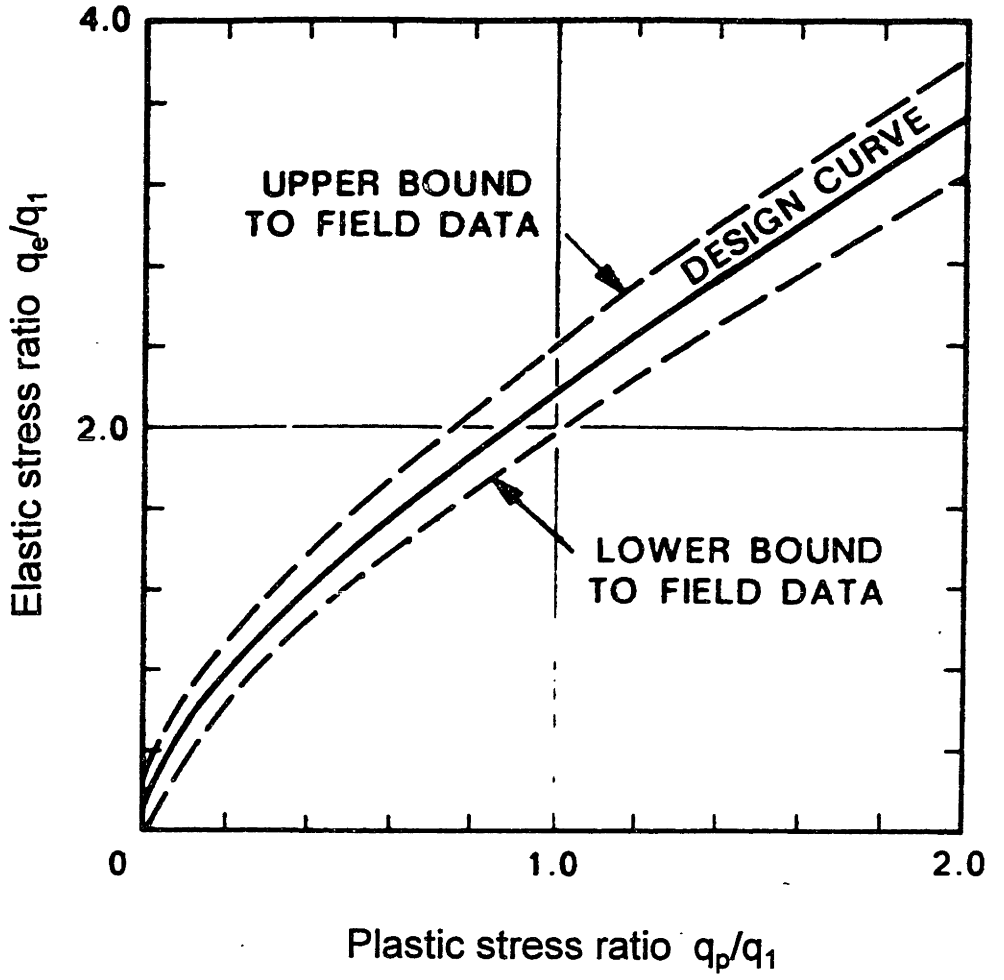

Figure 2.24 Normalized design curves for base resistance (after Williams et al. 1980)

6. Determine the actual total load Q_t corresponding to displacement w_t, as Q_s + Q_b.

7. Check if the load Q_t is close to the design load. If not, select a new trial design and repeat the above procedures.

2.5.2 Rowe and Armitage Design Method

A typical design chart developed from finite element analyses by Rowe and Armitage (1987a, b) is shown in Figure 2.25, in which the lower dashed line represents the elastic solution (no slip) and the upper dashed line represents full slip conditions ($\tau_{avg}/\tau_{max} = 1$). The following is a brief outline of the design procedure:

1. Determine the following design parameters:
   (i) allowable design displacement, w_t;
   (ii) diameter of the shaft, B;
   (iii) applied axial load, Q_t;
   (iv) unconfined compressive strength of the rock σ_c;
   (v) modulus of the shaft, E_p.

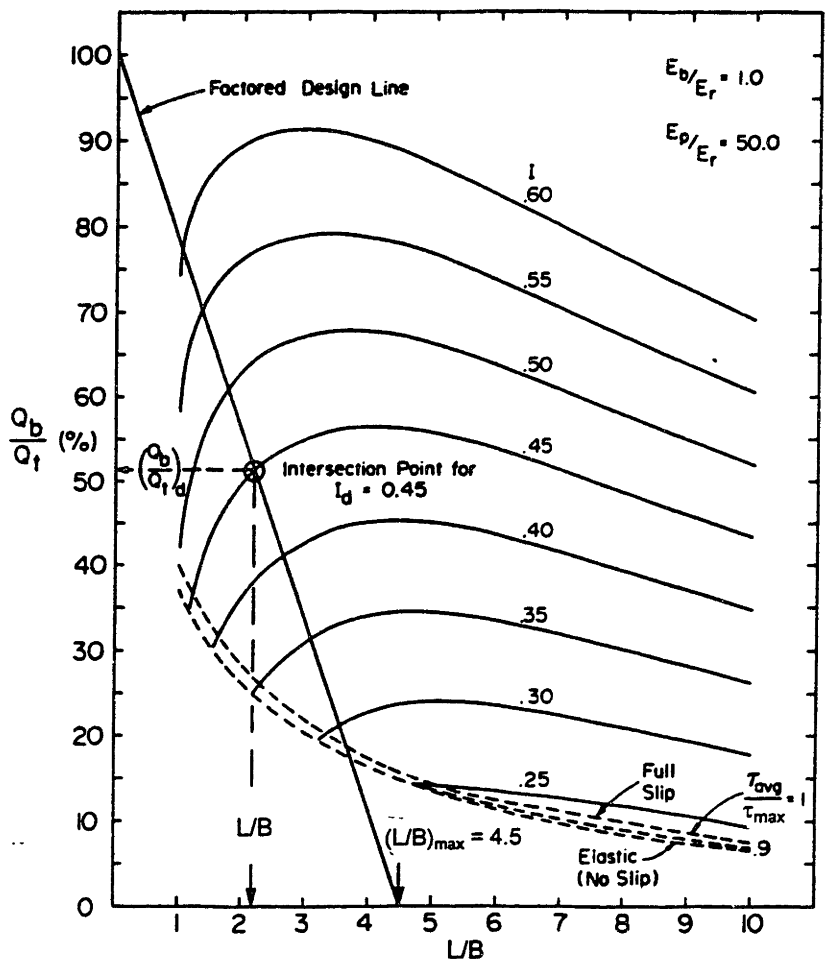

$I = E_r B w_t / Q_t$; B = shaft diameter; w_t = displacement at shaft head;
Q_t = total applied load at shaft head; Q_b = bearing load at shaft base;
E_r = Young's modulus of rock mass adjacent to the shaft;
E_b = Young's modulus of rock mass below the shaft base;
E_p = Young's modulus of the shaft; L = shaft length;
τ_{avg} = average side shear resistance; τ_{max} = ultimate side shear resistance.

Figure 2.25 Design of a socketed shaft allowing for slip (after Rowe and Armitage 1987b)

2. Estimate the maximum unit side shear resistance, τ_{max}, according to Eq. (2.9), i.e.,

$$\tau_{max} = 0.45(\sigma_c)^{0.5} \quad \text{for sockets with roughness R1, R2 or R3} \qquad (2.9a)$$

$$\tau_{max} = 0.6(\sigma_c)^{0.5} \quad \text{for sockets with roughness R4} \qquad (2.9b)$$

where τ_{max} and σ_c are in MPa.

3. Estimate the Young's modulus of the intact rock, E_i, as follows

$$E_i = 215\sqrt{\sigma_c} \qquad (2.47)$$

where E_i and σ_c are in Mpa.

4. Apply reduction factors to τ_{max} and E_i to obtain the design parameters for the side shear resistance and the rock mass modulus, i.e.,

$$\tau_d = f_\tau \tau_{max} \qquad (2.48)$$

$$E_d = f_E E_i \qquad (2.49)$$

where f_τ and f_E are reduction factors (or partial factors). According to Rowe and Armitage (1987b), a value of at least 0.7 should used for both f_τ and f_E. The partial factors of 0.7 are

chosen to meet a serviceability limit state such that the probability of exceeding the design settlement is less than 30% (Rowe and Armitage 1987b).

5. Calculate $(L/B)_{max}$ that will be required if the total load, Q_t, were to be carried in side shear only

$$(L/B)_{\max} = \frac{Q_t}{\pi B^2 \tau_d} \tag{2.50}$$

6. Calculate the settlement influence factor, I_d,

$$I_d = \frac{w_t E_d B}{Q_t} \tag{2.51}$$

7. This step involves selecting the length of the shaft required to give the 'design' displacement influence factor I_d, while allowing for possible slip at the shaft-rock interface. This is achieved by selecting an appropriate design chart for given values of $E_p/E_r = E_p/E_d$ and E_b/E_r from those produced by Rowe and Armitage (1987b) (e.g., see Figure 2.25) and proceeding as follows:

(a) Draw a straight line between the coordinates (L/B = 0, Q_b/Q_t = 100%) and ($L/B = L_{max}/B$, $Q_b/Q_t = 0$, where Q_b is the base load) (see Figure 2.25).

(b) Locate the intersection between the straight line and the design curve corresponding to the settlement influence factor I_d calculated in Step 6 (see Figure 2.25).

The coordinate of this intersection point represents the 'design' length-to-diameter ratio $(L/B)_d$ and the corresponding $(Q_b/Q_t)_d$.

If an intersection can be found, then a shaft of length L_d will satisfy the design displacement criterion and it simply remains to check that there is an adequate 'factor of safety' against over-stressing the rock beneath the shaft base. Proceed to step 8.

(c) If no intersection point can be established on the design chart, it is necessary to check whether the shaft can be designed for the given conditions. Select the appropriate chart from another solution set that represents the elastic solution (no slip conditions) (e.g., see Figure 2.26) and draw a horizontal line for $I = I_d$. Find the intersection of this line with the curve for the appropriate value of $E_p/E_r = E_p/E_d$:

(i) If there is an intersection point on this curve then the shaft can be designed elastically (i.e., negligible slip should occur under design conditions). The required L/B can be obtained as shown in Figure 2.26. The corresponding proportion of load transferred to the base Q_b/Q_t may be determined from curves as given in Figure 2.27. The shaft of length L/B satisfies the design displacement criterion. Proceed to step 8 to check bearing pressures below the shaft base.

(ii) If still no intersection point can established to find L/B, then no shaft of diameter B will satisfy the design requirements for the specified conditions. Go back to step 1 and either increase the design displacement or increase the diameter B and repeat the design procedure.

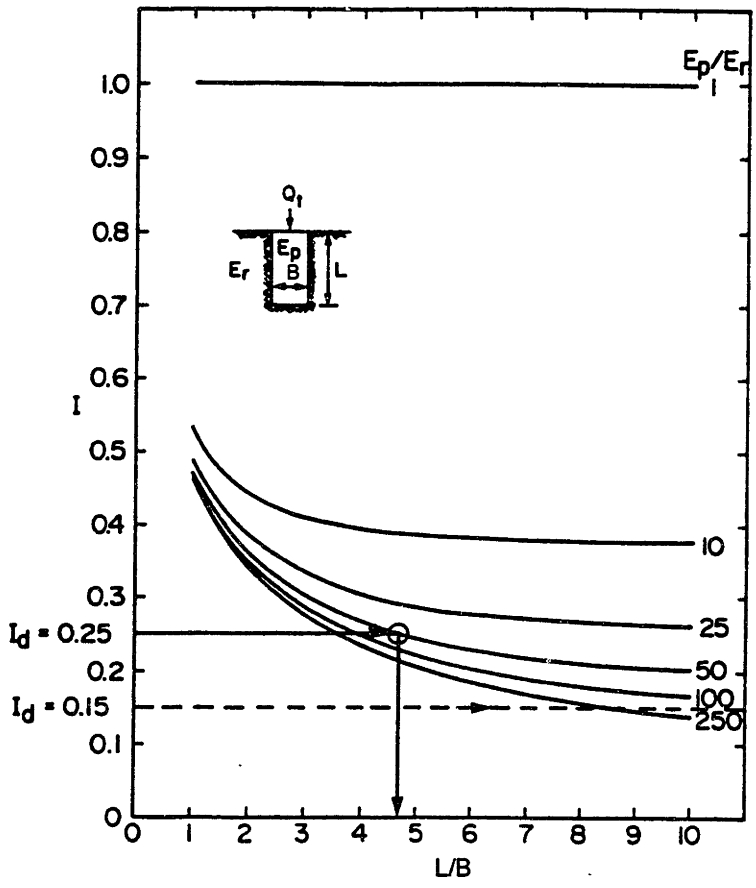

$I = E_r B w_t / Q_t$;
Q_t = total applied load at shaft head;
B = shaft diameter;
E_p = Young's modulus of the shaft.
w_t = displacement at shaft head;
E_r = Young's modulus of the rock mass;
L = shaft length;

Figure 2.26 Design of a socketed shaft for no slip conditions (after Rowe and Armitage 1987b)

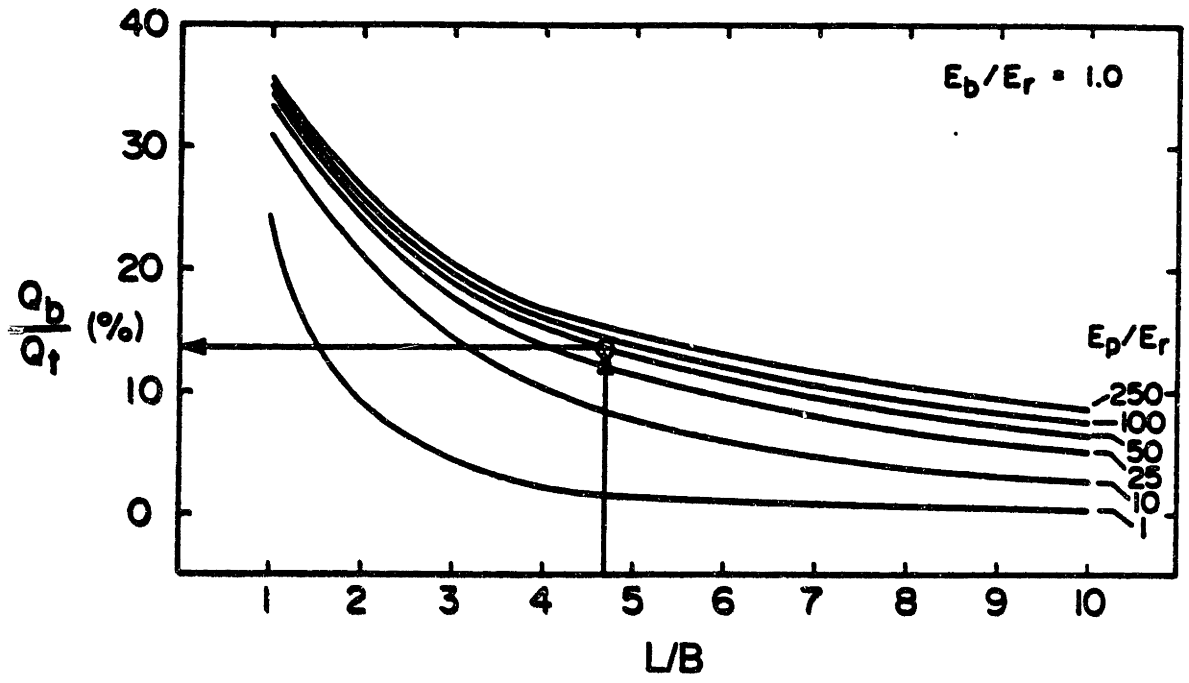

B = shaft diameter;
Q_t = total applied load at shaft head;
E_r = Young's modulus of rock mass;
L = shaft length;
Q_b = bearing load at shaft base;
E_p = Young's modulus of the shaft.

Figure 2.27 Design of a socketed shaft for no slip conditions (after Rowe and Armitage 1987b)

8. Once the design values of L/B and Q_b/Q_t are established, check that the end bearing pressure $q_b = Q_b/\pi B^2$, does not exceed the maximum recommended value of $2.5\sigma_c$.

In the case of rock with soil seams, Rowe and Armitage (1987b) suggest that τ_{max} and E_i used above be modified as follows:

$$\tau^*_{max} = S\tau_s + (1-S)\tau_{max} \tag{2.52}$$

$$E^*_i = SE_s + (1-S)E_i \tag{2.53}$$

where

S is the proportion of seams to total socket length (i.e., $S = \Sigma$(seam thickness)/L);

τ^*_{max} and E^*_i are the modified side shear resistance and the modulus of the intact rock, respectively.

τ_s and E_s are the side shear resistance along the seams and the modulus of the seams, respectively.

2.5.3 Comments on Current Design Methods

Several comments can be made about the papers referenced in the preceding section describing design methods for drilled shafts socketed into rock:

1. Current design methods can just model the rock mass as a single half space or, at best, as a two layer medium (i.e., the rock adjacent to and beneath the socketed shaft). In practice, however, the rock mass is often multi-layered and distinct differences in material properties exist from layer to layer. To use the available design methods for shafts in multi-layered rock mass, the common practice is to use weighted average values of material properties. This is a very crude approximation. To reasonably consider the multi-layer nature of rock mass, new design methods need to be developed.

2. Current design methods consider the end bearing resistance very crudely. To reasonably design a rock-socketed shaft, it is necessary to predict not only the ultimate side shear resistance but also the end bearing resistance.

CHAPTER 3

DESIGN MODEL FOR DRILLED SHAFTS SOCKETED INTO ROCK

3.1 General

As shown in the literature review of Chapter 2, current design methods just model the rock mass as a single half space or, at best, as a two layer medium (i.e., the rock adjacent to and beneath the rock socketed shaft). This is a very crude approximation to the multi-layered rock mass occurring in reality. The literature review also showed that the current design methods consider the end bearing resistance very crudely. To reasonably design a rock socketed shaft, it is necessary to consider the multi-layer nature of the rock mass and predict not only the ultimate side shear resistance but also the end bearing resistance. This chapter provides a general description of the main points of a proposed design model which can reduce the above limitations of the current design methods.

3.2 Allowable Load Capacity

The allowable load capacity, Q_a, of a drilled shaft socketed into rock can be obtained from the ultimate load capacity, Q_u, by

$$Q_a = \frac{Q_u}{FS} \tag{3.1}$$

where FS is the factor of safety. According the current design practice of pile foundations, FS of at least 2 to 3 should be used.

For a drilled shaft socketed into a multi-layered rock mass (see Figure 3.1), Q_u can be obtained as follows:

$$Q_u = \pi B \sum_{i=1}^{m} L_i (\tau_{\max})_i + \frac{\pi B^2}{4} q_{\max} \tag{3.2}$$

where

B is the diameter of the socket;

L_i is the length of the socket in layer i;

$(\tau_{\max})_i$ is the ultimate side shear resistance of the socket in layer i;

$q_{\max}$ is the end bearing resistance.

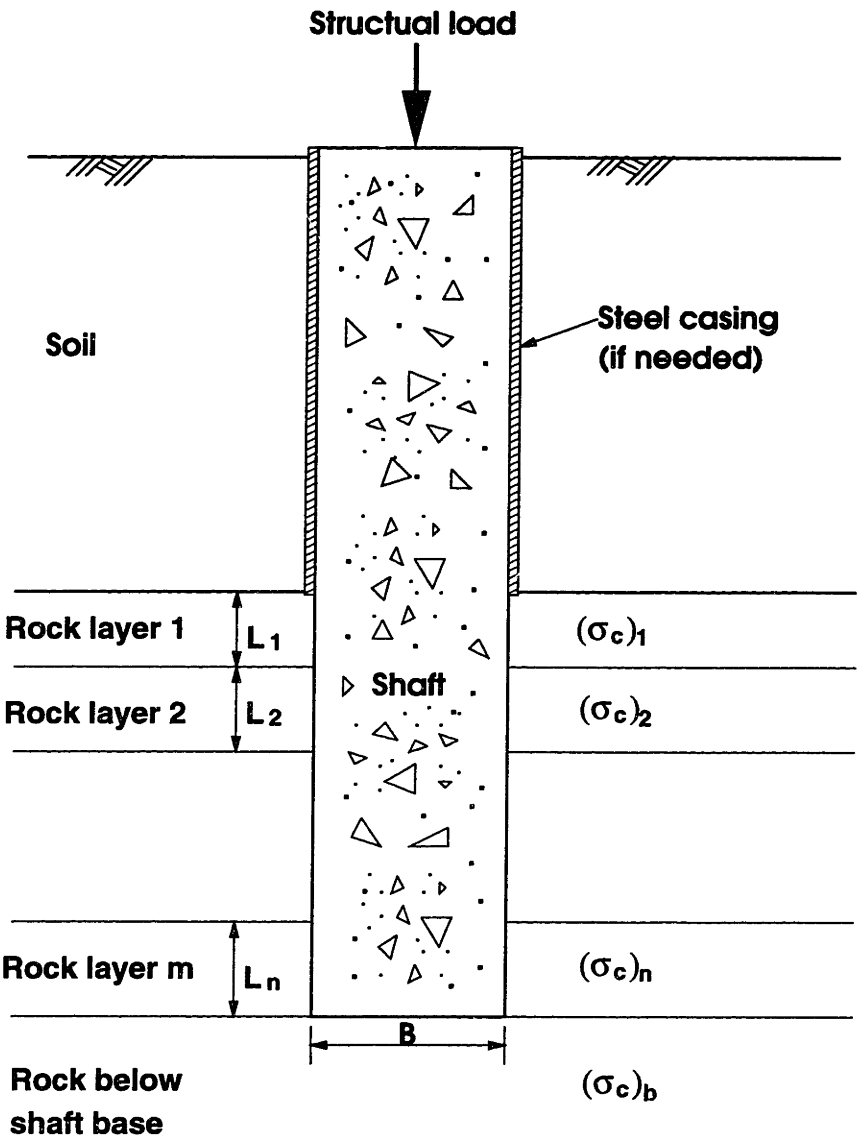

Figure 3.1 A drilled shaft sockted into a multi-layered rock mass.

$(\tau_{max})_i$ and q_{max} can be determined from the corresponding unconfined compressive strength, σ_c. The detailed procedure will be described in Chapter 4.

For a drilled shaft socketed into rock, the working load, Q_t, should not exceed the allowable load capacity, Q_a, obtained from Eq. (3.1). So if a drilled shaft with working load, Q_t, is to be designed, the required minimum ultimate load capacity, $(Q_u)_{min}$, should be

$$(Q_u)_{\min} = FS \cdot Q_t \tag{3.3}$$

From Eqs. (3.2) and (3.3),

$$\pi B \sum_{i=1}^{m} L_i (\tau_{max})_i + \frac{\pi B^2}{4} q_{max} \geq FS \cdot Q_t \tag{3.4}$$

With Eq. (3.4), shaft dimensions can be selected. Generally the shaft diameter is controlled by construction requirements or allowable concrete stresses. After a diameter is selected, the shaft length can be evaluated from Eq. (3.4).

3.3 Displacement of the Shaft at Working Load

A rational design method for drilled shafts socketed into rock should consider not Only the allowable load capacity but also the displacement at the working load.

After the shaft dimensions have been determined using the method described in the last section, the displacement of the shaft at the working load can be calculated using a yet to be determined method. If the calculated displacement values exceed the allowable displacement, the diameter and/or length of the shaft should be adjusted. For the proposed design method, a model is developed to predict the displacement of a shaft socketed into a multi-layered rock mass, at working load. The details of this model are presented in Chapter 5. The proposed model assumes that the shaft behaves linearly elastically up to the working load.

As described in Chapter 2, the general load-displacement curve for a drilled shaft under axial loading consists of three stages (see Figure 2.9). In the first stage (line OA in Figure 2.9), the shaft behaves essentially in a linear manner, and the displacement can be computed accurately using the theory of elasticity. Field scale and model tests show that the first stage can go up to 50% of the ultimate load (see, e.g., Goeke and Hustad 1979; Radhakrishana and Leung 1989; Leung and Ko 1993; Dykeman and Valsangkar 1996). Numerical and analytical results also show that the shaft behaves essentially in a linear manner up to 50% of the ultimate load (see Figure 2.14).

Since the shaft behaves essentially in a linear manner up to 50% of the ultimate load capacity, the displacement at working load (which is less than 50% of the ultimate load capacity if FS of 2 to 3 is used) can be computed accurately using the theory of elasticity.

3.4 Effect of Discontinuities

Soft seams, joints and faults frequently exist in rock formations. Occurrence of these discontinuities will reduce the load capacity and increase the displacement. The core recovery ratio, P_r, and rock quality designation, *RQD*, are commonly used to describe the quality of rock masses. Both P_r and *RQD* are related to the soundness and continuity of the rock. The relationship between the numerical value of *RQD* and rock engineering qualities are shown in Table 3.1 (Deere 1964). For the purpose of foundation design on a rock mass, Kulhawy and Goodman (1987) suggest that the design value of the rock mass strength be determined from the intact rock strength value based on the corresponding *RQD* values of the rock mass as shown in Table 3.2. Several methods are available for estimating the Young's modulus of rock masses (see, e.g., Bieniawski 1984, CGS 1992). Here only the empirical relations are presented. Figure 3.2 shows the relation between *RQD* and the modulus ratio E_m/E_i (Bieniawski 1984), where E_m and E_i are the moduli of the rock mass and intact rock, respectively. The empirical relationship between the rock mass rating (*RMR*) value and an in situ rock mass modulus is shown in Figure 3.3. Bieniawski (1978) studied seven projects and suggested the following equation to predict rock mass modulus from *RMR*:

$$E_m = 2RMR - 100 \quad \text{(GPa)} \tag{3.5}$$

Table 3.1 Relationship of *RQD* to rock engineering quality (after Deere 1964)

RQD (%)	Rock Quality
< 25	Very poor
25 - 50	Poor
50 - 75	Fair
75 - 90	Good
90 - 100	Very good

Table 3.2 Suggested design values of rock strength parameters (after Kulhawy and Goodman 1987)

	Rock mass properties		
RQD (%)	Unconfined compressive strength	Cohesion	Angle of friction (°)
0 - 70	$0.33\sigma_c$	$0.1\sigma_c$	30
70 - 100	$(0.33 - 0.8)\sigma_c$	$0.1\sigma_c$	30 - 60

σ_c = unconfined compressive strength of intact rock core.

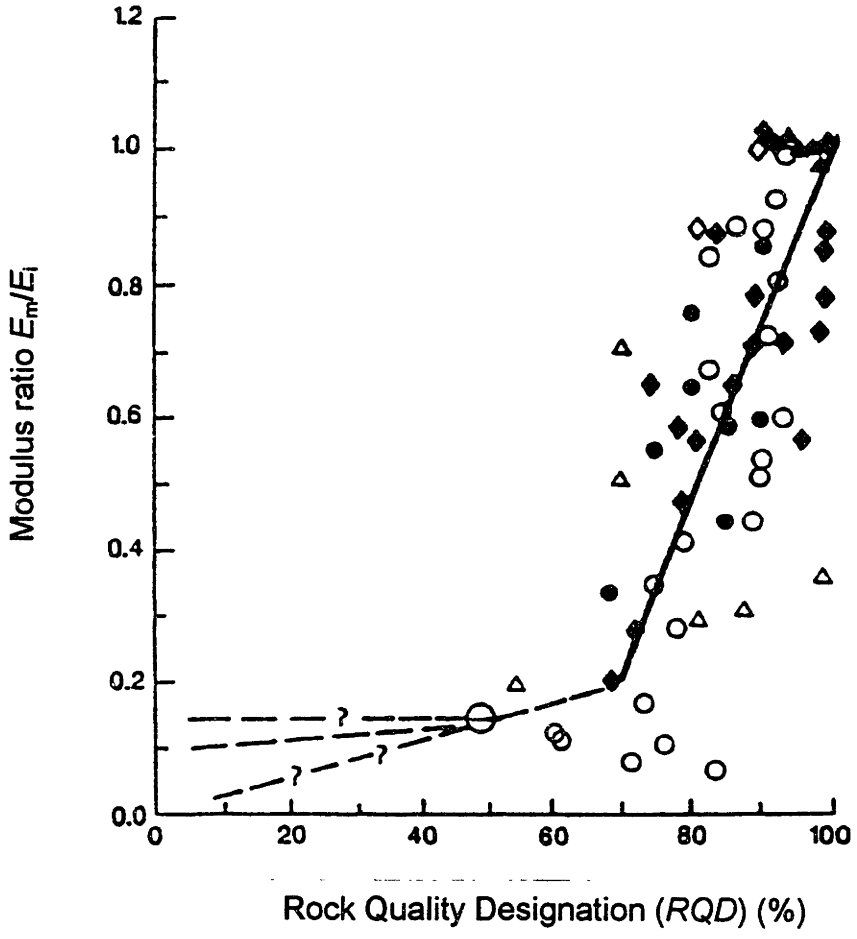

Figure 3.2 Correlation between *RQD* and modulus ratio E_m/E_i (after Bieniawski 1984)

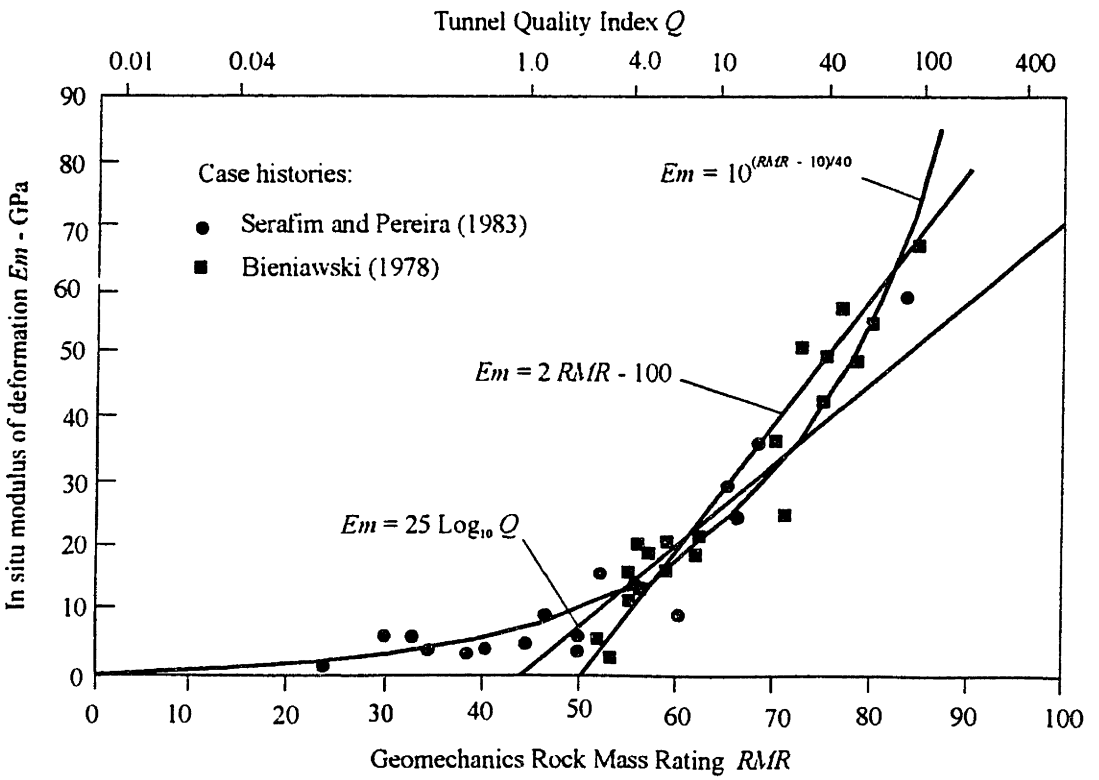

Figure 3.3 Relationship between in situ modulus and *RMR* (after Bieniawski 1978; Serafim and Pereira 1983)

The obvious deficiency of this equation is that it does not give modulus values for *RMR* values less than 50. Additional studies carried out on rock masses with qualities ranging from poor to very good indicated that the modulus could be related to *RMR* by (Serafim and Pereira 1983)

$$E_m = 10^{(RMR-10)/40} \quad \text{(GPa)} \tag{3.6}$$

More recently Barton et al. (1980), Barton et al. (1992) and Grimstad and Barton (1993) have found good agreement between measured displacements and predictions from numerical analyses using in situ deformation modulus values estimated from

$$E_m = 25 \log_e Q \quad \text{(GPa)} \tag{3.7}$$

where Q is the rock quality index (Barton et al. 1974).

It should be noted that all the above empirical relations suffer from the limitations mentioned, e.g., by Einstein et al. (1979).

There exist other empirical reduction factors which can then be used to calculate the ultimate load capacity. For example, according to Williams et al. (1980), the side shear resistance reduction factor, β_w, can be related to the rock mass modulus and intact rock modulus ratio, E_m/E_i, as shown in Figure 2.6. Hassan and O'Neill (1997) suggest that the friction along the interface at the soft seams be excluded. This can be done by

multiplying τ_{max} of a certain rock layer by the core recovery ratio, P_r, of this layer. The reduced end bearing resistance can be determined using the reduced unconfined compressive strength value (e.g., in Table 3.2).

It should be recalled, also, that the modulus used to predict the displacement is the rock mass modulus, E_m, not the intact rock modulus, E_i.

CHAPTER 4

ULTIMATE LOAD CAPACITY OF DRILLED SHAFTS SOCKETED INTO ROCK

4.1 General

As discussed in chapter 3, to predict the ultimate load capacity of a drilled shaft socketed into rock, it is necessary to predict the ultimate side shear resistance and the end bearing resistance. In this chapter, methods for predicting the ultimate side shear resistance and the end bearing resistance are developed. By analyzing the available methods for estimating the ultimate side shear resistance, relations are recommended respectively for smooth and rough sockets. In this chapter, the terms "smooth socket" and rough socket" are used to represent the extreme interface conditions as defined, for example, by Kodikara et al. (1992) (Table 2.2). As for the end bearing resistance, a data base of 35 load tests is developed and, based on this data base, a new relation is developed to predict the end bearing resistance from unconfined compressive strength. The Hoek-Brown strength criterion is used to analyze the end bearing resistance of rock

sockets. The results show that the agreement between the new relation and the theoretical solution is reasonable.

4.2 Ultimate Side Shear Resistance

As shown in Chapter 2, the available relations for estimating the ultimate side shear resistance can be divided in the following two major groups:

1) The ultimate side shear resistance is a simple constant times σ_c.

2) The relationship between the ultimate side shear resistance and σ_c is a power-curve.

Considering that the probable origin of these relations is by plotting the available data and noting trends, the relations can be simply explained. If the rock strength can be expressed as a Coulomb material (c and ϕ), with the interface skin friction approximating the rock's cohesion (see Figure 4.1), then (McVay et al. 1992)

$$\sin\phi = \frac{0.5\sigma_c}{(x + \sigma_t + 0.5\sigma_c)} \tag{4.1}$$

$$\tau_{max} = (x + \sigma_t)\tan\phi \tag{4.2}$$

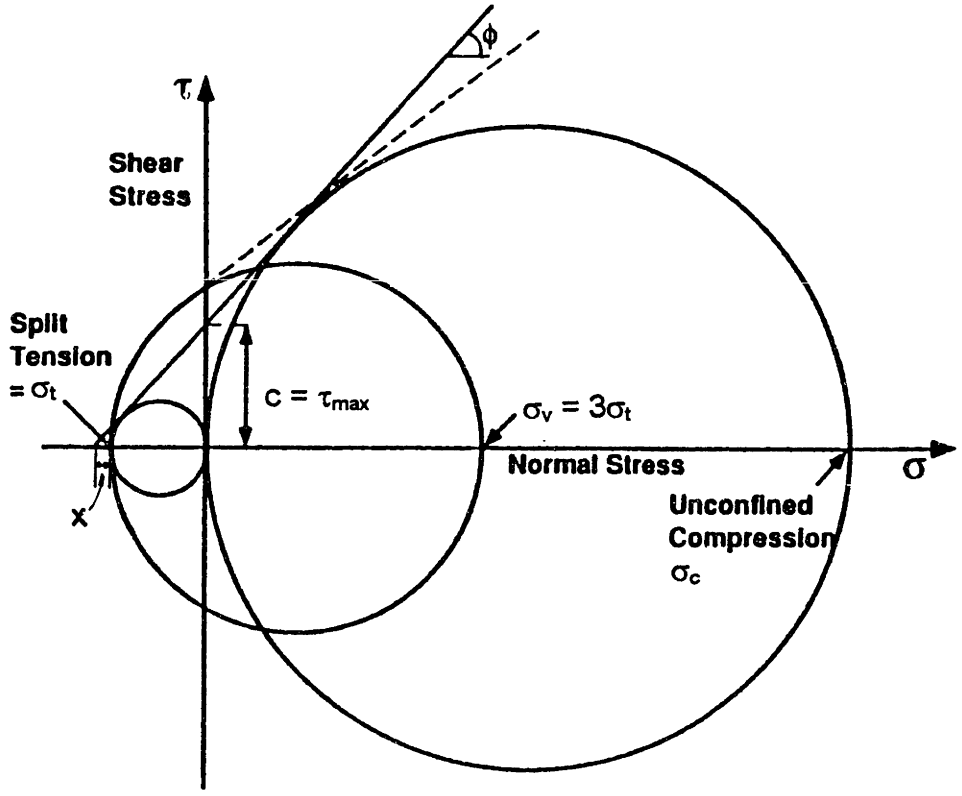

Figure 4.1 Strength envelope by McVay et al. (1992)

where σ_t is tensile strength of the intact rock. Combining Eq. (4.1) and (4.2) results in

$$\tau_{max} = \frac{\sigma_c(1-\sin\phi)}{2\cos\phi} \tag{4.3}$$

or

$$\alpha = \frac{\tau_{max}}{\sigma_c} = \frac{(1-\sin\phi)}{2\cos\phi} \tag{4.4}$$

So for a fixed strength envelope (constant ϕ), a constant relationship will exist between cohesion (skin friction) and σ_c. Alternatively, the relation using a power function suggests a rock with a variable ϕ. For example, as ϕ increases, the σ_c strength increases likewise, which in turn would lower the adhesion factor, α (see Eq. 4.4).

A study of extensive load test data (Williams and Pells 1981; Kulhawy and Phoon 1993) indicates that the power curve relationship is closer to the real cases. So only the power curve relations will be considered for the proposed design model.

The relations of Kulhawy and Phoon (1993) (Eq. 2.13) can be rewritten as

Mean Behavior: $$\tau_{max} = 0.90(\sigma_c)^{0.5} \tag{4.5a}$$

Upper bound (very rough): $$\tau_{max} = 1.35(\sigma_c)^{0.5} \tag{4.5b}$$

Lower bound: $$\tau_{max} = 0.45(\sigma_c)^{0.5} \quad (4.5c)$$

It can be seen that the lower bound relation of Kulhawy and Phoon (1993) (Eq. 4.5c) is the same as the relation of Rowe and Armitage (1997b) for sockets with roughness R1, R2 or R3 (Eq. 2.9a). However, the upper bound value from Kulhawy and Phoon (1993) (Eq. 4.5b) will be much higher than the value from Rowe and Armitage (1997b) for sockets with roughness R4 (Eq. 2.9b). Figure 4.2 is a plot of the ultimate side shear resistance, τ_{max}, versus the unconfined compressive strength, σ_c. Also plotted in this figure are the relations by Rosenberg and Gourneaux (1976) (Eq. 2.6), Meigh and Wolshi (1979) (Eq. 2.7) and Horvath (1982) (Eq. 2.8). Considering the fact that the relation of Kulhawy and Phoon (1993) is derived from a relatively extensive data base and that their upper bound value is much higher than the values from all other relations, the following relation is recommended for the proposed design method:

Smooth socket (R1, R2 or R3): $$\tau_{max} = 0.40(\sigma_c)^{0.5} \quad (4.6a)$$

Rough socket (R4): $$\tau_{max} = 0.80(\sigma_c)^{0.5} \quad (4.6b)$$

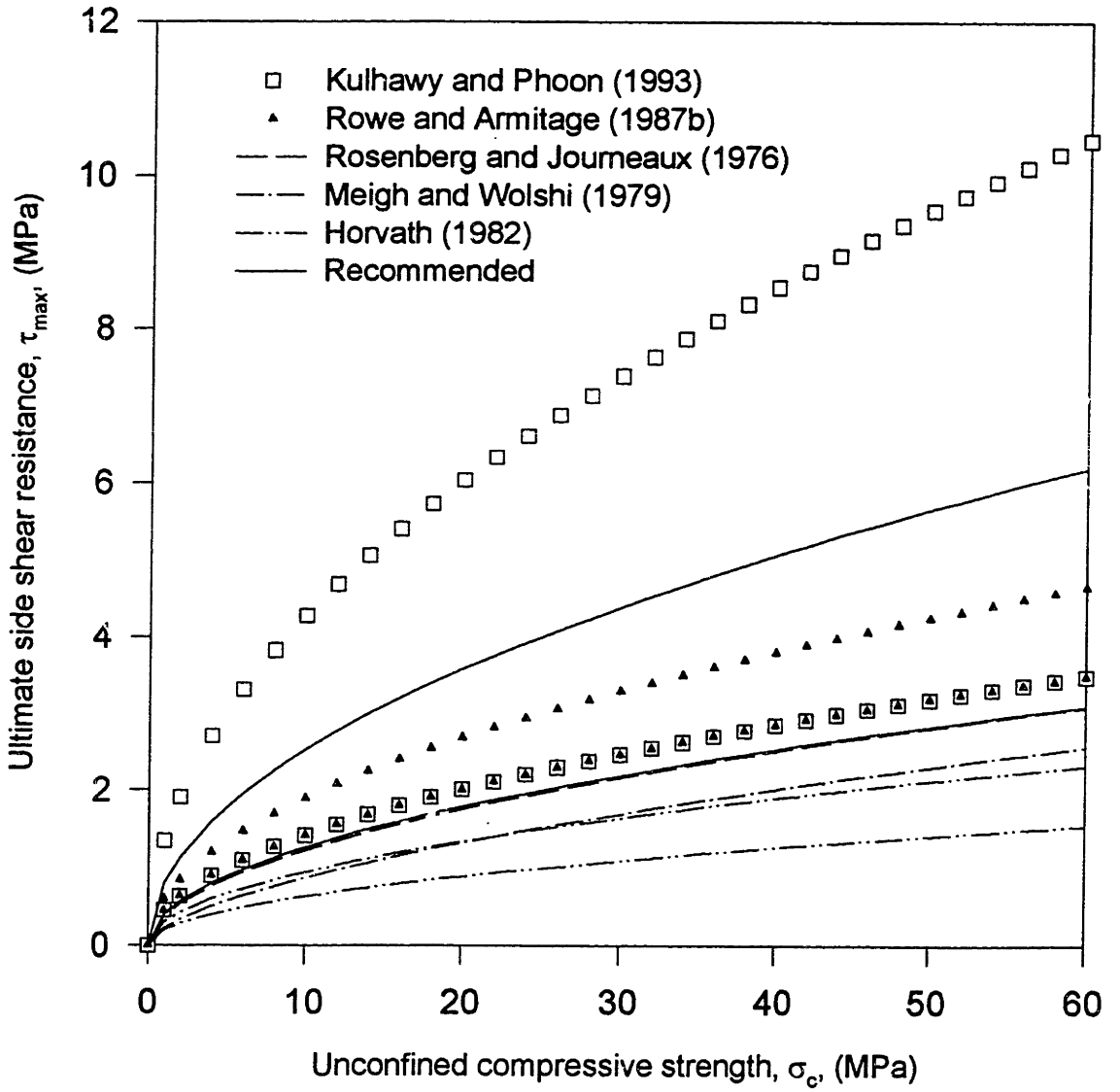

Figure 4.2 Ultimate side shear resistance vs. unconfined compressive strength

(There are two curves respectively for Kulhawy and Phoon 1993, Rowe and Armitage 1987b, Horvath 1982 and those recommended. In these thesis, for each shaft, the upper one is for rough interface and the lower one for smooth interface)

4.3 End Bearing Resistance

There has been considerable debate concerning the bearing capacity of circular foundations on rock. Numerous theories have been proposed and there is a significant variation in the predicted bearing capacity. The scatter in predicted results from various empirical relations is also quite high (see, for example, Eqs. 2.17 - 2.19). This may account for the fact that current design methods consider the end bearing resistance very crudely. Here a data base of 35 loading tests is developed and by analyzing the test data, a new relation is derived to predict the end bearing resistance of rock socketed shafts. The new relation is basically supported by the theoretical results derived from Hoek-Brown strength criterion (Hoek and Brown 1980, 1988; Hoek et al. 1992).

4.3.1 New Relation between End Bearing Resistance and Unconfined Compressive Strength

A data base of 35 loading tests is developed to study the variation of end bearing resistance with unconfined compressive strength. Data are obtained from the literature. Information for each load test is collected as comprehensively as possible. Table 4.1 is a summary of the data base.

All the load test data are plotted in Figure 4.3. It can be seen that the relation of q_{max} and σ_c is strong. Using linear regression, the relationship between q_{max} and σ_c can be obtained as follows:

$$q_{max} = 4.5(\sigma_c)^{0.57} \tag{4.7}$$

The end bearing capacity factor, N_c, defined by

$$N_c = \frac{q_{max}}{\sigma_c} \tag{4.8}$$

is often used in the literature. From Eqs. (4.7) and (4.8),

$$N_c = 4.5(\sigma_c)^{-0.43} \tag{4.9}$$

It can be seen that N_c decreases with increasing σ_c (see Figure 4.4). So the available relations such as Eqs. (2.17) – (2.19) assuming constant N_c values (i.e., q_{max} increases linearly with σ_c) are not accurate in predicting the end bearing resistance of rock socketed shafts. The theoretical solution presented in next section will also support the derived relations.

Table 4.1 Summary of the data base of load tests.

No.	Rock type	Dia-meter (mm)	Depth to base (m)	σ_c (MPa)	q_{max} (MPa)	N_c[1)]	Reference
1	Mudstone	670	6	4.2	6.88	1.64	Wilson (1976)
2	Shale	762	8.8	0.81	4.69	5.79	Goeke & Hustad (1979)
3	Shale	457	13.7	3.82	10.8	2.83	Hummert & Cooling (1988)
4	Shale	305	**	1.08	3.66	3.39	Jubenville & Hepworth (1981)
5	Gypsum[2)]	1064	5.32	2.1	6.51	3.1	Leung & Ko (1993)
6	Gypsum[2)]	1064	**	4.2	10.9	2.6	Leung & Ko (1993)
7	Gypsum[2)]	1064	**	5.4	15.7	2.9	Leung & Ko (1993)
8	Gypsum[2)]	1064	5.71	6.7	16.1	2.4	Leung & Ko (1993)
9	Gypsum[2)]	1064	**	8.5	23	2.7	Leung & Ko (1993)
10	Gypsum[2)]	1064	5.71	11.3	27.7	2.5	Leung & Ko (1993)
11	Till	762	**	0.7	4	5.71	Orpwood et al. (1989)
12	Till	762	**	0.81	4.15	5.12	Orpwood et al. (1989)
13	Till	762	**	1	5.5	5.5	Orpwood et al. (1989)
14	Diabase	615	12.2	0.52	2.65	5.1	Webb (1976)
15	Hardpan	1281	18.3	1.38	5.84	4.23	Baker (1985)
16	Till	1920	20.7	0.57	2.29	4.04	Baker (1985)
17	Hardpan	762	18.3	1.11	4.79	4.33	Baker (1985)
18	Sandstone	610	**	8.36	10.1	1.21	Glos & Briggs (1983)
19	Sandstone	610	**	9.26	13.1	1.41	Glos & Briggs (1983)
20	Mudstone	300	2.01	0.65	6.4	9.8	Williams (1980)
21	Mudstone	300	1	0.67	7	10.5	Williams (1980)
22	Mudstone	1000	15.5	2.68	5.9	2.2	Williams (1980)
23	Mudstone	1000	15.5	2.45	6.6	2.7	Williams (1980)

Table 4.1 Continued

No.	Rock type	Dia-meter (mm)	Depth to base (m)	σ_c (MPa)	q_{max} (MPa)	N_c	Reference
24	Mudstone	1000	15.5	2.45	7	2.9	Williams (1980)
25	Mudstone	1000	15.5	2.68	6.7	2.5	Williams (1980)
26	Mudstone	600	1.8	1.93	9.2	4.8	Williams (1980)
27	Mudstone	1000	3	1.4	7.1	5	Williams (1980)
28	Shale	**	**	34	28	0.82	Thorne (1980)
29	Sandstone	**	**	12.5	14	1.12	Thorne (1980)
30	Sandstone	**	**	27.5	50	1.82	Thorne (1980)
31	Shale	**	**	55	27.8	0.51	Thorne (1980)
32	Shale	740	7.24	1.42	5.68	4	Aurora & Reese (1977)
33	Shale	790	7.29	1.42	5.11	3.6	Aurora & Reese (1977)
34	Shale	750	7.31	1.42	6.11	4.3	Aurora & Reese (1977)
35	Shale	890	7.63	0.62	2.64	4.25	Aurora & Reese (1977)

[1] $N_c = q_{max}/\sigma_c$.

[2] Gypsum mixed with cement is used as pseudo-rock in centrifuge test. The diameters and depths are the equivalent prototype dimensions corresponding to 40 g in the centrifuge tests.

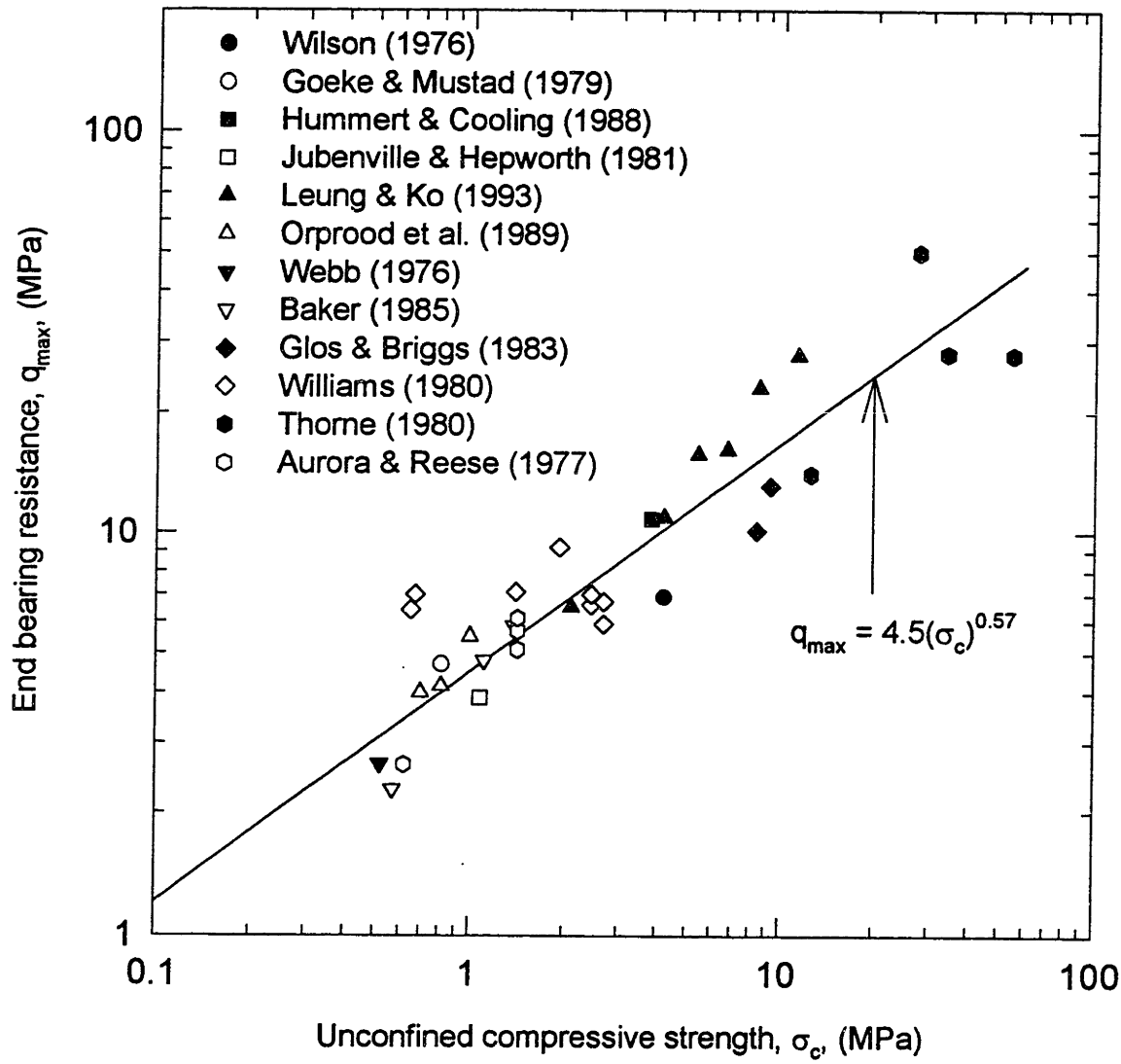

Figure 4.3 End bearing resistance vs. unconfined compressive strength

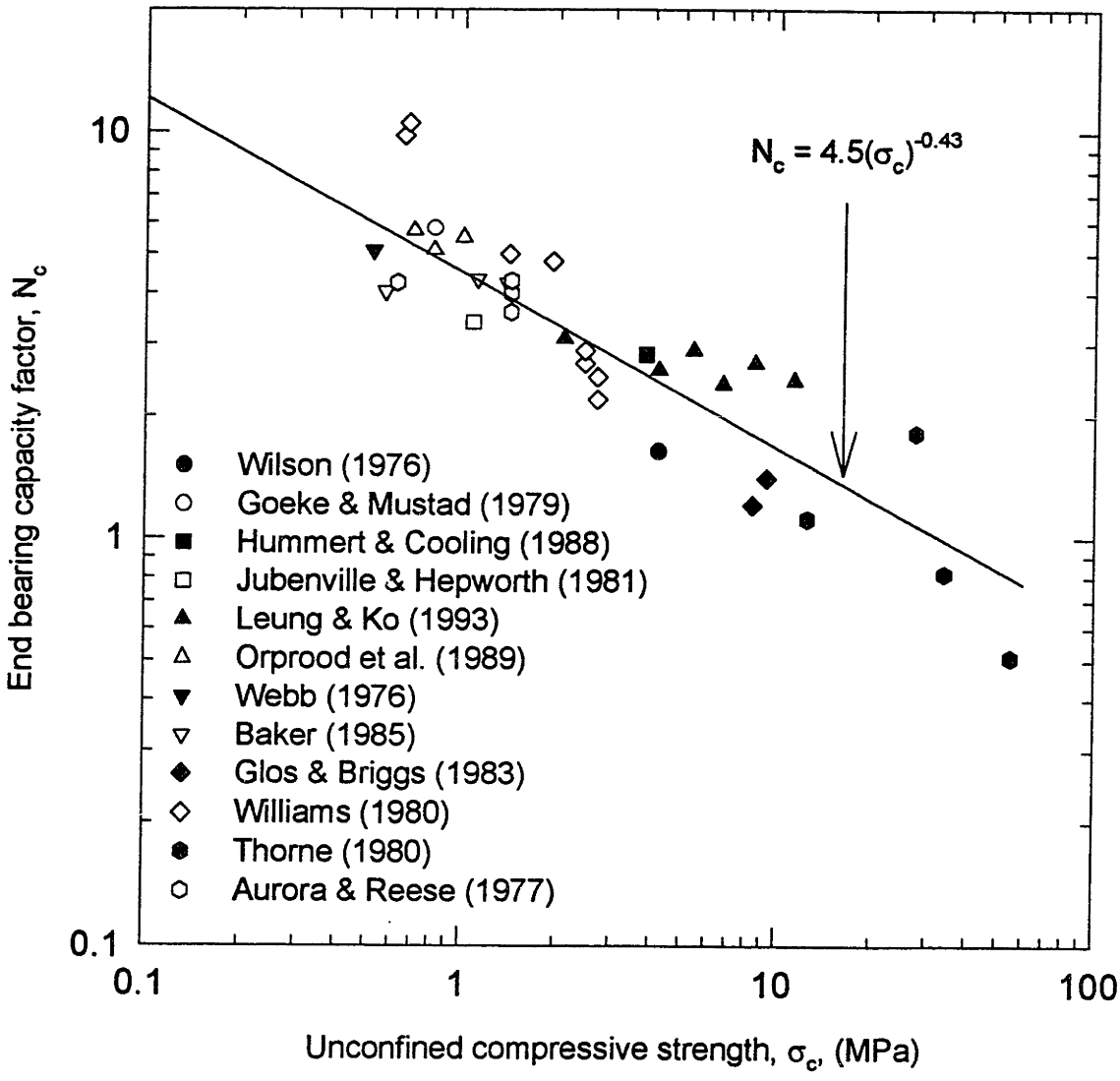

Figure 4.4 End bearing capacity factor vs. unconfined compressive strength

4.3.2 Theoretical consideration

A strength criterion for rock masses has been developed by Hoek and Brown (1980 and 1988) which is used in rock engineering. This is an empirical criterion that has been developed by trial and error and is based on the observed behavior of rock masses, model studies to simulate the failure mechanism of jointed rock, and triaxial compression tests of fractured rock. For intact rock, the Hoek-Brown criterion may be expressed in the following form

$$\sigma_1' = \sigma_3' + \sigma_c\left(m_i \frac{\sigma_3'}{\sigma_c} + 1\right)^{0.5} \tag{4.10}$$

where

σ_c is uniaxial compressive strength of the intact rock material;

σ'_1 and σ'_3 are the major and minor effective principal stresses respectively;

m_i is the material constant for the intact rock. m_i depends only upon the rock type (texture and mineralogy) as tabulated in Table 4.2.

For jointed rock masses, the Hoek-Brown criterion is given by the equation

$$\sigma_1' = \sigma_3' + \sigma_c\left(m_b \frac{\sigma_3'}{\sigma_c} + s\right)^{0.5} \tag{4.11}$$

Table 4.2. Values of parameter m_i for a range of rock types (after Hoek et al. 1995)

Rock type	Class	Group	Texture			
			Course	Medium	Fine	Very fine
SEDIMENTARY	Clastic		Conglomerate (22)	Sandstone 19	Siltstone 9	Claystone 4
				← Greywacke → (18)		
	Non-Clastic	Organic		← Chalk → 7		
				← Coal → (8-21)		
		Carbonate	Breccia (20)	Sparitic Limestone (10)	Micritic Limestone 8	
		Chemical		Gypstone 16	Anhydrire 13	
METAMORPHIC	Non Foliated		Marble 9	Hornfels (19)	Quartzite 24	
	Slightly foliated		Migmatite (30)	Amphibolite 31	Mylonites (6)	
	Foliated*		Gneiss 33	Schists (10)	Phyllites (10)	Slate 9
IGNEOUS	Light		Granite 33		Rhyolite (16)	Obsidian (19)
			Granodiorite (30)		Dacite (17)	
	Dark		Diorite (28)		Andesite 19	
			Gabbro 27	Dolerite (19)	Basalt (17)	
			Norite 22			
	Extrusive pyroclastic type		Agglomerate (20)	Breccia (18)	Tuff (15)	

*These values are for intact rock specimens tested normal to foliation. The value of m_i will be significantly different if failure occurs along a foliation plane (Hoek, 1983).

where

m_b is the value of the constant m for the rock mass;

s is a constant that depends on the characteristics of the rock mass.

Eq. (4.11) is of no practical value unless the values of the material constants m_b and s can be estimated in some way. Hoek and Brown (1988) proposed a set of relations between the 1976 version of Bieniawski's Rock Mass Rating (RMR) and the parameters m_b and s, as follows:

(i) disturbed rock masses

$$m_b = \exp\left(\frac{RMR-100}{14}\right) m_i \tag{4.12a}$$

$$s = \exp\left(\frac{RMR-100}{6}\right) \tag{4.12b}$$

(ii) undisturbed or interlocking rock masses

$$m_b = \exp\left(\frac{RMR-100}{28}\right) m_i \tag{4.13a}$$

$$s = \exp\left(\frac{RMR-100}{9}\right) \tag{4.13b}$$

Consider the failure pattern shown in Figure 4.5, which is similar to that in soil mechanics, i.e., active and passive wedges are developed in the rock below the shaft base.

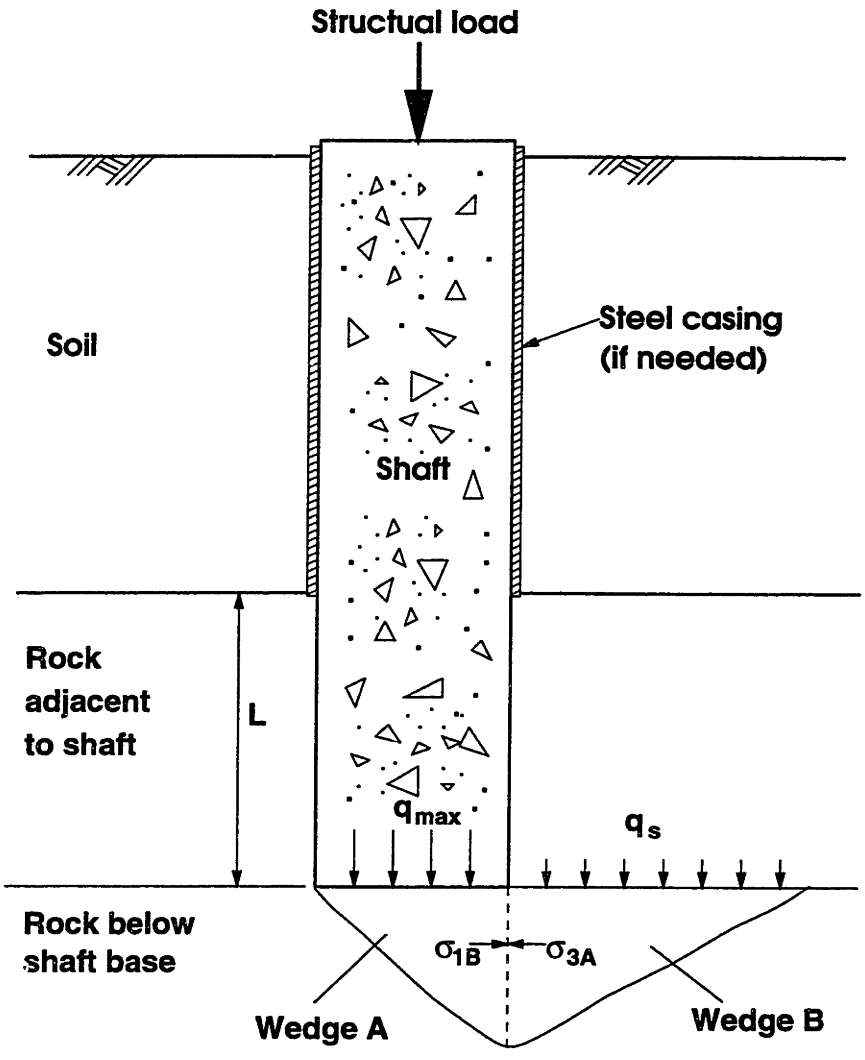

Figure 4.5 Assumed failure mode of rock below the shaft base.

The major principal stress in zone A is equal to the foundation pressure q. Zone B is like a triaxial loading extension test with the major principal stress acting horizontally. The minor principal stress on zone B is the average vertical stress q_s produced by the overburden soil and rock. At foundation failure both zones shear simultaneously and the minor principal σ'_{3A} in zone A is equal to the major principal stress σ'_{1B} in zone B. For zone B, using the Hoek-Brown criterion with σ'_{3B} equal to q_s

$$\sigma'_{1B} = q_s + \sigma_c \left(m_b \frac{q_s}{\sigma_c} + s \right)^{0.5} \tag{4.14}$$

For zone A, using the Hoek-Brown criterion with σ'_{3A} equal to σ'_{1B}, the ultimate end bearing resistance can be obtained as:

$$q_{\max} = \sigma'_{1A} = \sigma'_{1B} + \sigma_c \left(m_b \frac{\sigma'_{1B}}{\sigma_c} + s \right)^{0.5} \tag{4.15}$$

So with known values of rock properties (σ_c, m_b and s), the end bearing resistance of a rock socketed shaft at a given depth (so q_s can be obtained) can be calculated from Eq. (4.20) and (4.21).

Consider the data base shown in Table 4.1. Since the depths to shaft base range from 1 to 20.7 m, an average value of about 10 m is selected. This depth gives a q_s value

of about 0.2 MPa. Based on the rock types in the data base, m_i of 10 is selected according to Table 4.2. Consider a rock mass of good quality with *RMR* equal to 80. m_b and s can be calculated from Eq. (4.13) as:

$$m_b = 5; \qquad s = 0.11$$

With known values of m_b and s, the variation of can q_{max} with σ_c can be determined from Eqs (4.14) and (4.15). The results are shown in Figure 4.6. It can be seen that there a reasonable agreement between the new relation and the theoretical solution.

However, one should be cautious in applying the theoretical solution described above. The reasons are as follows:

1. The Hoek-Brown strength criterion was originally developed for intact rock and then extended to rock masses. The process used by Hoek and Brown in deriving their strength criterion for intact rock (Eq. 10) was one of pure trial and error. Apart from the conceptual starting point provided by the Griffith theory (Griffith 1921 and 1924), there is no fundamental relationship between the empirical constants included in the criterion and any physical characteristics of the rock. The justification for choosing this particular criterion (Eq. 10) over the numerous alternatives lies in the adequacy of its predictions of observed rock fracture behavior, and the convenience of its application to a range of typical engineering problems (Hoek 1983). The material constant m_i in Table 4.2 is derived based upon analyses of published triaxial test results on intact rock (Hoek 1983; Doruk 1991; Hoek et al. 1992). The strength criterion for rock masses (Eq. 4. 11) is just

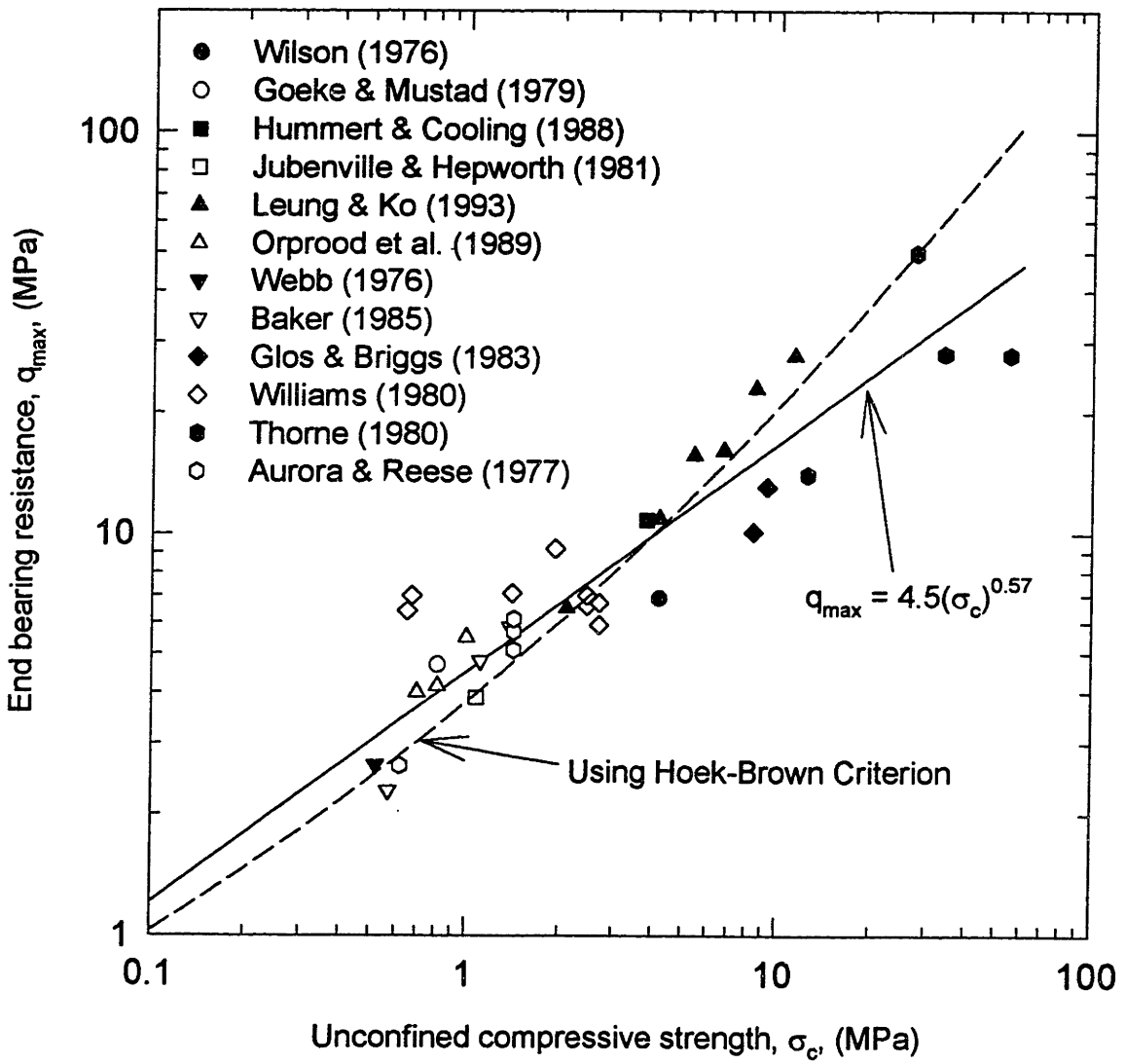

Figure 4.6 End bearing resistance vs. unconfined compressive strength with theoretical results included.

an empirical extension of the criterion for intact rock (Eq. 4.10). Since it is practically impossible to determine the material constants m_b and s using triaxial tests on rock masses, Hoek and Brown (1988) suggested empirical relations (Eqs. 4.12 and 4.13) to estimate constants from Bieniawski's rock mass rating (*RMR*). Bieniawski's rock mass rating (*RMR*) system is also empirical. Because of the empirical nature of the Hoek-Brown strength criterion for rock masses (Eq. 4.11) discussed above, it is uncertain if it will predict the real behavior of rock masses.

2. The failure pattern shown in Figure 4.5, which is similar to that in soil mechanics, implicitly assumes that the rock mass is isotropic and the rock failure is plastic. In reality, however, the rock mass may be anisotropic and the rock failure may be brittle.

CHAPTER 5

DISPLACEMENT OF DRILLED SHAFTS AT WORKING LOAD

5.1 General

Prediction of the displacement of drilled shafts at working load is in some cases as important as, or possibly more critical than, predicting the ultimate load capacity. The available theoretical solutions just model the rock mass as a single half space or, at best, as a two-layer medium (i.e., the rock adjacent to and beneath the rock-socketed shaft). Since, in practice, rock masses are usually multi-layered, a method which can reasonably consider the multi-layer nature of rock masses needs to be developed. In this chapter, a variational model for the analysis of axially loaded drilled shafts socketed in a multi-layer rock mass is presented. Governing differential equations and boundary conditions are derived for a shaft socketed in a rock mass with any number of layers. Theoretically, these differential equations can be solved to get a closed-form solution, no matter how many layers of rock is presented. For simplicity, however, only the closed-form solution for a shaft socketed in a three-layer rock mass is presented. The validation of the

proposed method is demonstrated by comparing with solutions of Pells and Turner (1979) Pells et al. (1980) and Carter and Kulhawy (1988).

5.2 Formulation of the Model

Figure 5.1 shows a typical concrete drilled shaft of length L and radius R, embedded within a multi-layered rock mass. Only the final equilibrium displacement (neglecting creep) at the head of the shaft is considered. The inherent assumptions in the proposed model are:

1. The shaft is an isotropic, homogeneous and elastic solid with a Young's modulus E_p and Poisson's ratio ν_p.
2. The shaft is perfectly connected to the rock. There is no slippage at the interface of the shaft and the surrounding rock.
3. The rock is considered to be isotropic and elastic. There are n layers of rock adjacent to the shaft and the rock beneath the shaft base is homogeneous. The Young's modulus and Poisson's ratio of each layer are as shown in Figure 5.1.

The problem is axisymmetric and therefore cylindrical coordinates (r, θ , z) are used. Based on practical considerations, the radial displacement, $u_r(r, z)$, in the rock mass is considered negligible, compared to the vertical displacement, $w_r(r, z)$, in the rock mass.

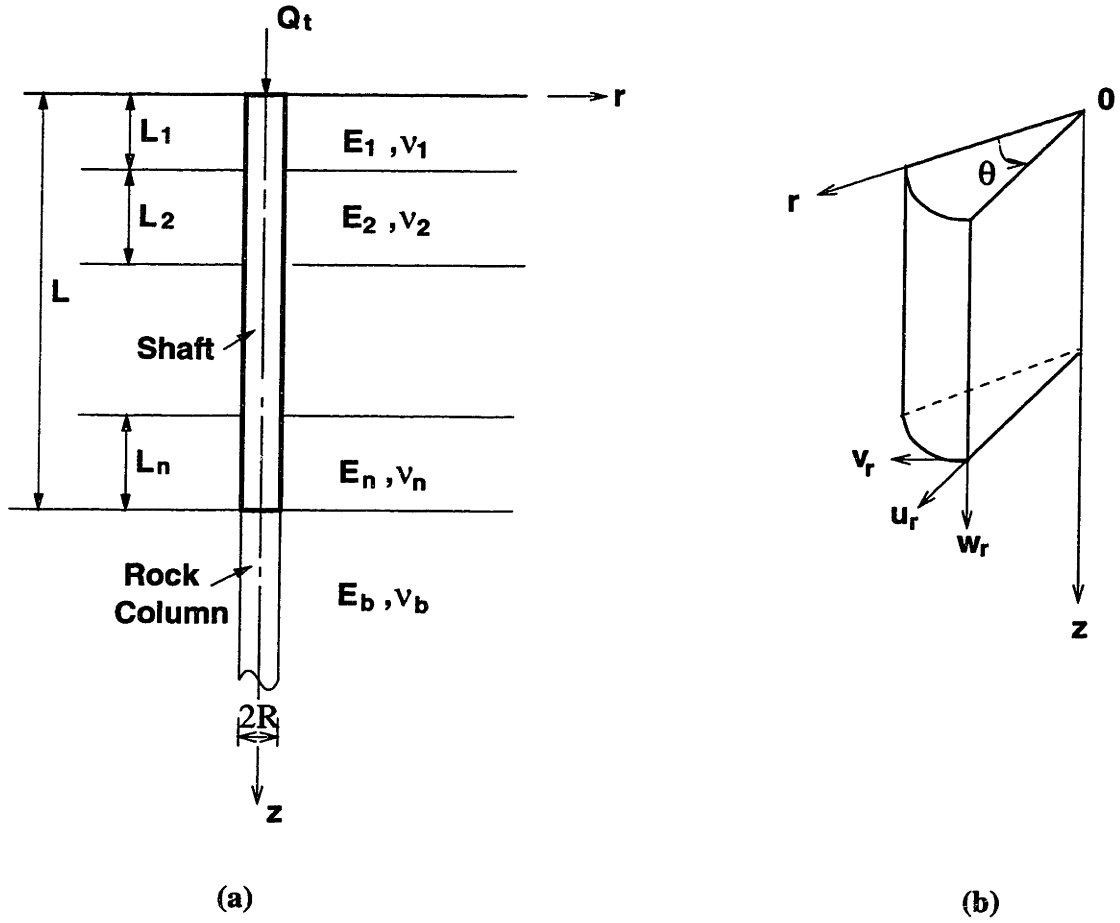

Figure 5.1 (a) Shaft-rock system; (b) Coordinate system and displacement components.

Furthermore, it is assumed that the vertical displacement, $w_r(r, z)$, in the rock mass around the shaft and the rock column (see figure 5.1) can be represented by

$$w_r(r,z) = w(z)\phi(r) \tag{5.1}$$

where

$w(z)$ is the axial displacement of the shaft and the rock column below the shaft base;

$\phi(r)$ is a dimensionless function representing the variation of the rock displacement in the r-direction.

Based on the assumed displacements, there are two non-zero internal strains in the rock mass, namely

$$\varepsilon_{zz} = \frac{dw}{dz}\phi \tag{5.2a}$$

$$\varepsilon_{rz} = \frac{1}{2} w \frac{d\phi}{dr} \tag{5.2b}$$

The corresponding non-zero stress components are

$$\sigma_{rr} = \lambda_i \frac{dw}{dz}\phi \tag{5.3a}$$

$$\sigma_{\theta\theta} = \lambda_i \frac{dw}{dz}\phi \tag{5.3b}$$

$$\sigma_{zz} = (\lambda_i + 2G_i)\frac{dw}{dz}\phi \tag{5.3c}$$

$$\sigma_{rz} = G_i w \frac{d\phi}{dr} \tag{5.3d}$$

where λ_i and G_i (i =1, 2, ..., n, b) are the Lamé parameters of the rock of layer i, which can be obtained by

$$\lambda_i = \frac{\nu_i E_i}{(1+\nu_i)(1-2\nu_i)} \qquad (i = 1,2,\ldots,n,b) \tag{5.4a}$$

$$G_i = \frac{E_i}{2(1+\nu_i)} \qquad (i = 1,2,\ldots,n,b) \tag{5.4b}$$

The total potential energy function of the shaft and rock system can be obtained as

$$\begin{aligned}\Pi = &\frac{1}{2}\int_0^L E_p A_p (\frac{dw}{dz})^2 dz + \frac{1}{2}\int_L^\infty E_b A_b (\frac{dw}{dz})^2 dz \\ &+ \pi\int_0^\infty\int_R^\infty [(\lambda_i + 2G_i)(\frac{dw}{dz})^2\phi^2 + G_i w^2 (\frac{d\phi}{dr})^2]rdrdz - Q_t w\big|_{z=0}\end{aligned} \tag{5.5}$$

where

A_p is the cross-sectional area of the shaft (= πR^2);

A_b is the cross-sectional area of the rock column below the shaft base ($= \pi R^2$);

Q_t is the axial load applied at the shaft head.

Minimizing the function Π with respect to w and using principles of variational calculus, the governing equations for the shaft and rock column can be obtained as

$$t_i \frac{d^2 w_i}{dz^2} - k_i w_i = 0 \qquad (i = 1, 2, ..., n, b) \tag{5.6}$$

with boundary conditions

$$t_1 \frac{dw_1}{dz} + Q_t = 0 \qquad (z = 0) \tag{5.7a}$$

$$w_i = w_{i+1} \qquad \text{(at the interface of layer } i \text{ and } i+1) \tag{5.7b}$$

$$t_i \frac{dw_i}{dz} = t_{i+1} \frac{dw_{i+1}}{dz} \qquad \text{(at the interface of layer } i \text{ and } i+1) \tag{5.7c}$$

$$w_b = 0 \qquad (z \to \infty) \tag{5.7d}$$

where w_i ($i = 1, 2, ..., n, b$) are displacements of the shaft or the rock column in layer i. Parameters t_i and k_i ($i = 1, 2, ..., n, b$) are

$$t_i = \pi R^2 [E_p + 2(\lambda_i + 2G_i) m_1] \qquad (i = 1, 2, ..., n) \tag{5.8a}$$

$$k_i = 2\pi G_i m_2 \qquad (i = 1, 2, ..., n) \tag{5.8b}$$

$$t_b = \pi R^2[E_b + 2(\lambda_b + 2G_b)m_1] \tag{5.8c}$$

$$k_b = 2\pi G_b m_2 \tag{5.8d}$$

in which the nondimensional parameters m_1 and m_2 are

$$m_1 = \frac{1}{R^2}\int_R^\infty r\phi^2 dr \tag{5.9a}$$

$$m_2 = \int_R^\infty r(\frac{d\phi}{dr})^2 dr \tag{5.9b}$$

Consider the differential equation for the rock column (see Figure 5.1a), i.e.,

$$t_b \frac{d^2 w_i}{dz^2} - k_b w_b = 0 \tag{5.10}$$

with boundary conditions

$$w_b = w_n \qquad (z = L) \tag{5.11a}$$

$$w_b = 0 \qquad (z \to \infty) \tag{5.11b}$$

The solution of Eq. (5.10) with boundary conditions of Eq, (5.11) can be derived as

$$w_b(z) = w_n(L)e^{-\alpha_b(z-L)} \tag{5.12}$$

where

$$\alpha_b = \sqrt{\frac{k_b}{t_b}} \tag{5.13}$$

Using Eq. (5.7c), the boundary condition at the shaft base can be derived as

$$t_n \frac{dw_n}{dz} = \sqrt{k_b t_b} w_n \qquad (z = L) \tag{5.14}$$

This shows that the boundary condition at the shaft base ($z = L$) is equivalent to a spring with a spring constant equal to

$$K_b = \sqrt{t_b k_b} \tag{5.15}$$

The boundary condition at $z = 0$ (see Eqs. 5.7a and 5.8a) means that the applied load is shared by the shaft and the rock. Considering the fact that the applied load is carried only by the shaft at $z = 0$, Eq. (5.7a) is modified as

$$E_p A_p \frac{dw_1}{dz} + Q_t = 0 \qquad (z = 0) \tag{5.16}$$

Similarly, minimizing the function Π with respect to ϕ for $R \leq r < \infty$, the following differential equation can be obtained

$$r^2 \frac{d^2\phi}{dr^2} + r\frac{d\phi}{dr} - (\frac{\gamma}{R})^2 r^2 \phi = 0 \tag{5.17}$$

with boundary conditions at $r = R$, $\phi = 1$, and at $r = \infty$, $\phi = 0$ (i.e., the displacement of the rock mass at $r = R$ is equal to the displacement of the shaft or the rock column, i.e., $w_r(r = R, z) = w(z)$, and the displacement of the rock mass at $r = \infty$ is equal to zero). γ is a nondimensional parameter that can be expressed as

$$(\frac{\gamma}{R})^2 = \frac{(\lambda_i + 2G_i)\int_{L_i} (\frac{dw_i}{dz})^2 dz + (\lambda_b + 2G_b)\frac{\alpha_b w_n^2(L)}{2}}{G_i \int_{L_i} w_i^2 dz + G_b \frac{w_n^2(L)}{2\alpha_b}} \qquad (i = 1, 2, ..., n) \tag{5.18}$$

Equation (5.17) is the modified Bessel's equation of order zero, and has the solution

$$\phi(r) = C_1 I_0(\gamma r / R) + C_2 K_0(\gamma r / R) \tag{5.19}$$

where $I_0(\gamma r/R)$ and $K_0(\gamma r/R)$ are the modified Bessel function of the first and second kind of order zero, respectively. Constants C_1 and C_2 can be determined using the boundary conditions in Eq. (5.17). The final solution is

$$\phi(r) = \frac{K_0(\gamma r / R)}{K_0(\gamma)} \tag{5.20}$$

After $\phi(r)$ is obtained, the dimensionless parameters m_1 and m_2 can be derived as

$$m_1 = \frac{1}{2[K_0(\gamma)]^2}\{[K_1(\gamma)]^2 - [K_0(\gamma)]^2\} \tag{5.21a}$$

$$m_2 = \frac{1}{2[K_0(\gamma)]^2}\{[K_1(\gamma) + \gamma K_0(\gamma)]^2 - (\gamma^2 + 1)[K_1(\gamma)]^2\} \tag{5.21b}$$

where K_1 is the modified Bessel function of the second kind of order one.

Summarizing the above derivations, the governing differential equations of the shaft socketed in a multi-layered rock mass are

$$t_i \frac{d^2 w_i}{dz^2} - k_i w_i = 0 \qquad (i = 1, 2, ..., n) \tag{5.22}$$

with boundary conditions

$$E_p A_p \frac{dw_s}{dz} + Q_t = 0 \qquad (z = 0) \tag{5.23a}$$

$$w_i = w_{i+1} \qquad \text{(at the interface of layer } i \text{ and } i+1) \tag{5.23b}$$

$$t_i \frac{dw_i}{dz} = t_{i+1} \frac{dw_{i+1}}{dz} \qquad \text{(at the interface of layer } i \text{ and } i+1) \tag{5.23c}$$

$$t_n \frac{dw_n}{dz} = \sqrt{k_b t_b} w_n \qquad (z = L) \tag{5.23d}$$

In principle, Eq. (5.22) can be solved analytically to get closed-form solutions for any number of layers. For simplicity, however, only the closed-form solutions for a shaft socketed in a three–layer rock mass are presented in next section.

5.3 Displacement of a Shaft socketed in a Three Layer Rock Mass

Consider a shaft socketed in a three-layer rock mass (see Figure 5.2), using the results from last section, the governing equations for the shaft can be written as (from Eq. 5.6)

$$t_s \frac{d^2 w_s}{dz^2} - k_s w_s = 0 \qquad (0 \le z \le L_s) \tag{5.24a}$$

$$t_r \frac{d^2 w_r}{dz^2} - k_r w_r = 0 \qquad (L_s \le z \le L) \tag{5.24b}$$

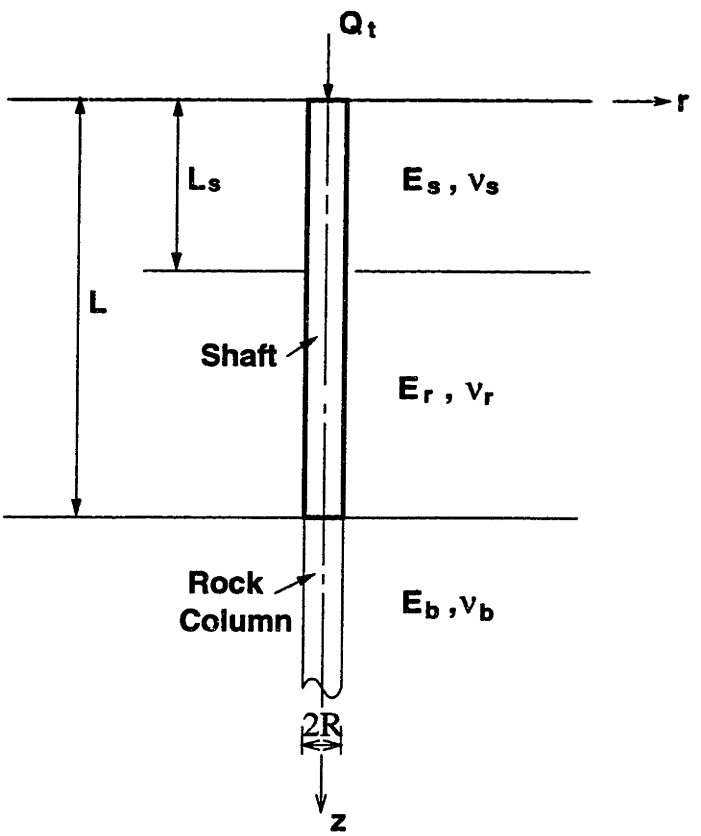

Figure 5.2 A shaft socketed in a three layer rock mass.

with boundary conditions (from Eq. 5.23)

$$t_s \frac{dw_s}{dz} + Q_t = 0 \qquad (z = 0) \tag{5.25a}$$

$$w_s = w_r \qquad (z = L_s) \tag{5.25b}$$

$$t_s \frac{dw_s}{dz} - t_r \frac{dw_r}{dz} = 0 \qquad (z = L_s) \tag{5.25c}$$

$$t_r \frac{dw_r}{dz} + \sqrt{t_b k_b} w_r = 0 \qquad (z = L) \tag{5.25d}$$

where w_s and w_r are displacements of the shaft at $0 \le z \le L_s$ and $L_s \le z \le L$, respectively. Parameters t_i and k_i ($i = s, r, b$) are

$$t_s = \pi R^2 [E_p + 2(\lambda_s + 2G_s)m_1] \tag{5.26a}$$

$$k_s = 2\pi G_s m_2 \tag{5.26b}$$

$$t_r = \pi R^2 [E_p + 2(\lambda_r + 2G_r)m_1] \tag{5.26c}$$

$$k_r = 2\pi G_r m_2 \tag{5.26d}$$

$$t_b = \pi R^2 [E_b + 2(\lambda_b + 2G_b)m_1] \tag{5.26e}$$

$$k_b = 2\pi G_b m_2 \tag{5.26f}$$

Solving Eq. (5.24)

$$w_s(z) = a_1 e^{-\alpha_s z} + a_2 e^{\alpha_s z} \qquad (0 \le z \le L_s) \tag{5.27a}$$

$$w_r(z) = b_1 e^{-\alpha_r z} + b_2 e^{\alpha_r z} \qquad (L_s \le z < \infty) \tag{5.27b}$$

where

$$\alpha_s = \sqrt{\frac{k_s}{t_s}} \tag{5.28a}$$

$$\alpha_r = \sqrt{\frac{k_r}{t_r}} \tag{5.28b}$$

The coefficients a_1, a_2 and b_1, b_2 in Eq. (5.27) can be obtained by applying boundary conditions in Eq. (5.25) as

$$a_1 = \frac{Q_t(K_s\Delta_1 - K_r\Delta_2)e^{2\alpha_s L_s}}{\alpha_s E_p A_p[K_s\Delta_1(e^{2\alpha_s L_s} - 1) - K_r\Delta_2(e^{2\alpha_s L_s} + 1)]} \tag{5.29a}$$

$$a_2 = \frac{Q_t(K_s\Delta_1 + K_r\Delta_2)}{\alpha_s E_p A_p[K_s\Delta_1(e^{2\alpha_s L_s} - 1) - K_r\Delta_2(e^{2\alpha_s L_s} + 1)]} \tag{5.29b}$$

$$b_1 = \frac{2Q_t K_s(K_r + K_b)e^{2\alpha_s L_s + 2\alpha_r L}}{\alpha_s E_p A_p[K_s\Delta_1(e^{2\alpha_s L_s} - 1) - K_r\Delta_2(e^{2\alpha_s L_s} + 1)]} \tag{5.29c}$$

$$b_2 = \frac{2Q_t K_s(K_r - K_b)e^{2\alpha_s L_s}}{\alpha_s E_p A_p[K_s\Delta_1(e^{2\alpha_s L_s} - 1) - K_r\Delta_2(e^{2\alpha_s L_s} + 1)]} \tag{5.29d}$$

where

$$\Delta_1 = (K_r + K_b)e^{(\alpha_s-\alpha_r)L_s+2\alpha_r L} + (K_r - K_b)e^{(\alpha_s+\alpha_r)L_s} \tag{5.30a}$$

$$\Delta_2 = -(K_r + K_b)e^{(\alpha_s-\alpha_r)L_s+2\alpha_r L} + (K_r - K_b)e^{(\alpha_s+\alpha_r)L_s} \tag{5.30b}$$

$$K_s = \sqrt{t_s k_s} \tag{5.30a}$$

$$K_r = \sqrt{t_r k_r} \tag{5.30b}$$

The displacement at the head of the shaft is

$$w_t = w(z=0) = \frac{Q_t[K_s\Delta_1(e^{2\alpha_s L_s}+1) - K_r\Delta_2(e^{2\alpha_s L_s}-1)]}{\alpha_s E_p A_p[K_s\Delta_1(e^{2\alpha_s L_s}-1) - K_r\Delta_2(e^{2\alpha_s L_s}+1)]} \tag{5.31}$$

The nondimensional parameter γ can be rewritten as

$$(\frac{\gamma}{R})^2 = \frac{(\lambda_s + 2G_s)M_s + (\lambda_r + 2G_r)M_r + (\lambda_b + 2G_b)M_b}{G_s N_s + G_r N_r + G_b N_b} \tag{5.32}$$

where M_s, M_r, M_b, N_s, N_r and N_b are parameters given by

$$M_s = \alpha_s[a_1^2(1-e^{-2\alpha_s L_s}) - 4a_1 a_2 \alpha_s L_s + a_2^2(e^{2\alpha_s L_s}-1)] \tag{5.33a}$$

$$M_r = \alpha_r[b_1^2(e^{-2\alpha_r L_s} - e^{-2\alpha_r L}) - 4b_1 b_2 \alpha_r (L-L_s) + b_2^2(e^{2\alpha_r L} - e^{2\alpha_r L_s})] \tag{5.33b}$$

$$M_b = \alpha_b (b_1 e^{-\alpha_r L} + b_2 e^{\alpha_r L})^2 \tag{5.33c}$$

$$N_s = \frac{1}{\alpha_s}[a_1^2 (1 - e^{-2\alpha_s L_s}) + 4a_1 a_2 \alpha_s L_s + a_2^2 (e^{2\alpha_s L_s} - 1)] \tag{5.33d}$$

$$N_r = \frac{1}{\alpha_r}[b_1^2 (e^{-2\alpha_r L_s} - e^{-2\alpha_r L}) + 4b_1 b_2 \alpha_r (L - L_s) + b_2^2 (e^{2\alpha_r L} - e^{2\alpha_r L_s})] \tag{5.33e}$$

$$N_b = \frac{1}{\alpha_b}(b_1 e^{-\alpha_r L} + b_2 e^{\alpha_r L})^2 \tag{5.33f}$$

To evaluate the solution w, the coefficients a_1, a_2 and b_1, b_2 should be obtained (see Eq. 5.27). As can be seen from Eqs. (5.21), (5.26), (5.28), (5.29) and (5.30), the parameter γ is needed to get a_1, a_2 and b_1, b_2. Note that γ defined by Eq. (5.32) depends on a_1, a_2 and b_1, b_2. Since we do not know the value of γ a priori, an iteration procedure is required to obtain its correct value. The procedure is composed of the following steps:

1. Assume $\gamma = 1.0$;

2. Calculate m_1 and m_2 from Eq. (5.21);

3. Calculate parameters t_i, k_i, α_i and K_i (i = s, r, b) using Eqs. (5.13), (5.15), (5.26), (5.28) and (5.30);

4. Calculate the displacement w along the shaft from Eqs. (5.27) and (5.29);

5. Calculate the new value of γ by using Eqs. (5.32) and (5.33);

6. Use the average of the old and new values of γ and repeat steps 2 - 5. Iteration is continued until the difference between the ith and (i + 1)th value of γ

$$|\gamma_{i+1} - \gamma_i| \leq \varepsilon \tag{5.34}$$

where ε is a prescribed convergence tolerance.

After γ is determined, the displacement of the shaft and the load in the shaft can be obtained.

A computer program has been written to execute the above iteration procedure.

5.4 Validation of the Proposed Method

To validate the proposed method, a set of results for the shaft head displacement has been obtained. To compare with the available theoretical solutions by Pells and Turner (1979), Pells et al. (1980) and Carter and Kulhawy (1988) (see chapter 2), two cases are considered: a single layer rock mass (i.e., $E_s = E_r = E_b$) and a two layer rock mass (i.e., $E_s = E_r \neq E_b$). The solutions obtained for the shaft head displacement are expressed in terms of an influence factor I_p defined as

$$I_p = \frac{E_r R w_t}{Q_t} \tag{5.35}$$

where w_t is the shaft head displacement.

The results are plotted in Figure 5.3 and 5.4 respectively for the single layer and the two layer rock mass. Poisson's ratios of 0.25 for the former case and 0.3 for the latter case (for both layers) are used in the calculations. Also plotted are finite element solutions by Pells and Turner (1979) and Pells et al. (1980) and approximate analytical solutions by Carter and Kulhawy (1988). The general agreement between the three solutions is reasonable and could be considered satisfactory for design purposes.

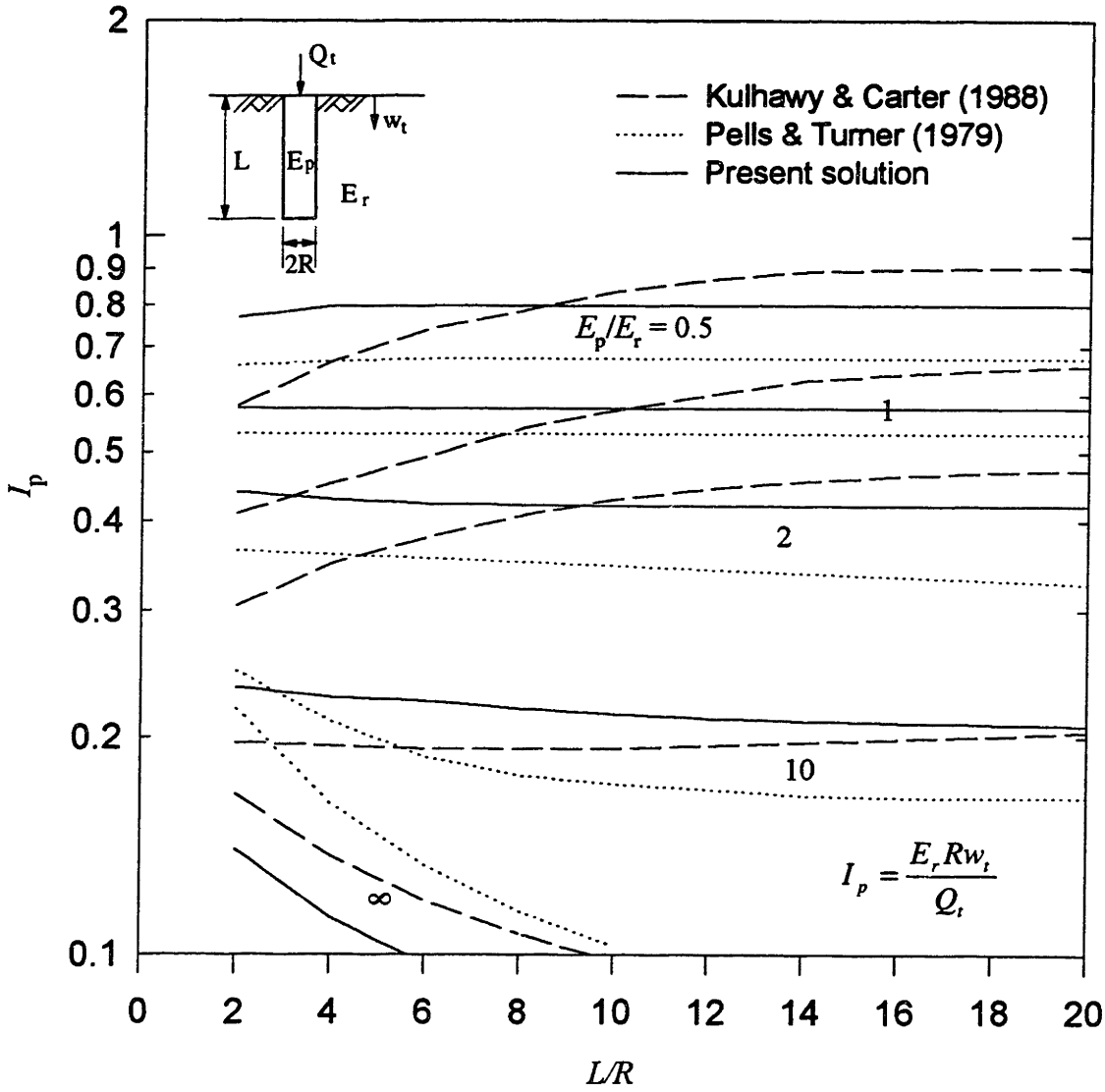

Figure 5.3 Elastic displacement of a drilled shaft in a homogeneous rock mass

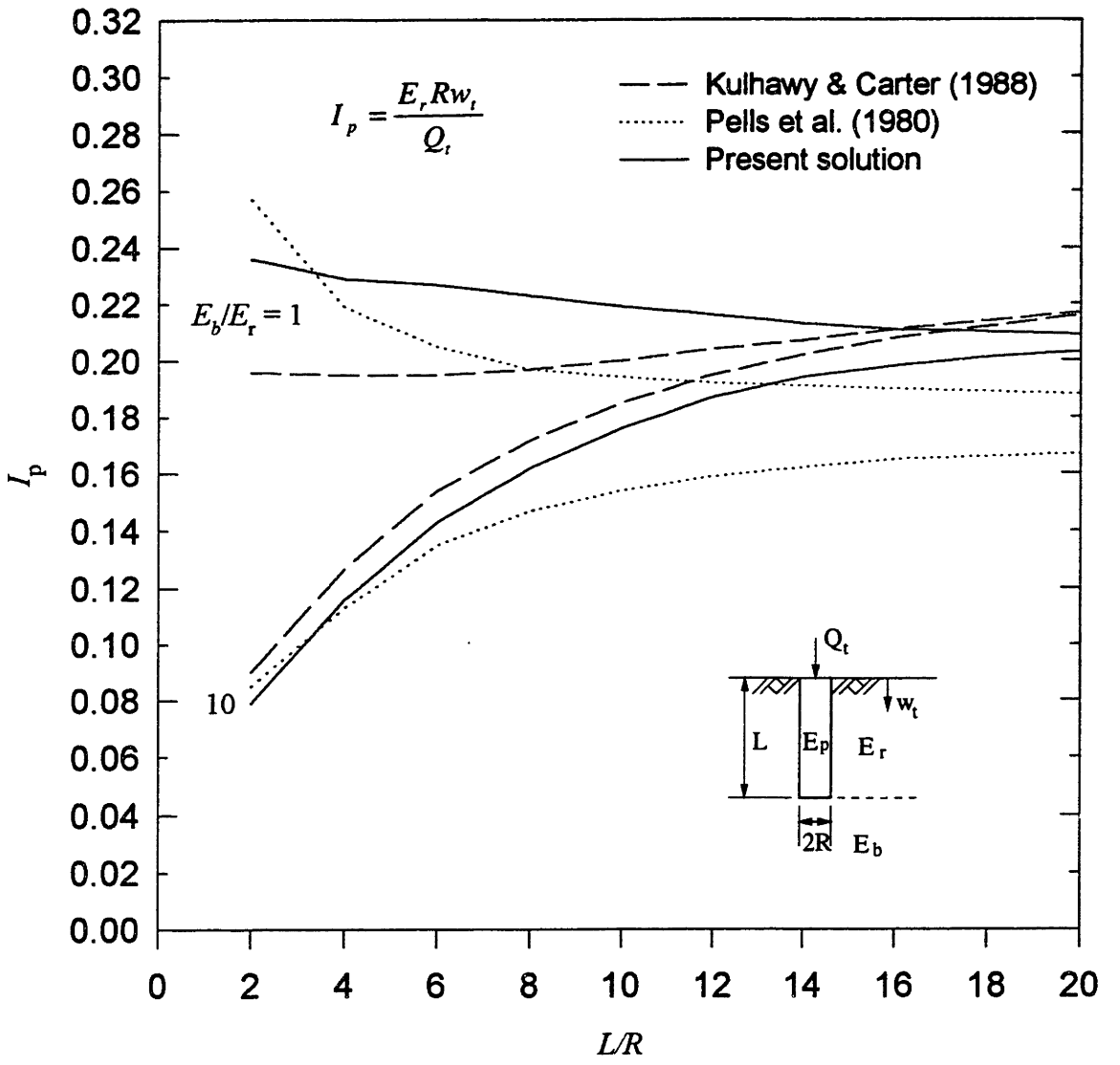

Figure 5.4(a) Elastic displacement of a drilled shaft in a two-layer rock mass ($E_p/E_r = 10$)

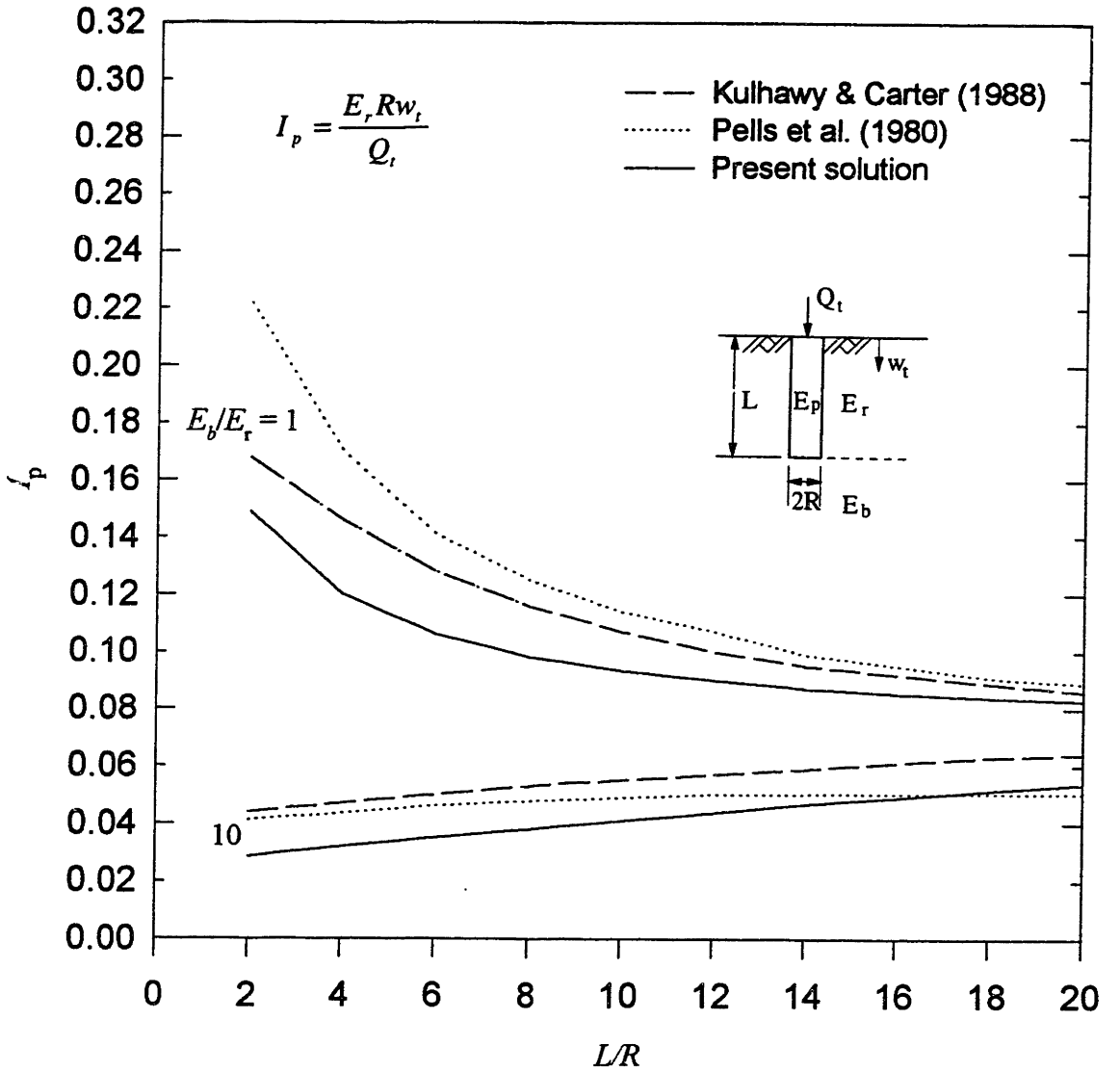

Figure 5.4(b) Elastic displacement of a drilled shaft in a two-layer rock mass ($E_p/E_r = 100$)

CHAPTER 6

SUMMARY AND APPLICATIONS OF THE RECOMMENDED DESIGN METHOD

6.1 General

This chapter provides a summary of the recommended design method for axially loaded drilled shafts socketed into rock. The summary is followed by two examples including three test shafts to show the use of the design method.

6.2 Summary of the Design Method

The proposed design method considers both the allowable load capacity and the displacement at working load. The following is an outline of the design procedure:

1. Determine the following design parameters:

   (i) allowable design displacement, w_a;

(ii) diameter of the shaft, B;

(iii) applied axial load (i.e., the working load), Q_t;

(iv) unconfined compressive strength, σ_c, for each rock layer;

(v) modulus of the shaft, E_p.

2. Estimate the maximum unit side shear resistance, τ_{max}, for each rock layer, as follows:

Smooth socket (R1, R2 or R3): $$\tau_{max} = 0.40(\sigma_c)^{0.5} \quad (4.6a)$$

Rough socket (R4): $$\tau_{max} = 0.80(\sigma_c)^{0.5} \quad (4.6b)$$

3. Estimate the end bearing resistance, q_{max}, as follows:

$$q_{max} = 4.5(\sigma_c)^{0.57} \quad (4.7)$$

4. Determine the socket length L ($= L_1 + L_2 + \ldots + L_n$) using

$$\pi B \sum_{i=1}^{n} L_i (\tau_{max})_i + \frac{\pi B^2}{4} q_{max} \geq FS \cdot Q_t \quad (3.4)$$

where FS is the factor of safety. A value of at least 2 to 3 should be used.

5. Estimate the Young's modulus of the rock mass, E_m, for each layer, using the empirical relations presented in Chapter 3. The Young's modulus of the intact rock, E_i, can be obtained as follows (Rowe and Armitage 1987b)

$$E_i = 215\sqrt{\sigma_c} \tag{2.45}$$

where E_i and σ_c are in MPa.

6. Predict the displacement of the shaft head using the method presented in Chapter 5. This can be done easily and quickly using the computer program.

7. Check if the predicted displacement, w_t, is smaller than the allowable displacement, w_a. If not, increase the socket length and/or diameter and repeat procedure 6. It should be noted that, in some cases, a factor of safety greater than 1 is also used for the displacement criterion.

6.3 Application of the Design Method

The design method for axially loaded drilled shafts socketed in rock, described above, is verified by applying it to field load tests. The following are two examples including three test shafts to illustrate the use of the design method.

6.3.1 Example 1

Aurora and Reese (1977) report four field tests of instrumented drilled shafts socketed into clay-shale. The shafts are constructed by three different construction procedures. Since the properties of the overburden soil are not reported, only the shaft with steel casing penetrating into clay-shale (shaft MT3) is analyzed here. Details of shaft MT3 are shown in Figure 6.1. Some of the properties for the rock socket are as follows:

Unconfined compressive strength of clay-shale σ_c = 1.42 MPa;

Total length of the shaft = 8.22 m;

Socket length L = 1.52 m;

Socket diameter B = 750 mm;

Measured ultimate load at the top of the shaft $(Q_u)_m$ = 5 MN.

Prediction of the ultimate load

Since there is no information about the interface roughness, both 'rough' and 'smooth' conditions are considered. Using Eq. (4.6), the ultimate side shear resistance can be obtained as

Smooth socket:

$$\tau_{max} = 0.40(\sigma_c)^{0.5} = 0.40(1.42)^{0.5} = 0.48\,\text{MPa}$$

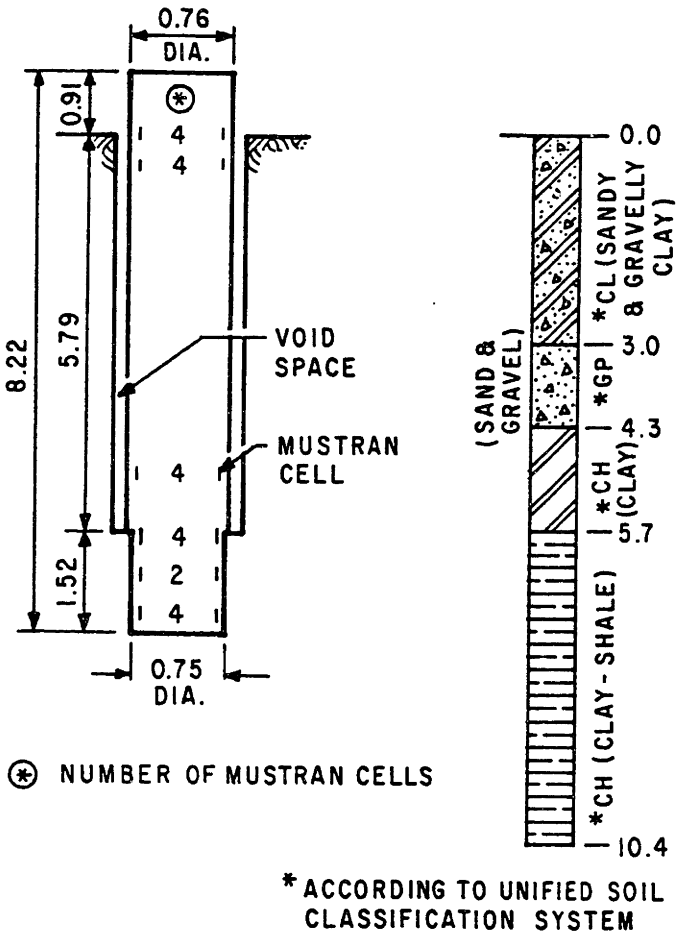

Figure 6.1 Details of shaft MT3 (after Aurora and Reese 1977)

Rough socket:

$$\tau_{max} = 0.80(\sigma_c)^{0.5} = 0.80(1.42)^{0.5} = 0.96 \text{ MPa}$$

The end bearing resistance, q_{max}, can be estimated using Eq. (4.7) as:

$$q_{max} = 4.5(\sigma_c)^{0.57} = 4.5(1.42)^{0.57} = 5.50 \text{ MPa}$$

So the ultimate load capacity can be predicted as:

Smooth socket:

$$Q_u = \pi B \sum_{i=1}^{n} L_i (\tau_{max})_i + \frac{\pi B^2}{4} q_{max}$$

$$= 3.14 * 0.75 * 1.52 * 0.48 + \frac{3.14 * 0.75^2}{4} * 5.5$$

$$= 4.15 MN$$

Rough socket:

$$Q_u = \pi B \sum_{i=1}^{n} L_i (\tau_{max})_i + \frac{\pi B^2}{4} q_{max}$$

$$= 3.14 * 0.75 * 1.52 * 0.96 + \frac{3.14 * 0.75^2}{4} * 5.5$$

$$= 5.89 MN$$

It can be seen that the measured value of $(Q_u)_m$ = 5 MN is in the range of the predicted values. The average of the predicted values is 5.02 MN which is almost the same as the measured value. Using the average of 5.02 MN for the predicted ultimate load and selecting a value of 2 for the factor of safety, the working load can be predicted as

$$Q_t = \frac{Q_u}{FS} = \frac{5.02}{2} = 2.51 MN$$

Displacement at working load

The elastic modulus of the shaft is not reported in the original paper. Since, in general, the elastic modulus of the shaft concrete is in the range of 25 to 35 MPa, an average value of E_p = 30 MPa is selected. The elastic modulus of the clay-shale is estimated from the unconfined compressive strength, i.e.,

$$E_m = 215\sqrt{\sigma_c} = 215\sqrt{1.42} = 256 MPa$$

With the known values of the moduli of the shaft and the clay-shale, the displacement of the top of the rock socket can be predicted using the method presented in Chapter 5. The total top displacement can be obtained by adding the elastic shortening of the portion of the shaft in the overburden to the corresponding displacement of the top of the rock socket. Figure 6.2 shows the predicted and observed load-top displacement curves. It can

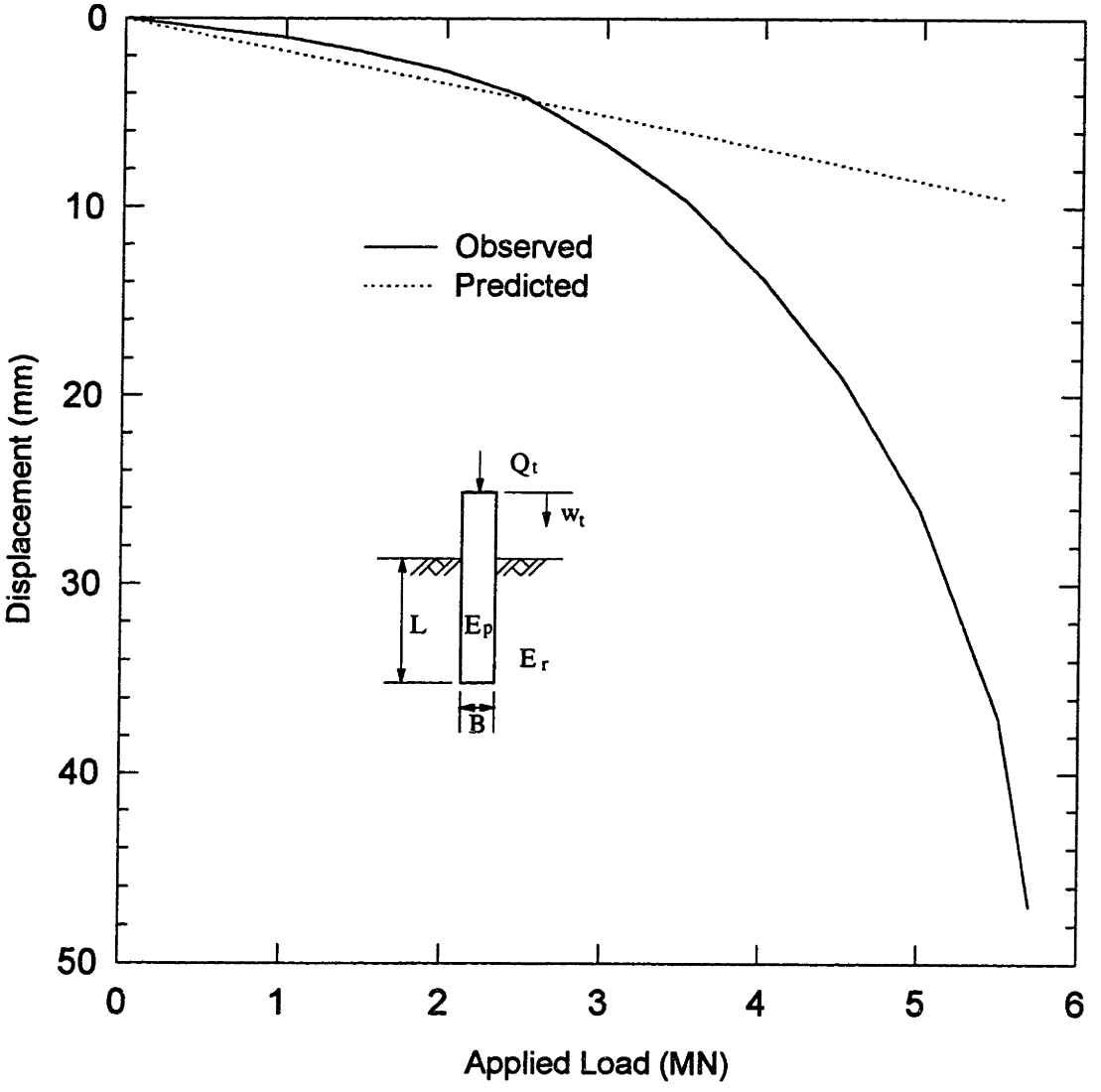

Figure 6.2 Predicted and observed load-displacement curves for example 1. (Displacements measured and predicted at top of the shaft)

be seen that, at the predicted working load of 2.51 MN, the predicted and observed displacements are in a good agreement.

6.3.2 Example 2

Two field tests of instrumented drilled shafts socketed into a layered rock mass are reported by Goeke and Hustad (1979). The subsurface profile and shaft embedments are shown in Figure 6.3. Since the clay-shale at a depth between 3.4 m and 5.8 m is soft and highly weathered and the measured load transfer curves show that little load is transferred in this zone, the side shear resistance in this zone is assumed to be zero in the following analyses.

(a) Shaft 1

Shaft 1 can be treated as a shaft socketed in a two layer rock mass (see Figure 6.4). The corresponding properties for the rock socket are as follows:

Unconfined compressive strength: $(\sigma_c)_r = 0.70$ MPa;

$(\sigma_c)_b = 0.81$ MPa;

Total length of the shaft = 8.8 m;

Socket length $L = 3.0$ m;

Socket diameter $B = 762$ mm;

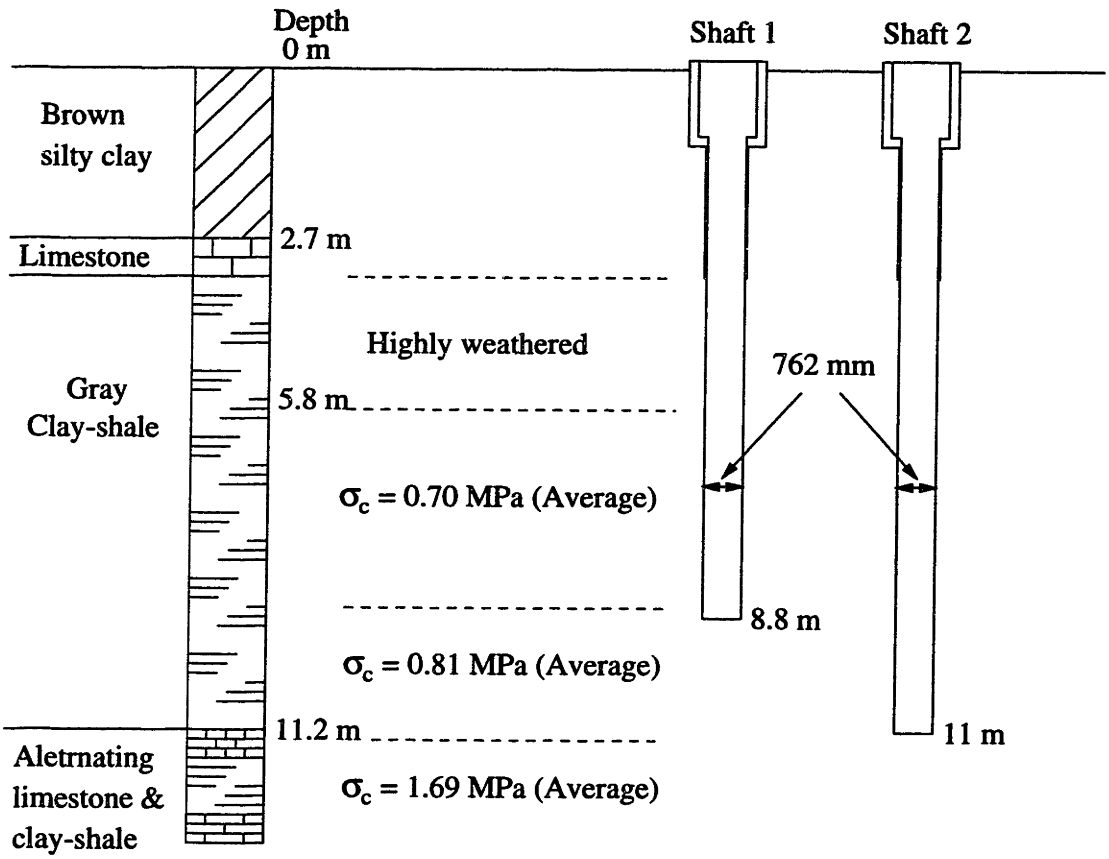

Figure 6.3 Subsurface profile and shaft embedments for example 2.

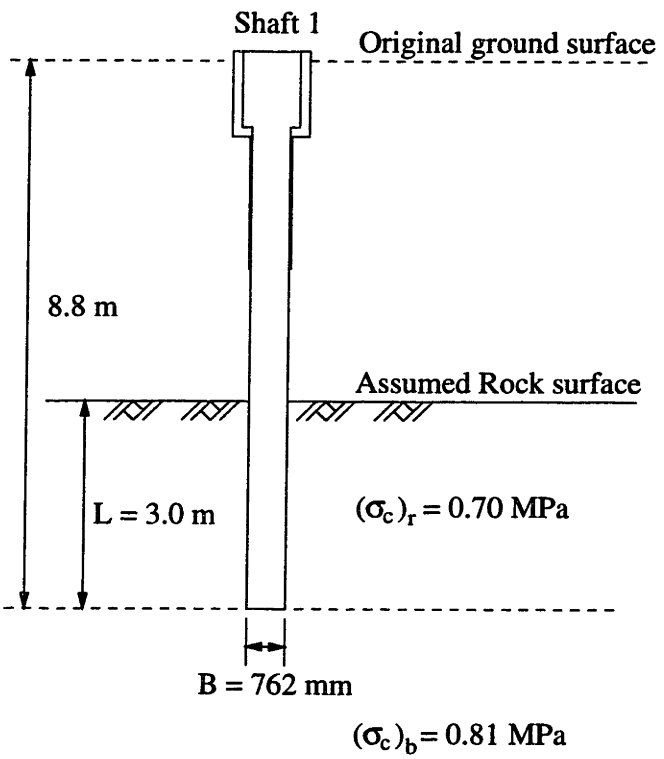

Figure 6.4 Idealization of shaft 1 as a socket in a two layer rock mass.

Measured ultimate load at the top of the shaft $(Q_u)_m = 4.98$ MN.

Prediction of the ultimate load

Since no information about the interface roughness is given in the original paper, both 'rough' and 'smooth' conditions are considered. Using Eq. (4.6), the ultimate side shear resistance can be obtained as

Smooth socket:

$$\tau_{max} = 0.40(\sigma_c)^{0.5} = 0.40(0.70)^{0.5} = 0.33\,\text{MPa}$$

Rough socket:

$$\tau_{max} = 0.80(\sigma_c)^{0.5} = 0.80(0.70)^{0.5} = 0.67\ \text{MPa}$$

The end bearing resistance, q_{max}, can be estimated using Eq. (4.7) as:

$$q_{max} = 4.5(\sigma_c)^{0.57} = 4.5(0.81)^{0.57} = 3.99\ \text{MPa}$$

So the ultimate load capacity can be predicted as:

Smooth socket:

$$(Q_u)_m = \pi B \sum_{i=1}^{n} L_i (\tau_{\max})_i + \frac{\pi B^2}{4} q_{\max}$$

$$= 3.14 * 0.762 * 3.0 * 0.33 + \frac{3.14 * 0.762^2}{4} * 3.99$$

$$= 4.19\,MN$$

Rough socket:

$$(Q_u)_m = \pi B \sum_{i=1}^{n} L_i (\tau_{\max})_i + \frac{\pi B^2}{4} q_{\max}$$

$$= 3.14 * 0.762 * 3.0 * 0.67 + \frac{3.14 * 0.762^2}{4} * 3.99$$

$$= 6.63\,MN$$

It can be seen that the measured value of $(Q_u)_m$ = 4.98 MN is in the range of the predicted values. The average of the predicted values is 5.41 MN which is close to the measured value. Using the average of 5.41 MN for the predicted ultimate load and selecting a value of 2 for the factor of safety, the working load can be predicted as

$$Q_t = \frac{Q_u}{FS} = \frac{5.41}{2} = 2.7\,MN$$

Displacement at working load

The elastic modulus of the shaft is not reported in the original paper. As in Example 1, a value of E_p = 30 MPa is selected. The elastic moduli of the rock masses are estimated from the unconfined compressive strengths, i.e.,

$$(E_m)_r = 215\sqrt{\sigma_c} = 215\sqrt{0.70} = 180\,MPa$$

$$(E_m)_b = 215\sqrt{\sigma_c} = 215\sqrt{0.81} = 194\,MPa$$

With the known values of the moduli of the shaft and the rock masses, the displacement of the top of the rock socket can be predicted using the method presented in Chapter 5. The total top displacement can be obtained by adding the elastic shortening of the portion of the shaft in the overburden to the corresponding displacement of the top of the rock socket. Figure 6.5 shows the predicted and observed load-top displacement curves. It can be seen that, at the predicted working load of 2.7 MN, the predicted and observed displacements are in a good agreement.

(b) Shaft 2

Shaft 2 can be treated as a shaft socketed in a three layer rock mass (see Figure 6.6). The corresponding properties for the rock socket are as follows:

Unconfined compressive strength: $(\sigma_c)_s$ = 0.70 MPa;

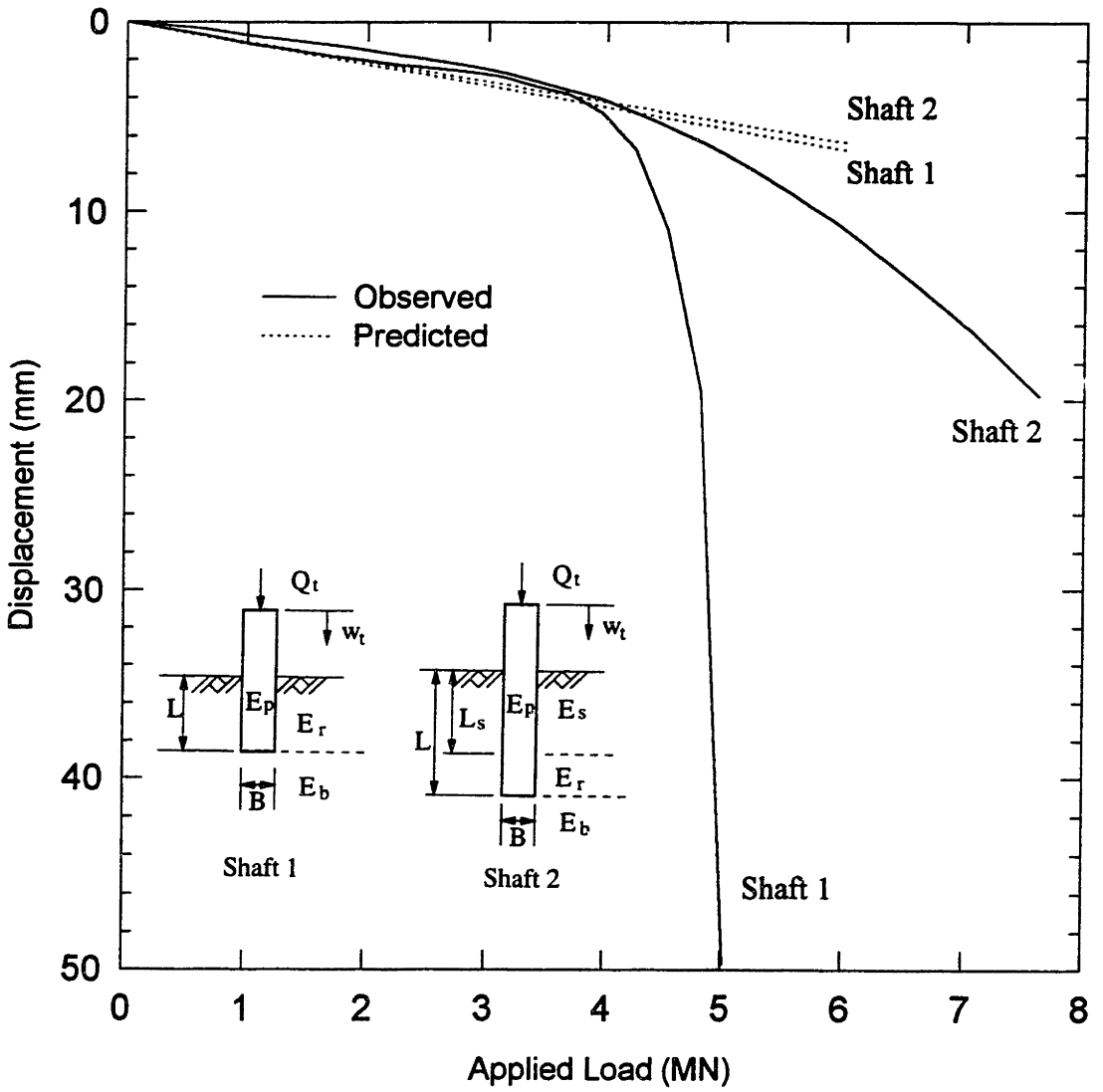

Figure 6.5 Predicted and observed load-displacement curves for example 2. (Displacements measured and predicted at top of the shaft)

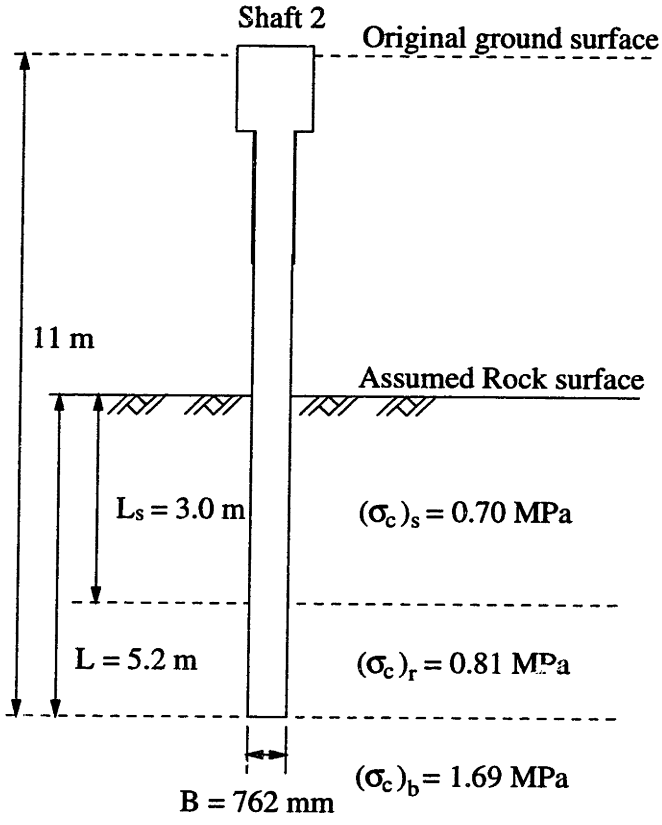

Figure 6.6 Idealization of shaft 2 as a socket in a three layer rock mass.

$(\sigma_c)_r = 0.81$ MPa;

$(\sigma_c)_b = 1.69$ MPa;

Total length of the shaft = 11 m;

Total socket length $L = 5.2$ m;

Length of the socket in layer 's' $L_s = 3$ m

Socket diameter $B = 762$ mm;

Measured ultimate load of the shaft $(Q_u)_m = 10$ MN.

Prediction of the ultimate load

Since there is no information about the interface roughness, both 'rough' and 'smooth' conditions are considered. Using Eq. (4.6), the ultimate side shear resistance can be obtained as

Smooth socket:

$$(\tau_{max})_s = 0.40(\sigma_c)_s^2 = 0.40(0.70)^{0.5} = 0.33\,\text{MPa}$$

$$(\tau_{max})_r = 0.40(\sigma_c)_r^2 = 0.40(0.81)^{0.5} = 0.36\,\text{MPa}$$

Rough socket:

$$(\tau_{max})_s = 0.80(\sigma_c)_s^2 = 0.80(0.70)^{0.5} = 0.67\,\text{MPa}$$

$$(\tau_{max})_r = 0.80(\sigma_c)_r^2 = 0.80(0.81)^{0.5} = 0.72\,\text{MPa}$$

The end bearing resistance, q_{max}, can be estimated using Eq. (4.7) as:

$$q_{max} = 4.5(\sigma_c)_b^{0.57} = 4.5(1.69)^{0.57} = 6.07 \text{ MPa}$$

So the ultimate load capacity can be predicted as:

Smooth socket:

$$(Q_u)_m = \pi B \sum_{i=1}^{n} L_i (\tau_{max})_i + \frac{\pi B^2}{4} q_{max}$$

$$= 3.14 * 0.762 * (3 * 0.33 + 2.2 * 0.36) + \frac{3.14 * 0.762^2}{4} * 6.07$$

$$= 7.03 MN$$

Rough socket:

$$(Q_u)_m = \pi B \sum_{i=1}^{n} L_i (\tau_{max})_i + \frac{\pi B^2}{4} q_{max}$$

$$= 3.14 * 0.762 * (3 * 0.67 + 2.2 * 0.72) + \frac{3.14 * 0.762^2}{4} * 6.07$$

$$= 11.38 MN$$

The measured value of $(Q_u)_m$ = 10 MN is in the range of the predicted values. The average of the predicted values is 9.21 MN which is close to the measured value. Using the average of 9.21 MN for the predicted ultimate load and selecting a value of 2 for the factor of safety, the working load can be predicted as

$$Q_t = \frac{Q_u}{FS} = \frac{9.21}{2} = 6.61 MN$$

Displacement at working load

The elastic modulus of the shaft is not reported in the original paper. As for shaft 1, a value of E_p = 30 MPa is selected. The elastic moduli of the rock masses are estimated from the unconfined compressive strengths, i.e.,

$$(E_m)_s = 215\sqrt{\sigma_c} = 215\sqrt{0.70} = 180 MPa$$

$$(E_m)_r = 215\sqrt{\sigma_c} = 215\sqrt{0.81} = 194 MPa$$

$$(E_m)_b = 215\sqrt{\sigma_c} = 215\sqrt{1.69} = 280 MPa$$

With the known values of the moduli of the shaft and the rock masses, the displacement of the top of the rock socket can be predicted using the method presented in Chapter 5. The total top displacement can be obtained by adding the elastic shortening of the portion

of the shaft in the overburden to the corresponding displacement at the top of the rock socket. The predicted and observed load-top displacement curves are also shown in Figure 6.5. At the predicted working load of 4.61 MN, the predicted and observed displacements are in a reasonable agreement.

CHAPTER 7

SUMMARY, CONCLUSIONS AND RECOMMENDATIONS

7.1 Summary and Conclusions

The preferred method to design drilled shafts socketed into rock would be on the basis of size specific large field tests. However, because field tests are very expensive, full-scale testing is seldom performed. As an alternative, empirical relations proposed by several authors are often used to predict ultimate loads (e.g., Williams and Pells 1981; Rowe and Armitage 1987b; Kulhawy and Phoon 1993). To predict the load deformation response at working loads, theoretical solutions have been developed by, for example, Pells and Turner (1979) and Rowe and Armitage (1987a). The literature review presented in Chapter 2 shows that

1. The available empirical relations for estimating the ultimate side shear resistance can be divided in two major groups: a) The ultimate side shear resistance is a simple constant times the unconfined compressive strength; and b) The relationship between the ultimate side shear resistance and the

unconfined compressive strength is a power-curve. The relations suggested by different authors give a wide range of values. This is because the relations are derived from different data bases.

2. The available relations for estimating the end bearing resistance assume a linear relationship between the end bearing resistance and the unconfined compressive strength. However, the linear relations produce results which deviate significantly from the field tests.
3. Current design methods just model the rock mass as a single half space or at best, as two-layer medium (i.e., the rock adjacent to and beneath the shaft). This is a very crude approximation to the multi-layered rock mass in reality.

Because of the limitations of the current design methods, a new design model was proposed. The new design method can reasonably predict the ultimate side shear resistance and the end bearing resistance. It also considers the multi-layer nature of the rock mass. The following are some of the main points about the new design method:

1. For the ultimate side shear resistance, a study of the results of many load tests indicated that a power-curve relationship between the ultimate side shear resistance and the unconfined compressive strength is closer to the real cases. By analyzing the available power-curve relations, a new relation (Eq. 4.6) was recommended.

2. For the end bearing resistance, a data base of 35 loading tests was developed. By analyzing the collected data, a new relation between the end bearing resistance and the unconfined compressive strength was derived (Eq. 4.7).
3. For the prediction of the displacement of drilled shafts at working load, a model was developed for the analysis of axially loaded drilled shafts socketed in a multi-layered rock mass. Governing differential equations and boundary conditions were derived for a shaft socketed in a rock mass with any number of layers. A closed-form solution for a shaft socketed in a three-layer rock mass was presented. The proposed model was validated by comparing it with available theoretical solutions.
4. The detailed procedure of the proposed design method is summarized in Chapter 6. Two examples including three test shafts are given to show the use of the design method. The results indicate that the proposed method can satisfactorily predict the ultimate loads and the displacements at working loads.

7.2 Recommendations for Future Research

The following are recommendations for future research:

1. The socket interface conditions significantly affect the performance of drilled shafts. Therefore, the load transfer mechanisms of "smooth sockets" and

"rough sockets" should be studied. This can be done theoretically and experimentally.

2. To reasonably design rock sockets, it is desirable to predict the borehole conditions, i.e., smooth, rough or smeared, during the design phase. It is believed that these conditions are related to the characteristics of the rock and the type of drilling techniques.
3. More field load test data should be collected to verify the derived relation for predicting the end bearing resistance. The physical experimentation should actually be expanded by controlled tests not only in the field but also in the laboratory. The finite element method or the boundary element method can be used to investigate the end bearing failure mechanism. Also, the fracture mechanisms that may develop at the base of the socket should be taken into account.
4. The long-term behavior of drilled shafts socketed into rock should be investigated.

References

Aurora, R. P., and Reese, L. C. (1977). "Filed test of drilled shafts in clay shale." *Proceedings, 9th International Conference on Soil Mechanics and Foundation Engineering*, Tokyo, Japan, 371-376.

Baker, C. N., Jr. (1985). "Comparison of caisson load tests on Chicago hardpan." Drilled Piers and Caissons II, Ed. By C. N. Jr. baker, ASCE, Denver, Colorado, 99-113.

Baker, C. N., Jr. (1994). "Current U.S. design and construction practice for drilled piers." *Proceedings, International Conference on Design and Construction of Deep Foundations.* Orlando, FL, 305-323,

Barton, N. (1976). "The shear strength of rock and rock joints." *International Journal of Rock Mechanics and Mining Science and Geomechanics Abstracts*, 13, 255-279.

Barton, N., Loset., F., Lien, R., and Lunde, J. (1980). "Application of the Q-system in design decisions." *Subsurface Space*, Ed. by M. Bergman, 2, 553-561.

Barton, N., and Bandis, S. C. (1982). " Effects of block size on the shear behavior of jointed rock." *23rd U.S. Symposium on Rock Mechanics*, Berkeley, 739-760.

Barton, N., and Bandis, S. C. (1990). "Review of predictive capabilities of JRC-JCS model in engineering practice." *Proceedings, International Symposium on Rock Joints, Loen, Norway*, Ed. by N. Barton and O. Stephansson, Balkema, Rotterdam, 603-610.

Bieniawski, Z. T. (1974). "Geomechanics classification of rock masses and its application in tunneling." *Proceedings, 3rd International Conference on Rock Mechanics.* Denver, Vol. 2, Part 2, 27-32.

Bieniawski, Z. T. (1976). "Geomechanics classification in rock engineering." *Proceedings, Symposium on Exploration for Rock Engineering.* Ed. by Z. T. Bieniawski, A. A. Balkema, Rotterdam, 97-106.

Bieniawski, Z. T. (1978). "Determining rock mass deformability: experience from case histories." *International Journal of Rock Mechanics and Mining Science and Geomechanics Abstracts*, 15, 237-248.

Bieniawski, Z. T. (1984). *Rock mechanics design in Mining and Tunneling*. Balkema, Rotterdam/Boston, 272pp.

Carter, J. P., and Kulhawy, F. H. (1988). "Analysis and design of drilled shafts foundations socketed into rock." *Report EL-5918*, Electric Power Research Institute, Palo Alto, California, 188pp.

CGS. (1992). *Canadian Foundation Engineering Manual*, 3rd Ed. Canadian Geotechnical Society, Toronto, Ont.

Coates, D. F. (1967). *Rock mechanics principle*. Energy Mines and Resources, Ottawa, Canada, Monograph 874.

Davis, E. H. (1968). "Theories of plasticity and the failure of soil masses." Chapter 6 in *Soil mechanics: Selected Topics*, Ed. By I. K. Lee, Butterworths, London, 341-380.

Donald, I. B., Sloan, S. N., and Chiu, H. K. (1980). "Theoretical analysis of rock-socketed piles." *Proceedings, International Conference on Structural Foundations on Rock*, Sydney, 1, 303-316.

Dykeman, P., and Valsangkar, A. J. (1996). "Model studies of socketed caissons in soft rock." *Canadian Geotechnical Journal*, 33(5), 747-759.

Glos, G. H., III, and Briggs, O. H., Jr. (1983). "Rock sockets in soft rock." *Journal of Geotechnical Engineering*, ASCE, 109(4), 525-535.

Goeke, P. M., and Hustard, P. A. (1979). "Instrumented drilled shafts in clay-shale." *Symposium on Deep Foundations*, Ed. by E. M. Fuller, ASCE National Convention, Atlanta, Georgia, 149-164.

Goodman, R. E. (1980). *Introduction to Rock Mechanics*, Wiley, New York.

Gupton, C., and Logan, T. (1984). "Design guidelines for drilled shafts in weak rocks of south Florida." *Proceedings, South Florida Annual ASCE Meeting*, ASCE.

Hassan, K. M., and O'Neill, M. W. (1997). "Side load transfer mechanism in drilled shafts in soft argillaceous rock." *Journal of Geotechnical Engineering*, ASCE, 123(2), 272-280.

Hassan, K. M., and O'Neill, M. W., Sheikh, S. A., and Ealy, C. D. (1997). "Design method for drilled shafts in soft argillaceous rock." *Journal of Geotechnical Engineering*, ASCE, 123(3), 272-280.

Hoek, E., and Brown, E. T. (1980). "Empirical strength criterion for rock masses." *Journal of Geotechnical Engineering*, ASCE, 106, 1013-1035.

Hoek, E. (1983). "Strength of jointed rock masses. 23rd Rankine Lecture." *Geotechnique*, 33(3), 187-223.

Hoek, E., and Brown, E. T. (1988). "The Hoek-Brown criterion - a 1988 update." Proceedings, *15th Canadian Rock Mechanics Symposium*, University of Toronto, Canada, 31-38.

Hoek, E., Wood, D., and Shah, S. (1992). "A modified Hoek-Brown criterion for jointed rock masses." *Proceedings, Rock Characterization, Symposium of ISRM: Eurock'92*, Ed: J A. Hudson, 209-214.

Hoek, E., Kaiser, P. K., and Bawden, W. F. (1995). *Support of Underground Excavations in Hard Rock*. A. A. Balkema, Rotterdam.

Horvath, R. G., Kenney, T. C., and Trow, W. P. (1980). "Results of tests to determine shaft resistance of rock-socketed drilled piers." *Proceedings, International Conference on Structural Foundations on Rock*, Sydney, 1, 349-361.

Horvath, R. G., Kenney, T. C., and Kozicki, P. (1980). "Method of improving the performance of drilled piers in weak rock." *Canadian Geotechnical Journal*, 20(4), 758-772.

Horvath, R. G. (1982). *Drilled piers socketed into weak shale – methods of improving performance*. Ph.D. Dissertation, University of Toronto, Toronto, Ontario, Canada.

Hummert, J. B., and Cooling, T. L. (1988). "Drilled pier test, Fort Collins Colorado." *Proceedings, 2nd International Conference on Case Histories in Geotechnical Engineering*, St. Louis, Missouri, 3, 1375-1382.

Johnston, I. W. (1992). "New developments in the predictions of side resistance of piles in soft rock." Civil Engineering Department, Monash University, Clayton, Victoria, Australia.

Jubenville, M. D., and Hepworth, R. C. (1981). "Drilled pier foundations in shale – Denver Colorado area." *Drilled Piers and Caissons, Proceedings of the Session at the ASCE National Convention*, St. Louis, Missouri, 66-81.

Kodikara, J. K., Johnston, I. W., and Haberfield, C. M. (1992). "Analytical predictions of shear resistance of piles in rock." *Proceedings, Sixth Australia-New Zealand Conference on Geomechanics*, Christchurch, New Zealand, 156-162.

Kulhawy, F. H. (1978). "Geomechanical model for rock foundation settlement." *Journal of Geotechnical Engineering*, ASCE, 104(2), 211-227.

Kulhawy, F. H., and Goodman, R. E. (1980). "Design of foundations on discontinuous rock." *Proceedings, International Conference on Structural Foundations on Rock*, Sydney, 1, 209-220.

Kulhawy, F. H., and Goodman, R. E. (1987). "Foundation in rock." Ground Engineering Reference Book, Ed. By F. G. Bell, Butterworth, London, 55/1-55/13.

Kulhawy, F. H. (1991). "Drilled shaft foundations." *Foundation Engineering Book.* Ed. by Fang, H. Y., Van Nostrand Reinhold, NY, 537-552.

Kulhawy, F. H., and Phoon, K. K. (1993). "Drilled shaft side resistance in clay soil to rock." *Proceedings, Conference on Design and Performance of Deep Foundations: Piles and Piers in Soil and Soft Rock*, Geotechnical Special Publication No. 38, 172-183.

Leung, C. F., and Ko, H-Y (1993). "Centrifuge model study of piles socketed in soft rock." *Soils and Foundations*, 33(3), 80-91.

McVay, M. C., Twonsend, F. C., and Williams, R. C. (1992). "Design of socketed drilled shafts in limestone." Journal of Geotechnical Engineering, 118(10), 1626-1637.

Meigh, A. C., and Wolski, W. (1979). "Design parameters for weak rocks." Proceeding, 7th European Conference on Soil Mechanics and Foundation Engineering, Brighton, British Geotechnical Society, 5, 57-77.

Orpwood, T. G., Shaheen, A. A., and Kenneth, R. P. (1989). "Pressuremeter evaluation of glacial till bearing capacity in Toronto, Canada." *Foundation Engineering: Current Principles and Practices*. Ed. By F. H. Kulhawy, ASCE, 1, 16-28.

Osterberg, J. O., and Gill, S. A. (1973). 'Load transfer mechanisms for piers socketed in hard soils or rock." *Proceedings, 9th Canadian Symposium on Rock Mechanics*, Montreal, 235-262.

Pabon, G., and Nelson, P. P. (1993). "Behavior of instrumented model piers in manufactured rock with a soft layer." *Geotechnical Special Publication No. 39*, ASCE, 260-276.

Pells, P. J. N., and Turner, R. M. (1979). "Elastic solutions for the design and analysis of rock-socketed piles." *Canadian Geotechnical Journal*, 16, 481-487.

Pells, P. J. N., and Turner, R. M. (1980). "End-bearing on rock with particular reference to sandstone." *Proceedings, International Conference on Structural Foundations on Rock*, Sydney, 1, 181-190.

Pells, P. J. N., Rowe, R. K., and Turner, R. M. (1980). "An experimental investigation into side shear for socketed piles in sandstone." *Proceedings, International Conference on Structural Foundations on Rock*, Sydney, 1, 291-302.

Poulos, H. G., and Mattes, N. S. (1969). "The behavior of axially-loaded end-bearing piles." *Geotechnique*, 19(2), 285-300.

Poulos, H. G., and Davis, E. H. (1974). *Elastic Solutions for Soil and Rock Mechanics.* Wiley and Sons, NY.

Randolph, M. F., and Wroth, C. P. (1978). "Analysis of deformation of vertically loaded piles." Journal of geotechical Engineering, 104(12), 1465-1488.

Reese, L. C., and O'Neill, M. W. (1987). "Drilled shafts: construction procedures and design methods." *Design manual*, U.S. Department of Transportation, Federal Highway Administration, Mclean, VA.

Reynolds, R. T., and Kaderabek, T. J. (1980). "Miami limestone foundation design and construction." ASCE, New York, N.Y.

Rosenberg, P., and Journeaux, N. L. (1977). "Friction and bearing tests on bedrock for high capacity socket design." *Canadian Geotechnical Journal*, 113(3), 324-33.

Rowe, R. K., and Armitage, H. H. (1987a). "Theoretical solutions for axial deformation of drilled shafts in rock." *Canadian Geotechnical Journal*, 24, 114-125.

Rowe, R. K., and Armitage, H. H. (1987b). "A design method for drilled piers in weak rock." *Canadian Geotechnical Journal*, 24, 126-142.

Serafim, J.L., and Pereira, J. P. (1983). "Considerations of the geomechanics classification of Bieniawski." *Proceedings, International Symposium on Engineering Geology and Underground Construction*, Lisbon, 1, II33-II42.

Teng, W. C. (1962). *Foundation Design.* Prentice-Hall Inc., Englewood Cliffs, N.J.

Thone, C. P. (1980). "The capacity of piers drilled into rock." *Proceedings, International Conference on Structural Foundations on Rock*, Sydney, 1, 223-233.

Webb, D. L. (1976). "The behavior of bored piles in weathered diabase." *Geotechnique*, 26(1), 63-72.

Williams, A. F. (1980). *The design and performance of piles socketed into weak rock.* Ph.D. dissertation, Monash university, Clayton, Victoria, Australia.

Williams, A. F., Johnston, I. W., and Donald, I. B. (1980). "The design of socketed piles in weak rock." *Proceedings, International Conference on Structural Foundations on Rock*, Sydney, 1, 327-347.

Williams, A. F., and Pells, P. J. N. (1981). "Side resistance of rock sockets in sandstone, mudstone, and shale." *Canadian Geotechnical Journal*, 18, 502-513.

Wilson, L. C. (1976). "Tests of bored and driven piles in cretaceous mudstone at port Elizabeth, South Africa." *Geotechnique*, 26(1), 5-12.

Winterkorn, H.F., and Fang, H.-F.(1975). *Foundation Engineering Handbook.* Van Nostrand Reinhols, New York, 601-615.

THESIS PROCESSING SLIP

FIXED FIELD: ill. _____ name _____

index _____ biblio _____

▶ COPIES: (Archives) Aero Dewey (Eng) Hum

Lindgren Music Rotch Science

TITLE VARIES ▶☐ _____

NAME VARIES: ▶☐ _____

IMPRINT: (COPYRIGHT) _____

▶COLLATION: 167 l

▶ADD. DEGREE: _____ ▶DEPT.: _____

SUPERVISORS: _____

NOTES:

cat'r: date:

page: 5129

▶DEPT: C.E.

▶YEAR: 1997 ▶DEGREE: M.S.

▶NAME: ZHANG, Lianyang